Master's thesis

NTNU
Norwegian University of Science and Technology
Faculty of Engineering
Department of Energy and Process Engineering

Jomar Mandal Leth-Olsen

Design of refrigeration system for freeze-concentration of fish protein hydrolysates using CO_2 as working fluid

Master's thesis in Mechanical Engineering
Supervisor: Armin Hafner
Co-supervisor: Ignat Tolstorebrov
June 2022

NTNU
Norwegian University of Science and Technology

Jomar Mandal Leth-Olsen

Design of refrigeration system for freeze-concentration of fish protein hydrolysates using CO_2 as working fluid

Master's thesis in Mechanical Engineering
Supervisor: Armin Hafner
Co-supervisor: Ignat Tolstorebrov
June 2022

Norwegian University of Science and Technology
Faculty of Engineering
Department of Energy and Process Engineering

NTNU
Norwegian University of
Science and Technology

Preface

This master thesis is written in the spring semester of 2022 and concludes my 2-year master in Mechanical Engineering at the Department of Energy and Process Engineering at the Norwegian University of Science and Technology (NTNU).

I want to thank Armin Hafner and Ignat Tolstorebrov for the guidance and advice during the project and master work, and Muhammad Umar Khan and Prem Kumar Sherman for the great co-operation during the spring and autumn semester. A special thanks also goes to my fellow students for the great social and academic environment.

Trondheim, June 2022
Jomar Mandal Leth-Olsen

Abstract

The processing of fish leaves a large amount of rest raw material (RRM) only utilized for low-quality byproducts. In some cases, the rest raw material can make up over 50% of the total weight of the white fish when filleted. Utilizing the high nutritional values still contained in the RRM for the production of fish protein hydrolysates (FPH) using enzymatic hydrolysis can produce high-quality hydrolysate. Further concentrating and drying can yield human-grade powder which is a more sustainable way to handle the RRM.

Freeze concentration is an energy-efficient and gentle manner to de-water the FPH prior to drying, better preserving the nutritional values and sensory characteristics of the product. The freeze concentration crystallizes and removes water, increasing the concentration of the solution.

To evaluate the heat transfer from the bulk hydrolysate to the refrigerant and determine the rate of ice formation in the contact freezing vessel, a simulation program has been written in Python to calculate the overall heat transfer coefficient, and the impact of the following factors is investigated:

- Vertical pipes vs coiled pipes
- Mass flux of refrigerant
- Uniform thermal gel layer between the pipe and vessel wall
- Diameter of the vessel and scrape velocity
- Saturation temperature of the refrigerant

The findings were; that the difference between the vertical and coiled configuration was negligible. Changing the mass flux of the refrigerant is impactful on the initial heat transfer coefficient, but in the range of $< 5\%$ on U_{avg}. The diameter and scrape velocity have the largest impact on the U_{avg} with values ranging $[475, 660]$ for the diameters considered. The saturation temperature of the refrigerant impacts the heat transfer Q and ice growth rate because of the change in temperature difference.

The overall heat and cooling demand are determined for the FPH process. Two CO_2 refrigeration systems are designed to meet the required heat and cooling loads; CASE 1 & CASE 2. The systems have two-stage compression and expansion, with the high stage having super-critical heat rejection. The system performance is investigated. **CASE 1** has the operational range of $[-28°C, -20°C]$ and the resulting COP_R ranges from [1.76,2.06]. The operational range of **CASE 2** extends from $[-40°C, -20°C]$, and the resulting COP_R ranges from [1.35, 1.86].

Design of refrigeration system for freeze-concentration of fish protein hydrolysates using CO2 as a working fluid

Sammendrag

Foredling av fisk etterlater store mengder restmateriale kun benyttet til lavkvalitets biprodukter. I noen tilfeller kan restmaterialet utgjøre over 50% av den totale vekten av hvit fisk. Utnyttelse av den høye næringsmengden fortsatt tilgjengelig i restmaterialet for produksjon av fiskeprotein-hydrolysat (FPH) ved å benytte enzymatisk hydrolyse, kan gi høykvalitets hydrolysat. Videre konsentrering og tørking kan produsere proteinrikt pulver til menneskelig konsum, som er en mer bærekraftig måte å bruke restmaterialet på.

Frysekonsentrasjon er en energieffektiv og skånsom måte å avvanne FPH før tørking, og bevarer næringsverdiene og sensoriske egenskaper til produktet bedre. Frysekonsentrasjonen krystalliserer og fjerner vannet, og øker konsentrasjonen av løsningen.

For å evaluere varmeoverføringen fra hydrolysatet til kjølemediet og bestemme hastigheten på isdannelsen i kontakt-fryseren, er det skrevet et simuleringsprogram i Python for å beregne den totale varmeoverføringskoeffisienten, og virkningen av følgende faktorer er undersøkt:

- Vertikale rør vs. kveilrør
- Massefluks av kjølemedium
- Jevnt lag termisk gel mellom rør- og sylinder-vegg
- Diameter på sylinder og skrapehastighet
- Metningstemperatur for kjølemediet

Resultatene var; at forskjellen mellom vertikal- og kveil-konfigurasjon var ubetydelig. Endring av massefluksen til kjølemediet har innvirkning på den opprinnelige varmeoverføringskoeffisienten, men i området $< 5\%$ på gjennomsnittlig varmeoverføringskoeffisienten U_{avg}. Diameteren og skrapehastigheten har størst innvirkning på U_{avg} med verdier som varierer $[475, 660]$ for diameterne ble vurdert. Metningstemperaturen til kjølemediet påvirker varmeoverføringen Q og vekstfarten på islaget grunnet endringen i temperaturforskjell.

Det totale varme- og kjølebehovet regnes ut for FPH-prosessen. To CO_2 kjølesystemer er designet for å møte de nødvendige varme- og kjølebelastningene; CASE 1 & CASE 2. Systemene har to-trinns kompresjon og ekspansjon, der det øvre trinnet har superkritisk varmeavgivning. Systemytelsen undersøkes.**CASE 1** har operasjonsområdet $[-28°C, -20°C]$ og den resulterende COP_R varierer fra [1.76,2.06]. Operasjonsområdet til **CASE 2** strekker seg fra $[-40°C, -20°C]$, og den resulterende COP_R varierer fra [1.35, 1.87].

Contents

List of Figures

List of Tables

Nomenclature

Symbols

q”	Local heat flux	[W/m^2]
k	Thermal conductivity constant	[W/mk]
T	Temperature	[^oC]
h	Heat transfer coefficient	[W/m^2k]
R	Thermal resistance	$[K/W]$
U	Overall heat transfer coefficient	$[W/m^2K]$
A	Area	$[m^2]$
G	Mass flux	$[kg/m^2s]$
ρ	Density	[kg/m^3]
P	Pressure	[bar]
V	Volume	[m^3]
H	Height	[m]
g	Gravitational acceleration	[m/s^2]
$\dot{Q}$	Heat flux	[W/s]
$\dot{Q}$”	Local heat flux	$[W/m^2]$
C_p	Specific heat capacity	[kJ/kgK]
$\dot{W}$	Work	$[W]$
η_{is}	Isentropic efficiency	$[-]$
h	Specific enthalpy	$[kj/kg]$
Pr	Prandtl number	$[-]$
Nu	Nusselt number	$[-]$
Re_D	Reynolds number pipe flow	[$-$]
$\dot{m}$	Mass flow	[kg/s]
D_h	Hydraulic diameter	[m]
μ	Kinematic viscosity	[m^2/s]
x	Length	[m]
x	gas fraction	$[-]$
f	Darcy friction factor	[$-$]
Co	Convection number	$[-]$
Fr	Froude number	$[-]$
Bo	Boiling number	$[-]$
r	Radius	$[m]$
D	Diameter	$[m]$

Subscripts

Ref	Refrigerant
R	Refrigeration
HP	Heat pump
E	Evaporator
Sat	Saturated
D_h	Hydraulic diameter
l	liquid
AC	Cross-sectional area
s	Surface
surf	Surface
lam	Laminar
turb	Turbulent
Cyl	Cylinder
req	Required
avg	Average
out	Outlet
hyd	hydrolysate
low	Lower stage
int	Intermediate stage
high	High stage

List of abbreviations

CFD	Computational fluid dynamics
SSHE	Scraped surface heat exchanger
SFC	Suspension freeze concetration
PFC	Progressive freeze concentration
RRM	Rest raw material
FPH	Fish protein hydrolysate
RPM	Rounds per minute
IHX	Internal heat exchanger
HP	High pressure
LP	Low pressure
GWP	Global Warming Potential
FC	Freeze concettration
ODP	Ozone depletion potentail

1 Introduction

1.1 Motivation

Fish and marine products are a large source of protein for human consumption. However, the processing of fish leaves a large amount of rest raw materials (RRM) only utilized for the production of cheap byproducts such as fish flour, fish oil, or animal feed[1]. In some cases, the RRM can make up over 50% of the total weight of the white fish when filleted. Utilizing the RRM for the processing of fish protein hydrolysates (FPH) and further processing into human-grade powder is a more sustainable way to handle the RRM. A considerable challenge with FPH is the low solid content of $< 10\%$, short shelf life, and sensitivity to heat treatment.

Freeze concentration is a measure for increasing the solid content in a more gentle manner compared to traditional evaporation techniques. The processing involves the fractional crystallization of water to ice and further removal of the ice [1] in order to stabilize the product. Freeze concentration is an energy-efficient way of removing water from food products sensitive to heat treatment. However freeze concentration (FC) requires expensive equipment, and has higher capital costs compared to traditional evaporation equipment. FC is therefore mainly used for high-value food products. Decreasing the water content of high moisture foods greatly reduces the energy consumption and the required equipment size for further drying of the product.

Using natural refrigerants with low global warming potential and ozone depletion potential (GWP) (ODP) such as CO2 instead of synthetic refrigerants is important to be able to reduce emissions of greenhouse gases (GHG) from refrigerants. In order to make an energy-efficient and sustainable operation of FPH processing. Integration of energy recovery and utilizing the surplus heat is essential when designing a refrigeration system for high energy efficiency.

1.2 Task Description

Project Work

The project work was performed during the autumn of 2021 and contained the initial calculation of the composition through the steps of processing and the corresponding heat and cooling loads imposed upon the refrigeration system. An investigation of the internal energy recovery potential was conducted. Initial design considerations were made and a CO_2 refrigeration and heat pumping system for the production of fish protein hydrolysate was proposed. Further, the steady-state performance of the system was analyzed along with investigating the impact of adding ejectors in the lower and higher pressure levels. The focus of the results was on the energy consumption per produced hydrolysate the system would produce.

Continuation of the Project Thesis

This master thesis is a continuation of the project work performed throughout the autumn of 2021. Some of the parts of the project work will be relevant for the master thesis. Therefore some parts will be reused in the master thesis to rather shift focus to the continuation of the work. This decision has been made in agreement with my supervisors Armin Hafner and Ignat Tolstorebrov. Some chapters will therefore have overlapping contents. The reproduction will predominantly be contained but not limited to the chapters listed in the following table:

Chapters
2 Theory
4 System design

Table 1.1: Partially reused material

This thesis will further investigate the system and the following tasks are to be considered:

- Review of relevant literature
- Develop models using EES and relevant modeling/simulation software, in order to simulate the different parts of the process plant with focus on the integration of both sides of the vapor compression cycle.
- Investigate the design and heat transfer of the evaporator design
- Perform detailed design investigations, and simulations, using the developed models.
- Analyze and discuss the results in terms of system performance and overall energy demand
- Master thesis report including chapters discussion, summary, and proposal for further work

1.3 Goal And Structure

Theory

This chapter will include the theory backing the research done in the thesis, and literature regarding the state of the field. It concerns among other things: the hydrolysis process, the process of freeze concentration, refrigeration cycles, and configurations for increasing performance as well as fundamental heat transfer theory.

Method

The chapter concerns the methodology and the approach taken in developing the programs/simulations of the overall heat transfer and refrigeration system. It includes documentation of the equations and algorithm used and the assumptions made in order to get final results.

System Design

The system design chapter contains the design of the CO_2 refrigeration systems and includes the main components of the different system configurations and illustrations. The background and reasoning for the different components of the design are included here.

Results

This chapter includes the results of the work performed during the master thesis. The main results and the impact are presented and discussed here. The chapter is divided into the heat transfer coefficient simulations and CO_2 systems performance. The impacting factors on the heat transfer,

such as temperature, mass flux, thermal gel layers, and varying diameters are investigated and key figures laid out. The CO_2 system specification and further performance for the different system configurations are presented.

Discussion

The impact of the results, the initial assumptions, and performed work is discussed in this chapter. The weaknesses and strengths of the methodology and simulations will be reviewed, and trends are observed.

Conclusion

The conclusion is a short summary of the findings of the work performed, including key figures such as COP, and heat transfer coefficients.

Further Work

List of work and ideas that can be further investigated in the future correlating to, or further developing the models and designs introduced in this thesis.

Appendix

Includes documentation of the simulations and scripts relevant to the work performed including EES scripts and Python scripts.

1.4 CoolFish

This thesis is in cooperation with the CoolFish project, which seeks to "develop technologies and concepts for more integrated, energy-efficient and climate-friendly cooling, freezing and heating onboard fishing vessels. It will also increase the knowledge transfer between research and industry, both nationally and internationally." [2]

Figure 1.1: Logo for the CoolFish project[2]

The duration of the project is 2019-2023 and is being led by SINTEF Ocean. The project includes research partners SINTEF Energy Research and NTNU and industry partners MMC First Process, Bluewild, Selvåg Senior/Sørheim Holding, GASNOR, Danfoss, Perfect Temperature Group, and Isotherm Inc. [2]

2 Theory

Section 2 will contain the essential theory and literature needed to present the methodology and contents of the master thesis.

2.1 Fish Protein Hydrolysate - FPH

Fish protein hydrolysis (FPH) is a process for utilizing the high nutritional values still remaining in the by-products of fish processing. The rest raw materials typically consist of heads, back,s and the tail of the different fish after filleting.

Fish protein hydrolysis is done by mixing the rest raw materials with water and adding either enzymes or chemicals. The solution subsequently breaks down the proteins in the fish tissues into smaller peptides and finally into amino acids.[3]

The primary constituents of fish; water, protein, fat, and ash varies with factors, such as the different batches of rest raw material, the type of fish, and the quality of initial processing. The composition of the product affects the shelf life of the products, freezing points, and heat capacity and further characteristics. It is imperative to understand how to handle and store the products in an effective and gentle manner to produce high-quality products.

Byproducts (%)	Heads	Backbones	Average
Moisture	79.5	75.0	77.3
Lipids	0.3	0.4	0.4
Proteins	13.9	15.2	14.6
Ash	5.6	9.0	7..3

Table 2.1: Composition of Cod byproducts[3]

The chemical composition for cod is presented in table 2.1 and the average protein value of 14.6% makes up a considerable mass fraction of the RRM. The main problem is the difficulty to extract the protein-rich part with mechanical equipment. FPH is a way to separate the protein from the other parts of the fish, therefore opening up for utilization as a nutrient for high-quality feeds.

There are two main approaches for protein hydrolysis: Enzymatic and Acidic/Alkali hydrolysis[3]. The main advantage of enzymatic hydrolysis is that the bones do not dissolve in the solution, which makes for a higher quality product compared to Acidic/Alkali hydrolysis. Another advantage is the inactivation of the enzymatic hydrolysis can be done by increasing the temperature, while the Acidic/Alkali hydrolysis forms a solution that needs to be neutralized by either adding water or adjusting the pH value by other means before dehydration.

A way of achieving a high-quality hydrolysate is by using enzymes from animals, plants, or microbial sources[4], such as papain and bromelain. The enzymatic reaction takes place at somewhat elevated temperatures of ca $35 - 60°C$ over a period of one to several hours at a certain pH according to the efficiency of the enzymes chosen and the quality required[3]. An advantage of enzymatic hydrolyzing of fish using papain and bromelain is the high quality of FPH and avoiding the development of undesirable products of racemization which occurs in acid and alkali hydrolysation.[3]

The finished hydrolysate mixture will be of high water content $\approx 90\%$ and will need considerable filtration to remove the bones and other undissolved solids contained in the mixture. The product

will also have a relatively short shelf life and to achieve a stable and high quality product, unwanted solids needs to be filtrated and further concentration and drying of the solution.

2.2 Refrigeration

2.2.1 Basic refrigeration cycle

The purpose of refrigeration is to cool reservoirs or products to temperatures lower than the ambient. Since heat travels in the direction of higher to lower temperatures, refrigeration is not possible without putting work into the process.

The most basic refrigeration principle is the vapor compression cycle, which is based on the Carnot cycle and is used for the majority of refrigeration systems. It circulates a fluid and manipulates the pressure and temperature for heat rejection and absorption at the desired temperature levels utilizing the latent heat in the two-phase region of gas & liquid. The circulating fluid is chosen by evaluating the thermo-physical properties as well as environmental and economic considerations. The basic refrigeration cycle includes 4 main components;

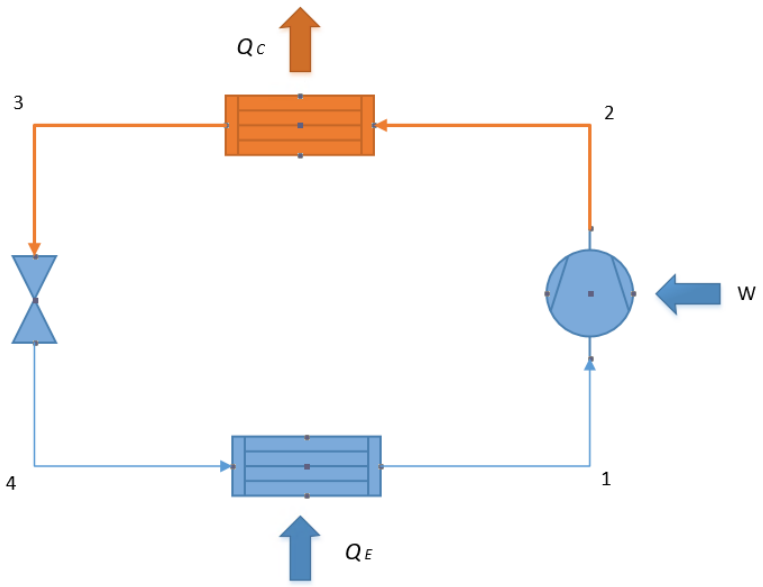

Figure 2.1: Illustration of a simple refrigeration cycle

The simplified process is illustrated in figure 2.1 where the following numbers refer to the state in the figure.

- **Compressor 1-2** isentropic compression of the gas coming from the evaporator. The pressure and temperature increases, yielding superheated gas at the compressor outlet. Real compression will not be isentropic due to losses, therefore an isentropic efficiency is introduced: η_{is}. The compressor work can be expressed as following:

$$\dot{W}_C = \frac{\dot{W}_{is}}{\eta_{is}} = \dot{m}_{ref} \times \frac{(h_{2s} - h_1)}{\eta_{is}} = \dot{m}_{ref} \times (h_2 - h_1) \tag{1}$$

- **Condenser 2-3** Constant pressure heat rejection to a secondary fluid or the ambient. Sensible heat removal from the superheated gas to the saturated gas line and subsequent con-

densation of the working fluid, yielding saturated liquid at the outlet.

$$\dot{Q}_C = \dot{m}_{ref} \times (h_2 - h_3) \tag{2}$$

- **Expansion valve 3-4** Isenthalpic expansion to the evaporator pressure. reducing the pressure & temperature, a mixture of gas and liquid at the outlet.

$$h_3(p_C) = h_4(p_E) \tag{3}$$

- **Evaporator 4-1** Gas and liquid mixture enter, absorbs heat at constant pressure evaporating the working fluid. Saturated gas exits the evaporator to the compressor. The heat absorbed in the evaporator can be expressed as:

$$Q_E = \dot{m}_{ref} \times (h_1 - h_4) \tag{4}$$

The stages in list 2.2.1 is illustrated in figure 2.2, where the log P-h and T-s diagrams for a simple subcritical refrigeration cycle is presented.

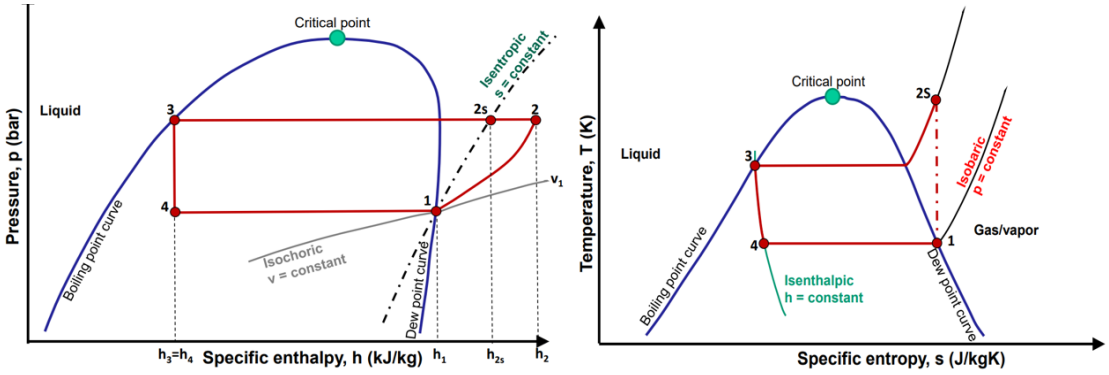

Figure 2.2: Log p-h, & T-s diagrams of a simple refrigeration cycle [5]

Refrigeration cycles have different requirements for the condensing- and evaporation pressures and temperatures depending on the system design. There are numerous refrigerants to choose from, with different properties and characteristics. Due to the increased focus on ozone depletion and greenhouse gas emissions, natural refrigerants with low global warming potential (GWP) and ozone depletion potential (ODP) are desired and are increasingly prioritized over their synthetic counterparts. The most common natural refrigerants are R717 - Ammonia, R744 - CO_2, and hydrocarbons.

2.2.2 CO_2 refrigeration

CO_2 has a long history as a refrigerant and has been used since the 1890s. The widespread availability made it the refrigerant of choice for freezing and transporting foods around the world. With the introduction of synthetic refrigerants, the use of CO_2 as refrigerant plummeted and by the 1960s it was almost entirely replaced.[6] In the last decades, CO_2 has made a resurgence as a refrigerant due to the increased focus on the environmental impact of refrigerants, prioritizing refrigerants with low ODP and GWP. Advances in materials science have made high-pressure systems cheaper and more efficient, leading it to be proposed as the main refrigerant for domestic hot water (DHW) and supermarket systems [6].

CO_2 has several beneficiary properties as a refrigerant and has proven to be a promising replacement for synthetic refrigerants. It is a natural refrigerant, with a ODP = 0 and a GWP = 1. Due to the relatively low critical temperature of CO_2 it is achievable to operate both sub-critical and trans-critical cycles.

The properties of CO_2 have made it popular in low-temperature applications as either a secondary fluid or lower part of a cascade. Another popular application is for the heating of district hot water with trans-critical operation.

2.2.3 Sub-critical

A sub-critical refrigeration cycle is designed as described earlier in list 2.2.1, where the entire cycle operates below the critical point. Both heat rejection and absorption will happen isobaric with phase change at constant temperature. For sub-critical CO_2 the lower evaporation boundary is at the triple point, approximately -55°C & 5.7 bars, and the practical upper condensing boundary is slightly under the critical point at 28/30 °C. Because of the low critical temperature the expansion loss is larger for CO_2 compared to other refrigerants.[5] The compressor efficiency and heat transfer coefficients in the condenser and evaporator are advantageous while the temperature loss for a given pressure loss $\frac{dT}{dp}$ is smaller than other refrigerants.

2.2.4 Trans-critical cycle

Taking the low critical temperature into account, trans-critical operation is possible and should be considered when using CO_2 as the refrigerant. Trans-critical processes have the heat rejection above the critical pressure and temperature, and the heat absorption below the critical point. The heat rejection at supercritical pressures occurs at a gliding temperature compared to the constant temperature condensation in the sub-critical cycle. The sensible heat rejection is advantageous when the receiving fluid requires a large temperature lift e.g. domestic hot water heating. Since trans-critical CO_2 COP_{HP} is highly dependent on the outlet temperature of the gas cooler, refrigeration systems without heat recovery and sub-cooling will perform worse during higher ambient temperatures compared to other systems due to the high outlet temperature and subsequent high gas fraction.

2.2.5 Refrigeration Losses

As opposed to the ideal vapor compression cycle, real refrigeration cycles have losses that contribute to increased energy consumption. The losses are illustrated in a T-s diagram in figure 2.3. The main losses are:

- **Heat exchanger loss** - Heat exchanger losses occur due to the temperature difference between the cold/warm reservoir and the evaporation/condensation temperature which increases the required work for the compression.
- **Super heat loss** - caused by the compression being carried out in the superheated region. Causing excess work.
- **Expansion loss** - caused by an isenthalpic expansion rather than an isentropic expansion. Utilizing the available exergy with an expansion machine or ejector reduces expansion loss.

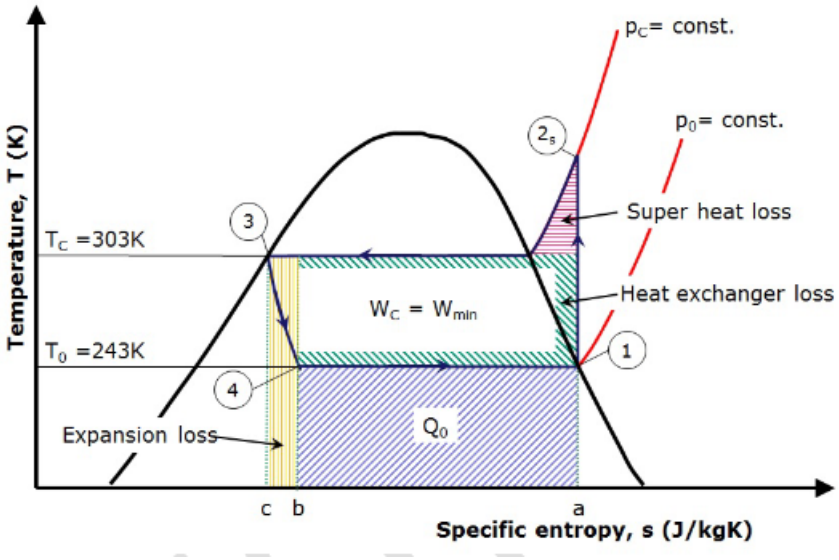

Figure 2.3: Refrigeration losses of an isentropic cycle in T-s diagram [5]

2.2.6 Two-stage compression

When the pressure difference between the evaporation and condensing/gas-cooler pressure is large, a two-stage compression should be considered. Two-stage compression opens up for and is necessary for systems with several evaporation levels. Two-stage compression with inter-cooling will always be more energy efficient than one-stage compression operating under the same conditions, due to increasing compression loss at higher temperatures[5]. The two-stage system allows for heat transfer at larger temperature and pressure differences than conventional one-stage systems since materials and lubricating oils have higher temperature limits. By introducing intermediate cooling between the compressor stages, the specific volume and the compressor work reduces. Figure 2.4 illustrates the

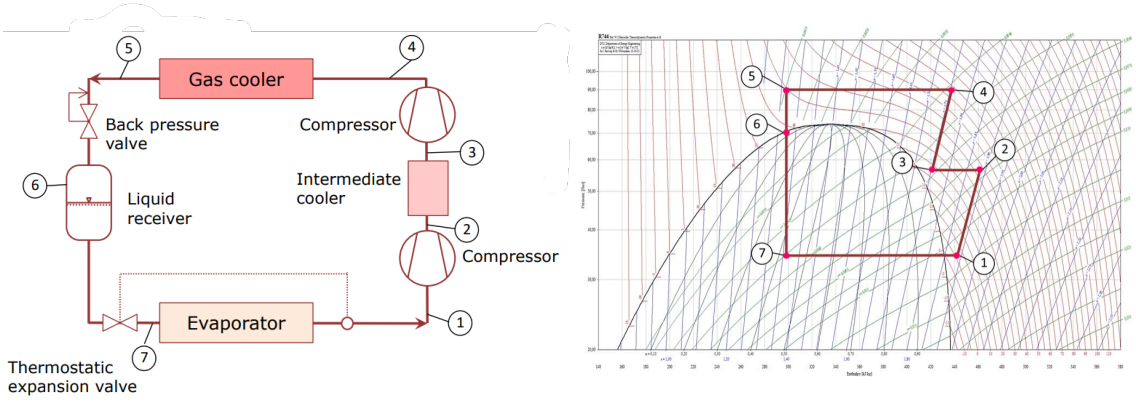

Figure 2.4: Schematic and log ph diagram for two-stage, trans-critical compression with inter-cooling[5]

Another consideration for the two-stage systems is the possibility of using two different refrigerants in a cascade, therefore utilizing the advantageous properties of several working fluids. This does however come with the increased heat exchanger loss from the necessary temperature difference when transferring heat from the low-pressure side to the high-pressure side since the refrigerants have separate closed loops. Supermarket refrigeration commonly uses a cascade solution with NH_3

on the upper cycle and CO_2 on the low-pressure side.

Two-stage systems using the same working fluid do not need heat transfer between the low and high-pressure side and can instead use a de-superheater and intermediate pressure receiver so the inlet of the high-pressure compressor is at the saturated gas line, minimizing the compression loss, removing the heat exchanger loss and increasing the volumetric efficiency.

Only parts of the refrigerant need to be compressed in two stages for cases with heat rejection at different pressures. A fraction of the refrigerant will be compressed to the high stage while the liquid is expanded to the lower stage. This system solution can be used when there is surplus heat in the cycle and less heating demand at higher temperatures.

2.2.7 Internal heat exchanger

The internal heat superheats the saturated gas going to the compressor while subcooling the gas or saturated liquid coming out of the gas cooler/condenser by transferring heat from the high pressure to the low pressure. The increased temperature of the gas leads to increased superheat loss and increased compression work, while the subcooling will reduce the expansion loss and increase the refrigeration capacity. The IHX has a positive effect on the refrigeration system if the specific refrigeration capacity increases more than the effect of the increased gas volume at the compressor inlet[5].

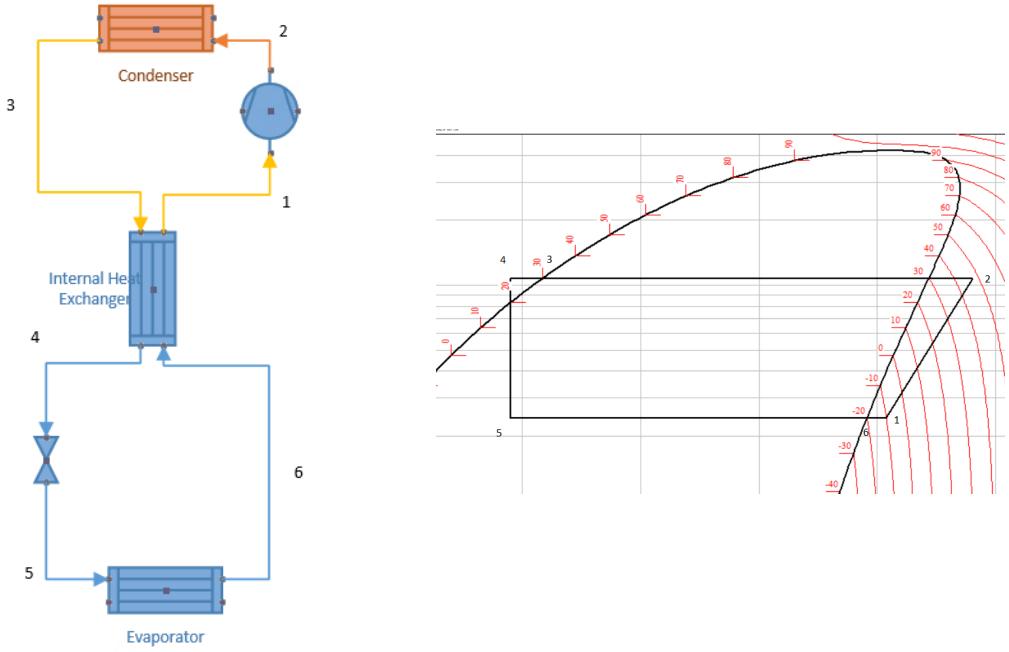

Figure 2.5: Schematic and log ph diagram of a system with IHX

2.3 Freeze Concentration

The concentration of food products is the process of removing undesired components to achieve a product of satisfactory quality and desired composition. Due to water being so abundant in foods and beverages and the dramatic effect water content has on the shelf life of food products, regulating the moisture is paramount for achieving a satisfactory and stable product.

The goal of hydrolysation of rest raw materials is to utilize proteins still contained in the fish. Since drying is such an energy-intensive process it is preferable to further concentrate the solution before drying occurs.

Freeze concentration is a less aggressive method of removing water from a product compared to evaporation at ambient pressures, better preserving the nutritional values and sensory characteristics. Due to the delicate handling, freeze concentration and freeze-drying are used for products that can be damaged by excessively high temperatures.[1]

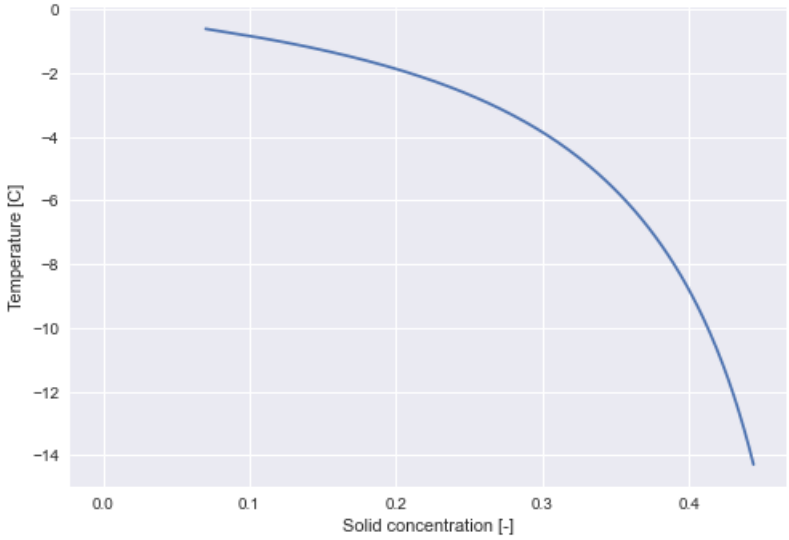

Figure 2.6: Freezing depression of the FPH mixture [7]

Freeze concentration is done by bringing the solution below the initial freezing point where some of the water in the solution crystallizes. The ice crystals are then separated from the mixture. The remaining unfrozen part of the solution is therefore of a higher concentration, further decreasing the freezing point of the solution. The temperature of the solution can be lowered, further repeating the process. The freezing depression of the FPH solution is illustrated in figure 2.6.[7] Several freezing steps can be implemented at different temperatures and separation of the ice can happen continuously or batch-wise depending on system design and configuration.

The FC process does however have high refrigeration costs, high capital costs for equipment, high operating costs, and low production rates compared with concentration by boiling.[1] Freeze concentration can achieve higher concentration compared with membrane processes, but lower than concentration using boiling. Due to its expensive nature, it is mainly used for high-value products.

Freeze concentration can be divided into two parts, which are suspension freeze concentration (SFC) and progressive freeze concentration (PFC).[9] PFC progressively produces ice crystal layers on a cooled surface until it forms a large crystal block.[9] The efficiency of PFC is found to be lower than SFC. SFC produces many small ice particles in the suspension of the solute. The system consists of crystalization, growth, and separation of the ice crystals.[9] The ice forms on a scraped-surface heat exchanger (SSHE) where the initial ice crystallization happens. The crystals are then removed with blades, cleaning the surface and keeping a high heat transfer rate.[10] Further, the ice crystals grow in the solution and are then separated.[10]. The heat transfer of an SFC system is investigated due to the higher productivity and well-tested nature of SFC, compared to PFC.

A general process for freeze concentration is shown in 2.7, and the main components needed for

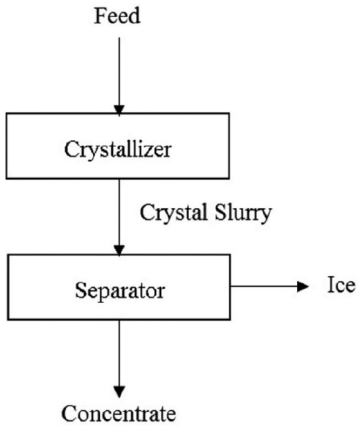

Figure 2.7: General process for freeze concentration[8]

suspension freeze concentration are:

- A direct freezing system
- A mixing SSHE for the ice crystals to grow
- A separation system to remove the crystals from the solution

Separation can be achieved by using several techniques such as centrifugation, filtration, filter pressing, or wash columns. [1]

Concentration can be accomplished with single-stage or multi-stage equipment. Multi-stage equipment will maintain a lower energy consumption and has the potential for higher production rates but run a higher capital cost. A solid concentration of 45% is possible due to improvements to washing and ice crystal generation.[1]

2.4 Industrial Drying Processes

Drying (or dehydration) is the process of removing the majority of water present in a food by evaporation. Drying can remove considerably more water than other processes, such as freeze concentration, membrane concentration, and mechanical separation.

The main reason for drying food products is to stabilize the product and extend the shelf life, minimizing the microbiological growth and enzyme activity. Due to the lower weight of a dry product, transportation and storage costs will be reduced.

2.4.1 Drying using heated air

When using heated air for the removal of moisture, three factors determine the capacity of air to remove moisture.[1]

1 The relative humidity of the air

2 The temperature of the air

3 The air velocity over the product

The three factors are intertwined, as the relative humidity changes with air temperature, and the energy efficiency depends on the mass flow of air and the temperature. When the hot air blows over the product, the water vapor diffuses through the boundary film and gets transported away. The driving force for diffusion is the vapor pressure gradient from the product to the hot air. [1]

Considering the low solid content in the fish protein hydrolysate, the drying will have to be carried out in a suitable manner. Therefore it will not be possible to dry using methods meant for solids, but rather use other techniques such as spray drying or roll dryer technologies. The efficiency of these methods will be dependent on the thermophysical properties of the hydrolysate, especially considering rheology aspects will be crucial for an efficient drying process. A more detailed description of drying methods applicable to FPH can be found in the parallel work "Sustainable Architecture in producing fish protein hydrolysates" by Prem Kumar Sherman.[11]

2.5 Heat transfer & pressure loss

Heat transfer consists of three main parts: convection, conduction, and radiation. This thesis will include the mechanisms of convection and conduction as the radiation is assumed to be negligible due to the low temperature differences considered.

Conduction, k is the transfer of heat through solid materials and is defined as the diffusion of energy due to the random molecular motion [12] and the rate equation is presented in equation 5.

$$q_x" = -k\frac{dT}{dx} \tag{5}$$

For a wall consisting of several materials with different conductive values, the conductive thermal resistance R_{cond} $[m^2K/W]$ is calculated using equation 6.

$$R''_{cond} = \sum_{n=i}^{\infty} \frac{x_i}{k_i} \tag{6}$$

where q''_x $[W/m^2]$ is the heat flux, k $[W/mK]$ is the conduction coefficient and dT & dx is the temperature difference and thickness of the material

The convection h is the heat transfer between a solid surface and a fluid, it can be defined as the diffusion of energy due to random molecular motion plus energy transfer due to bulk motion.[12]

$$q'' = h(T_s - T_\infty) \tag{7}$$

where T_s is the surface temperature and T_∞ is the temperature of the fluid. The thermal resistance R_{conv} $[m^2K/W]$ of the convection can be expressed as:

$$R_{conv} = 1/h \tag{8}$$

For one-dimensional conduction and convection, the temperature through the wall is dependent on the thermal resistances of the wall elements and convection. figure 2.8 illustrates heat transfer and

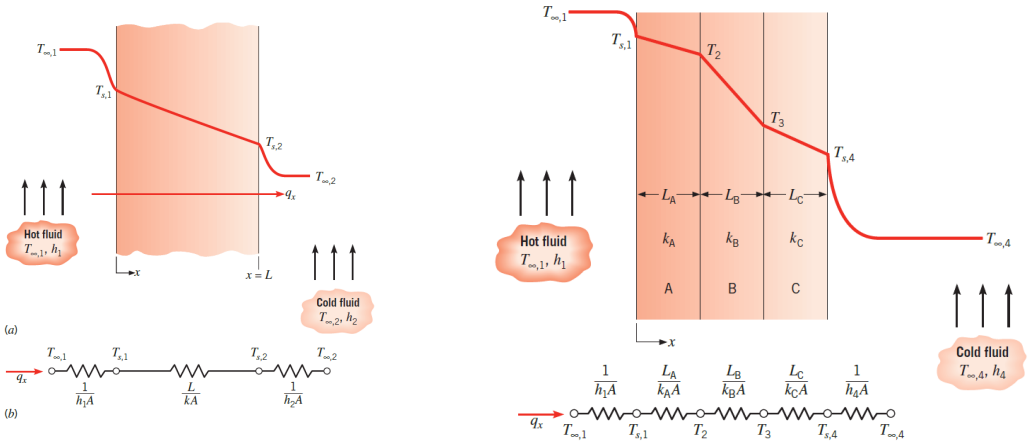

Figure 2.8: Heat transfer through a plane and composite series wall with temperature distribution and thermal circuit[12]

varying temperature differences between a hot to a cold fluid through a plane, and a composite series wall.

To find the heat transfer through the wall, consisting of several materials and convection on both sides, the overall heat transfer coefficient, or U-value can be calculated using equation 9 and further use the U-value to find the heat transfer using equation 10.

$$U = \frac{1}{R_{tot}} = \frac{1}{R_{conv,i} + R_{cond} + Rconv, o} = \frac{1}{\frac{1}{h_i} + \sum \frac{x_j}{k_j} + \frac{1}{h_o}} \tag{9}$$

$$Q = UA\Delta T \tag{10}$$

Pressure Drop

The pressure drop of evaporating two-phase refrigerant is complex and difficult to estimate accurately. There have been developed several correlations and papers reviewing these correlations to experimental data available. According to Xu & Fang (2012) [13] The correlation presented by Friedel (1979) [14] preformed advantageously at predicting the pressure drop for CO_2 compared to 3 of the 5 correlations included.

Pressure drop can affect the saturation temperature and mass flow rate of the refrigerant, but will not be taken into account in this thesis.

3 System Design

The system design considerations regarding the viability and calculations affecting the design are presented in this chapter.

The main components of the hydrolysis process were introduced and several assumptions were determined which form the rudimentary demand and further boundaries for the design of the CO_2 refrigeration system. The initial system and heat load calculations are described in greater detail in the project work "Design of CO2 refrigeration system for production of fish protein hydrolysate" (Leth-Olsen, 2021).[15] A short explanation with partial paraphrasing will be presented.

3.1 FPH processing

The flow sheet of the process for enzymatic hydrolysis is illustrated in figure 3.1. The heat loads are calculated by using existing data of the compositions of the fish found in table 2.1, and further determining the loads by calculating the composition and thermal loads at the different parts of the process. Assumptions have been made for the initial ratio of RRM and water of 1000kg:1000kg and a complete filtration of both ash and an 80:20 ratio of unsolved proteins and water from the initial composition in stage (6).

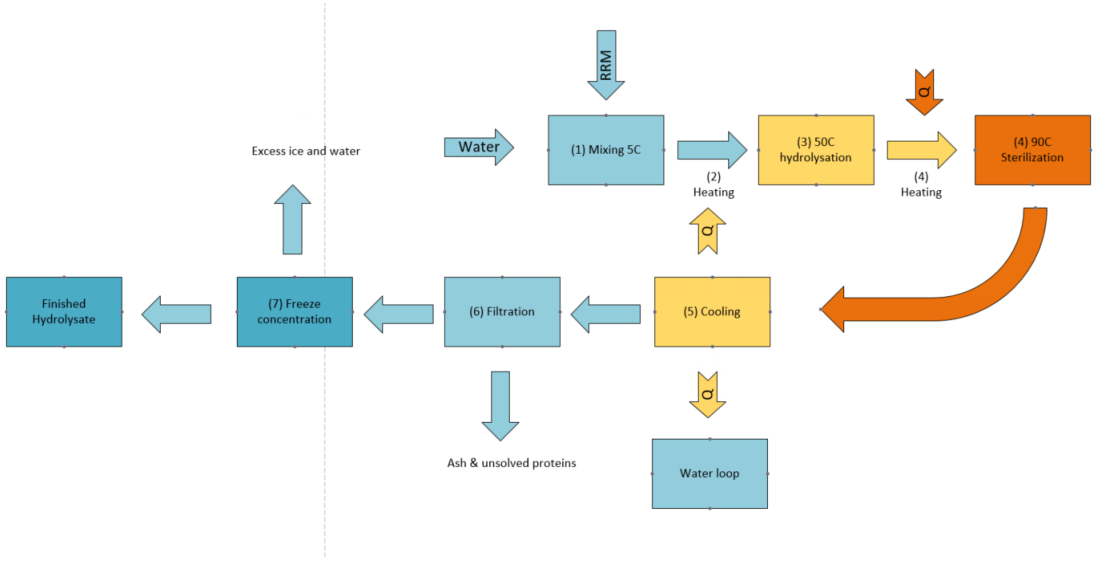

Figure 3.1: Flow sheet of the hydrolysate proces

The process is based on the experiments performed during the summer of 2021 at the lab facilities belonging to the department of energy and process engineering (EPT) at NTNU. The procedure of making and concentrating the FPH is explained in the following steps, where the numbering corresponds to figure 3.1:

1. The RRM is crushed and mixed with water in a 1:1 ratio, enzymes are added and the mixture is assumed to be at $T \approx 5°C$
2. Heating of the mixture to $50°C$
3. Hydrolysis in progress at constant temperature for 30 minutes to several hours
4. Heating the mixture to $T \approx 90°C$ for inactivation of enzymes and sterilization

5. Cooling the mixture to $T \approx 4°C$
6. Filtration, separating the Ash and unsolved solids, leaving only the hydrolysate with a protein concentration of $\approx 6.6\%$
7. Freeze concentration of the hydrolysate to 30% solids concentration

The entirety of the processing method has several heating and cooling loads which makes a considerable potential for heat recovery when considering the system design. The choice of refrigerant for the process favors CO_2 due to the low evaporation temperature, additionally, CO_2 will be able to meet the sensible temperature required in step 4 in trans-critical operation due to the gliding temperature rejection.

The required heat & cooling loads without integration of heat recovery can be found in table 3.1. The loads are based on the case of a continuous 1000kg RRM and 1000kg water mixture being handled by the system per hour.

Loads	$-18/5°C$	$5/50°C$	$50/90°C$	$90/4°C$	FC	WC
	68.7 kW*	97.8 kW	87.2 kW	-187.1 kW	-143.0 kW	129.1 kW
Total Heating Load	314.1 kW	382.8 kW*				
Total Cooling Load	330.1 kW					

*When RRM is frozen at arrival

Table 3.1: Heat & cooling loads without heat recovery integrated

By implementing two heat exchangers to cool the hydrolysate from 90-4°C, the stage 2 heating in list 3.1 from 5-90°C can be covered as well as partial coverage of the load required for melting of the ice coming from the wash column. The resulting heat & cooling loads with heat recovery are found in table 3.2.

Loads	$-18/5°C$	$5/50°C$	$50/90°C$	$90/4°C$	FC	WC
	68.7 kW*	0 kW	87.2 kW	0 kW	-143.0 kW	39.8 kW
Total Heating Load	127.0 kW	195.7 kW*				
Total Cooling Load	143.0 kW					

*When RRM is frozen at arrival

Table 3.2: Heat & cooling loads with heat recovery integrated

The integration of two heat exchangers reduces the thermal loads imposed on the refrigeration system significantly. The total cooling load decreases by approximately 57% and the total heating load similarly decreases by approximately 49% when the RRM arrives in a frozen state, and decreases by approximately 60% when the RRM arrives at 5°C

Water-loop & Wash column

The water loop is illustrated in Figure 3.2. The wash column functions to separate the ice from the hydrolysate coming from the freeze concentrator. The remaining slurry consisting of water and ice after separation melts and gets fed back into the water loop. A more detailed description of

the wash column and freeze concentration can be found in the parallel work "Design and analysis of freeze concentrator for processing of fish protein hydrolysate" by Muhammad Umar Khan [7].

To maintain a positive density gradient, the water temperature of the inlet and outlet for the water loop is chosen as 0.5°C & 3.5°C as the density of water is highest at approximate 4°C, and to avoid freezing. The small temperature difference makes for a large flow through the wash column and subsequent parallel heat exchangers. The majority of the heating load gets covered by the cooling of the unfiltered hydrolysate as figure 3.1 implies. The remaining load is heated by the surplus heat from the refrigeration system.

The water separated in the wash column gets led to the storage tank, and further to the heat exchangers connected in parallel in order to minimize the flow rate and increase the temperature difference in the heat exchangers. The mass of ice removed from the hydrolysate to achieve the desired solid concentration of 30% is 1392 kg. 1000 kg of water is reused for another batch as figure 3.1 shows. The excess water of 392 kg is disposed of. The accumulation tank connected to the water-loop assures a stable temperature and sufficient water for the mixture.

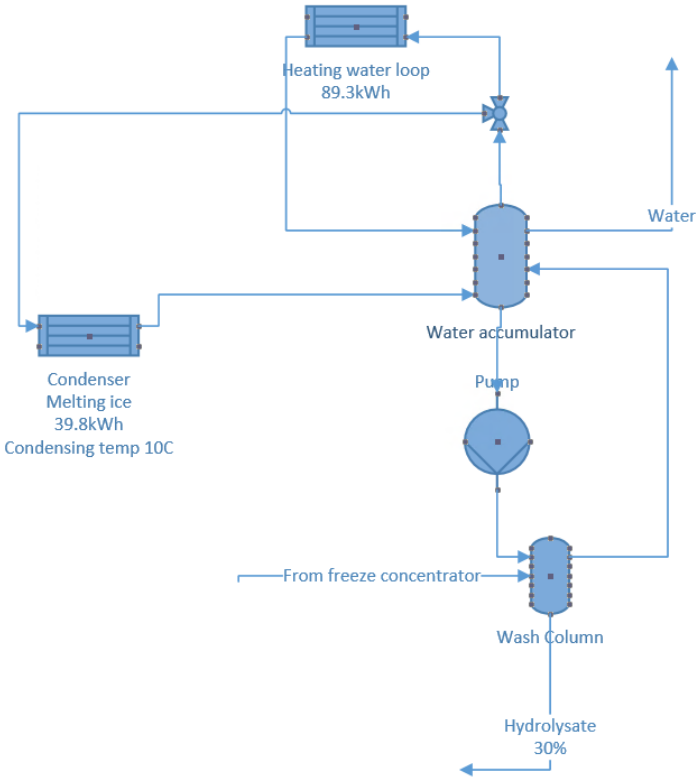

Figure 3.2: Illustration of the proposed water-loop

3.2 CO_2 Refrigeration System

To cover the heating and cooling loads, 2 different CO_2 system configurations are investigated; CASE 1 & CASE 2

CO_2 System, CASE 1

Any given refrigeration cycle needs somewhere to reject the surplus heat for the system to be feasible and operate reliably. Due to the marine nature of fish processing, the refrigeration plant is assumed to be in the vicinity of the sea, and seawater at lower depths is assumed to have a constant temperature of $\approx 5°C$. The minimum temperature to reliably reject heat to the ambient is set to $10°C$. The water-loop for melting the ice in the wash column is of low enough temperature that the temperature of $10°C$ is sufficient.

Due to the a max pressure difference of 30 bar in the compressors investigated, the minimum saturation temperature achievable -28°C. At -28°C a single-stage trans-critical is not feasible due to excess hot gas temperature, pressure ratio, and pressure difference of the compressor.

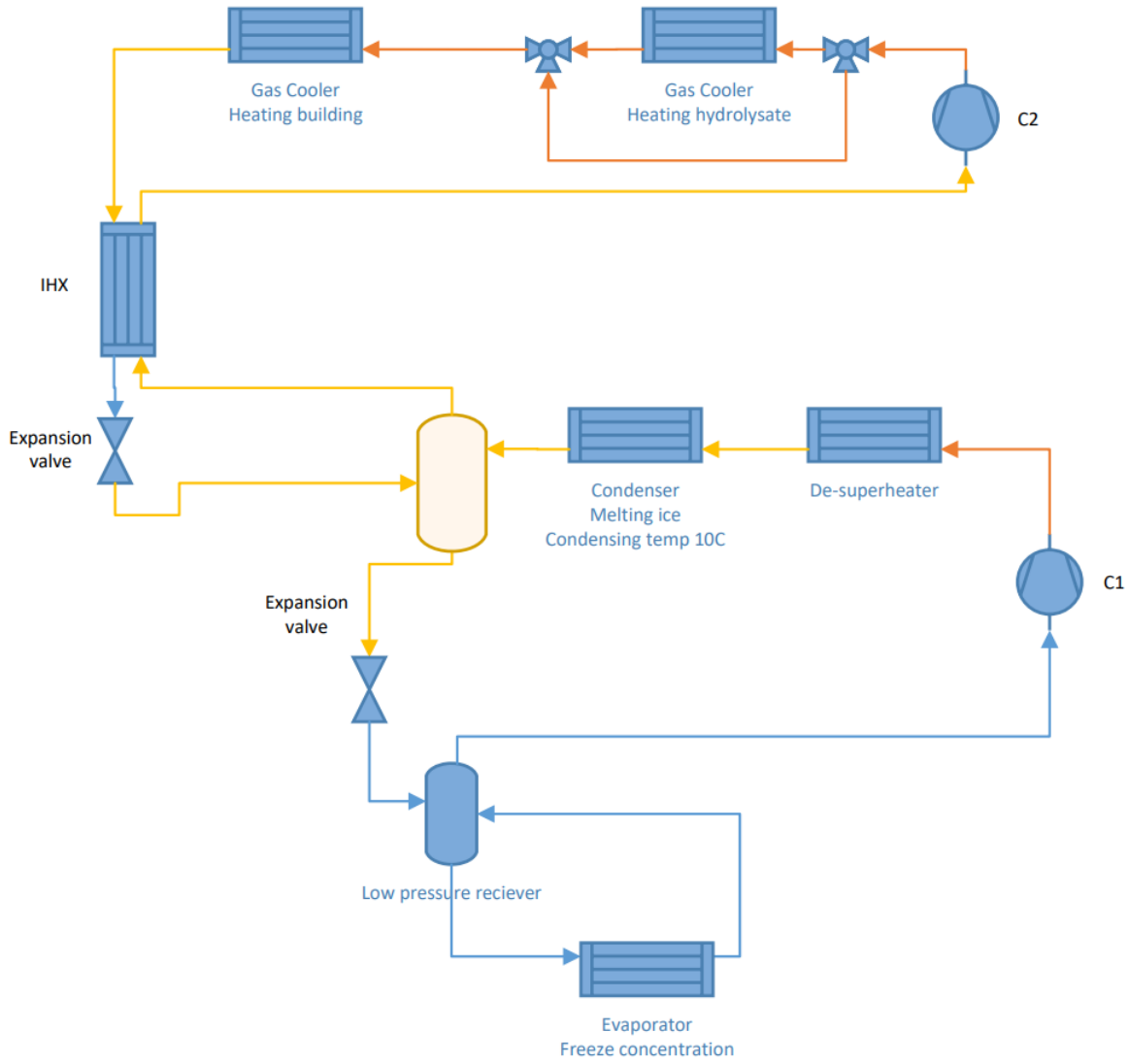

Figure 3.3: CASE 1 CO_2 system

To cover the heating of the mixture from $50-90°C$, a high pressure, 2. stage is added rejecting heat at trans-critical pressure, setting a minimum temperature difference of 5°C. An open intermediate-pressure receiver is introduced. The receiver separates the gas and liquid. The gas coming from the intermediate pressure condenser and the expansion valve is compressed to the high-pressure

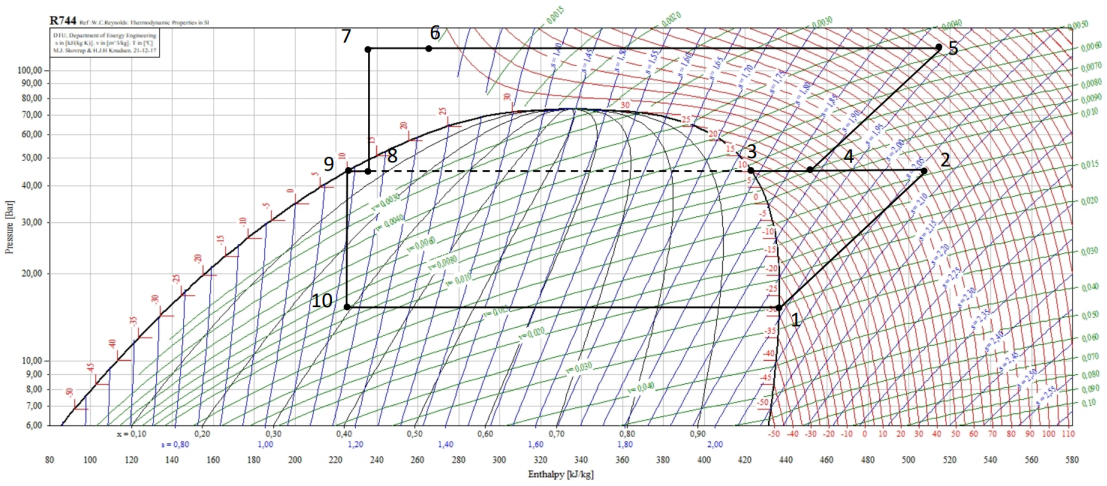

Figure 3.4: CASE 1 example visualized in log P-h diagram

side while the liquid is led to the expansion valve and low-pressure side.

Due to the relatively high intermediate temperature and pressure. The hot gas temperature exiting the high-pressure compressor (C2) with saturated gas at the inlet of the compressor is lower than the desired inlet temperature for the gas cooler of 95°C for pressures below 120 bar. An internal heat exchanger is introduced in order to increase the hot gas temperature to be able to meet the temperature and heating requirement of hydrolysate from 50 - 90°C (4). The IHX superheats the gas going to the compressor by 15°C.

The steady-state mass flows of gas and liquid in the intermediate pressure receiver need to be in equilibrium for the system to be able to operate reliably. The mass flow of the high-pressure stage is determined by the heating duty for heating the hydrolysate, and the lower side is determined by the cooling duty for the freeze concentration. The heating duty for the condenser of the intermediate stage will therefore be determined by the mass flow of the high-pressure stage and outlet enthalpy of the gas cooler, which decides the gas quality entering the intermediate-pressure receiver.

The gas cooler covers the entire heating duty of heating the mixture from 50-90°C, the required mass flow of the high-pressure side is directly linked to the enthalpy difference of the gas cooler inlet and $P = P_{GC}, T = 55°C$. An optimal gas cooler pressure will exist as the required mass flow decreases with higher pressure which increases the specific work of the compressor.

Since the mass flow of the high-pressure stage is determined by the Δh & Q_{Hyd}, adjusting the outlet temperature of the gas cooler will not have an impact on the overall energy consumption of the system. If the increase in heating duty from lowering the outlet temperature of the gas cooler can be utilized, the overall COP_{hp} will increase. There are therefore two gas coolers connected in series, one for the heating of the hydrolysate and the other for rejecting of the heat below 55°C. A bypass is also needed for the cases where there is no heating duty for the hydrolysate, as visualized in figure 3.3.

The outlet temperature of the last gas cooler is set to be 30 °C since the surplus heat from the can be utilized for preheating domestic hot water or space heating of adjacent buildings. The proposed system is visualized in figure 3.3, with an example of the process in the p-h diagram in figure 3.4.

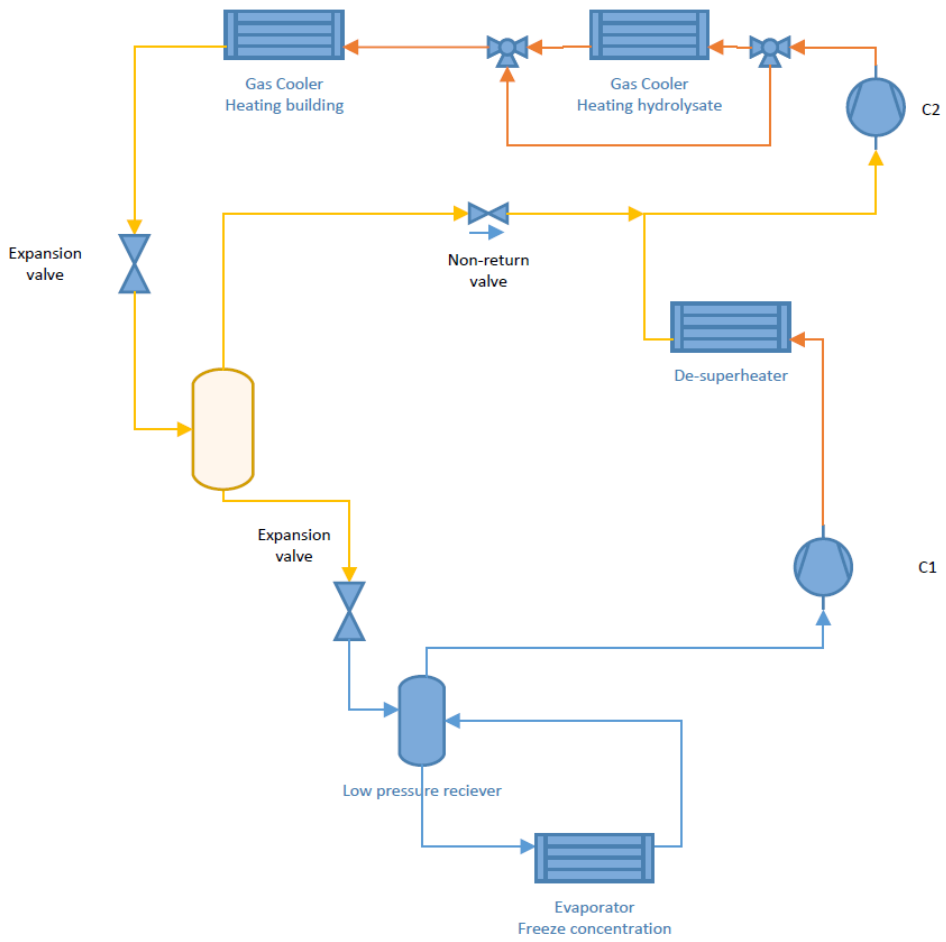

Figure 3.5: CASE 2 CO_2 system

CO_2 System, CASE 2

The other configuration of the CO_2 system does not have the partial condensation at the intermediate stage. The de-superheater partially de-superheats the CO_2 gas to a temperature of 10°C in order to maintain a sufficient temperature difference to the heat sink. The intermediate pressure is limited by the pressure difference between the low stage of 30bar and a maximum pressure of 50bar.

The high-pressure compressor has a higher pressure limit of 160 bar, and the lubricating oil and materials in the compressor have temperature limitation. An exit temperature out the gas-coolers of 30°C is set prior to expansion to the intermediate stage.

The gas exiting the gas cooler expands to the intermediate pressure increasing the gas fraction. The gas moves through the one-way valve, bypassing to the high-stage compressor. By removing the formed gas at the intermediate stage only liquid is further expanded to the evaporator stage. The mass flow of the low-pressure compressor will then decrease while maintaining the cooling capacity. The liquid is further expanded to the evaporator pressure.

CASE 2 has a higher operational range due to the partial de-superheating and lack of condensing at the intermediate stage. Therefore, lower evaporation temperatures reaching -40 °C can be reached.

Factors to investigate are varying the intermediate and high-side pressure, and determining the impact on energy consumption. The mass flow of the high-pressure stage is however dependent on the determining cooling load $Q_E = 143kW$, contrary to CASE 1, where the mass flow and pressure of the high stage can be varied. The outlet temperature of the gas-cooler for CASE 1 will impact the overall COP_R of the system, as the reduction in gas quality reduces the mass flow of the high-side compressor. The mass flow of the high-side compressor will in turn affect the optimal intermediate and high-side pressures.

4 Method

4.1 Software & Simulations

The main software tool used for making basic models and calculations is EES - Engineering Equation Solver for the performance of the refrigeration system. A program written in Python is used for the numerical solutions investigating the overall heat transfer, using the CoolProp library for gathering the thermodynamic properties for different states.

4.2 Evaporator Design

The evaporator has the design of a cylinder where the bulk, low concentrate hydrolysate. Water contained in the solution freezes on the walls. The ice gets removed by a scrape moving along the cylinder wall at a set time interval. The CO_2 flows through a pipe coiled or vertical and parallel to the cylinder.

4.2.1 Coiled pipes

A well-tested and common heat exchanger design for the heat transfer is evaporating the refrigerant by leading it through a coil around the cylinder. The downside to this solution is the relatively small contact area between the coil and the cylinder. In order to increase the heat transfer coefficient, a thermal gel can be applied in the gap between the coil and cylinder wall. To further evaluate the thermal resistance and temperature distribution through the materials, the overall heat transfer coefficient needs to be determined.

The evaporator and freeze concentration equipment is assumed to be thoroughly insulated to the ambient. Therefore the heat loss to the ambient will be assumed to be negligible. Due to the symmetry of the coil and cylinder, it will only be necessary to calculate the upper part of the center-line of one coil. The evaporating coil and surface wall have a certain thickness, and the space between the coil and wall is filled with heat transfer gel. Therefore there is assumed to be no convection and radiation through the pipe wall. There will be convection from the refrigerant to the wall and likewise from the bulk of hydrolysate to the cylinder wall. The conduction through the wall is assumed to be 1-dimensional. The design and heat flux is illustrated in Figure 4.1.

The cylinder is further discretized and the thermal resistance through the elements is calculated at the different heights relative to the evaporating coil. In this design, the main variables to change are the evaporation temperature of the refrigerant, the thickness of the heat transfer gel, and the diameter of the vessel.

4.2.2 Vertical pipes

Another geometry considered is placing the evaporating tubes vertically, parallel to the vessel rather than coiling the pipes horizontally around the vessel. The pipes will have similar conduction as the point of contact with the cylinder will remain at the center of the pipe. The size of the cylinder will have some impact on the amount of thermal gel needed as the distance between the tube and cylinder increases with decreasing cylinder diameter since the cylinder is circular and parallel to the pipe. In the case of increasingly large cylinder diameter, the geometry of vertical and horizontal

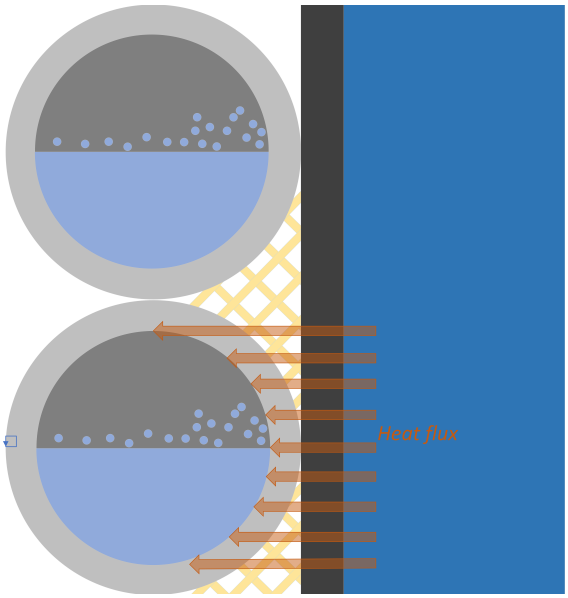

Figure 4.1: Proposed evaporator design w/coiled pipes

pipes converges.

The length of the pipes in this configuration is equal to the height of the vessel. A simplified sketch of the configuration is illustrated in figure 4.2.

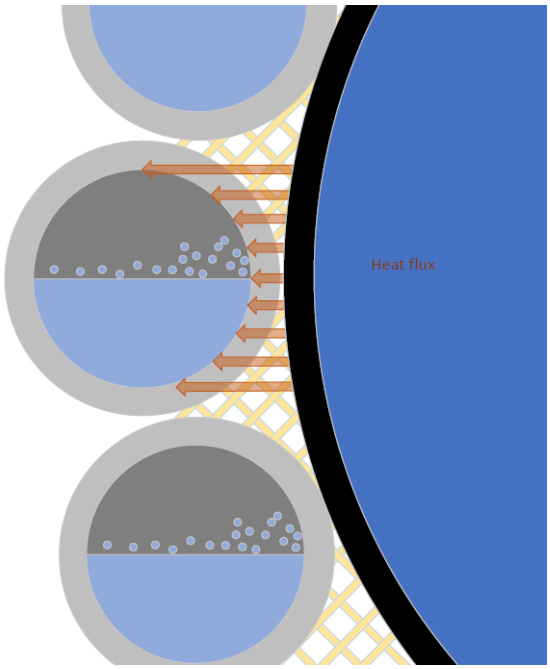

Figure 4.2: Verical pipes configuration, seen from above

The size of the pipe for both configurations is set to an outer diameter of 3/8" [in] / 9.5 [mm] & 0.76 [mm] wall thickness, as specified for K65 pipes produced by Wieland.[16] The pipe is able to withstand a maximum pressure of 87 bar which is adequate to withstand the pressure of CO_2 at ambient pressures when the refrigeration system is shut off. CO_2 is in the supercritical phase at the given pressure and temperatures above 30°C which equates to a pressure of 78 bar.

4.2.3 Heat transfer coefficient

The overall heat transfer coefficient, the U-value determines the rate of heat transfer per area and temperature difference. In order to determine the U-value, the thermal resistance of the fluids and materials must be calculated. The convection coefficient on each side of the wall and the conduction coefficient and width of the materials will influence the overall heat transfer coefficient.

$$U = \frac{1}{R_{conv,i} + R_{Cond} + R_{Conv,o}} = \frac{1}{\frac{1}{h_i} + \frac{x_{wall}}{k_{wall}} + \frac{1}{h_o}} \tag{11}$$

where h_i is the convection coefficient corresponding to the fluid inside the wall, $x_{wall}\&k_{wall}$ is the width and conduction coefficient of the wall while h_o is the convection coefficient corresponding to the fluid outside the wall.

For numerous materials, especially solids there are tabulated values for the conduction coefficient ranging for most temperatures. Copper and Aluminium have an approximately linear relation between the conduction coefficient and temperatures. The thermal gel used to fill the spaces between the outside of the pipe and cylinder wall is in agreement with co-supervisor assumed to have a low but constant conduction coefficient $k_{gel} = 10[W/mK]$.

Conduction

Due to the geometry of the pipes and cylinder wall, and the lower conductivity of the thermal gel, a notable increase in conductive resistance is to be expected moving further from the horizontal center-line of the pipes.

The pipe is discretized to determine the thermal conductive resistance at the different widths of the solid components. Subsequently calculations of the temperature throughout the wall. An average conduction coefficient is determined and used in further calculations

$$R_{cond} = \frac{x_{cu}}{k_{cu}} + \frac{x_{gel}}{k_{gel}} + \frac{x_{al}}{k_{al}} + \frac{x_{ice}}{k_{ice}} \tag{12}$$

The conduction coefficient will vary with the transient formation and subsequent removal of ice on the cylinder wall. The formation will be dependent on the thermal resistance at the given point of the wall, while the removal will occur at frequent and timed intervals.

CO_2 Convection

Liquid CO_2 enters the pipe evaporating partially, resulting in 2-phase flow in the pipes. Due to the more complicated physical situation occurring in the 2-phase flow, the correlations for the flow boiling and heat transfer coefficients are therefore more complex.[17] The correlations are somewhat limiting and have large bands of uncertainty, fortunately, the heat transfer coefficients relating to flow boiling are rarely the limiting thermal resistance in heat exchangers.[17] A review of many of the available and well-accepted correlations was performed by Shah.[18] The conclusion of the paper finds that the correlation proposed by Shah (1976,1982)[19][20] provides the least mean deviation of less than 20%. Another advantage of the correlation is the applicability for horizontal and vertical tubing. The steps and equations used in the correlation are explained below:

$$\tilde{h} = \tilde{h}(Co, Bo, Fr) = \frac{h}{h_l} \tag{13}$$

$\tilde{h}$ is a dimensionless heat transfer coefficient related by the convection number Co, boiling number Bo, and Froude number Fr. $\tilde{h}$ is defined as the ratio of the local convection coefficient for flow boiling and h_l, the convection coefficient that would occur if only the liquid fraction of the two-phase flow were present.

$$h_l = \left[\frac{(\frac{f_l}{8})(Re_{D_h,l} - 1000)Pr_{l,sat}}{1 + 12.7(Pr_{l,sat}^{2/3} - 1)\sqrt{\frac{f_l}{8}}} \right] \frac{k_{l,sat}}{D_h} \tag{14}$$

Where f_l is the Darcy friction factor, $Pr_{l,sat}$ is the Prandtl number of the saturated liquid, $k_{l,sat}$ is the conduction coefficient of the saturated liquid and D_h is the hydraulic diameter. The convection coefficient occurring in equation 14 predicts the Nusselt number using the Gnielinski correlation for fully developed flow under turbulent conditions.[17]

$$Re_{D_h,l} = \frac{G\,(1-x)\,D_h}{\mu_{l,sat}} \tag{15}$$

Where G is the mass velocity of the flow, x is the gas quality, and $\mu_{l,sat}$ is the dynamic viscosity of the saturated liquid. The $Re_{D_h,l}$ occurring in equation 14 is the liquid superficial Reynolds number, based on the hydraulic diameter and the flow rate of the liquid phase only.

$$G = \frac{\dot{m}}{A_c} \tag{16}$$

$$Co = \left(\frac{1}{x} - 1\right)^{0.8} \sqrt{\frac{\rho_{v,sat}}{\rho_{l,sat}}} \tag{17}$$

$G[kg/m^2 s]$ is the mass flux passing through the cross-section of the pipe. The dimensionless parameter Co is dependant on $x, \rho_{v,sat}, \rho_{l,sat}$ which is the gas quality and the saturated density in vapour and liquid form.

$$Bo = \frac{q_s''}{G\Delta i_{vap}} \tag{18}$$

Bo is the boiling number, which relates the heat flux at the wall to the heat flux required to completely vaporize the fluid.

$$Fr = \frac{G^2}{\rho_{l,sat}^2 g D_h} \tag{19}$$

The Froude number Fo relates the inertial force of the fluid to the gravitational one where g is the gravitational acceleration, and G is the mass flux calculated from equation 16.

The correlation used for the equations(11-17) are valid for horizontal pipes. The correlation is also valid for vertical pipes with $Fr > 0.04$ and will therefore be used when the prerequisite is fulfilled.

Hydrolysate Convection

The nature of the flow inside the cylinder is complex due to the scrape removing the ice being the only source of momentum and propulsion of the flow. Since the cylinder is large and the scrape moves radially and continuously along the inner wall of the cylinder, the flat plate correlation is chosen for the calculations of the thermal boundary layer and subsequent convection coefficient.

The relatively low speed of the scrape and blunt leading edge makes for a sudden increase in boundary layer thickness, and turbulent conditions in the wake. At a fixed position along the wall, the flow is initially turbulent as the scrape passes, and starts decelerating and the turbulent boundary layer dissipates.

In order to consider both the turbulent and laminar impact on the heat transfer at the wall. Krischer and Kast [21] presented a correlation for heat transfer for air the at Reynolds numbers from $10^1 < Re_l < 10^6$ based on collected data. Gnielinski [22] presented equation 20 for the average Nusselt number in the ranges of $10^1 < Re < 10^7$ and $0.5 < Pr < 2000$ where the physical properties are evaluated at the mean temperature $T_m = (T_{in} + T_{out})/2$.

$$Nu_{l,0} = \sqrt{Nu_{l,lam}^2 + Nu_{l,turb}^2} \tag{20}$$

where $Nu_{l,0} = \dfrac{hl}{k}$ and $Nu_{l,lam}$ & $Nu_{l,turb}$ are refering to the equations below.

$$Nu_{l,lam} = 0.664\sqrt{Re_l}\sqrt[3]{Pr} \tag{21}$$

$$Nu_{l,turb} = \frac{0.037 Re_l^{0.8} Pr}{1 + 2.443 Re_l^{-0.1}(Pr^{2/3} - 1)} \tag{22}$$

The Nusselt number equations, correlations, and references are gathered from VDI Heat Atlas[23]

4.3 Transient model & U-value

In order to initially calculate the convection coefficient of the forced flow boiling occurring with the CO_2, the heat flux at the wall $q_s''[W/m^2K]$ is required, which is not available due to the lack of experimental data. Consequently, an initial heat flux is guessed, and an equilibrium equation is set up to ensure the convection coefficient and heat flux are proportional and the heat flow is equal. One of the reasons for the heat flux and convection coefficient coupling is increased boiling, causing higher volumetric flow and turbulence in the pipe, increasing the disorder and heat transfer from the fluid. In one-phase flows, this effect is not present, and the initial mass flux needs to be higher for equivalent convection coefficients.

The algorithm used to determine the convection coefficient for the boiling CO_2 is illustrated in figure 4.3. The algorithm runs for n iterations until the overall heat transfer coefficient converges.

The overall heat transfer coefficient will be affected by the growing ice layer which forms on the inner surface of the cylinder. The iterative algorithm is important to be able to determine the growth speed, the change of U-value, and further analyze the impact of altering the speed of the scrape and flow regime of the refrigerant. Evaluating the U-value as a function of time will also

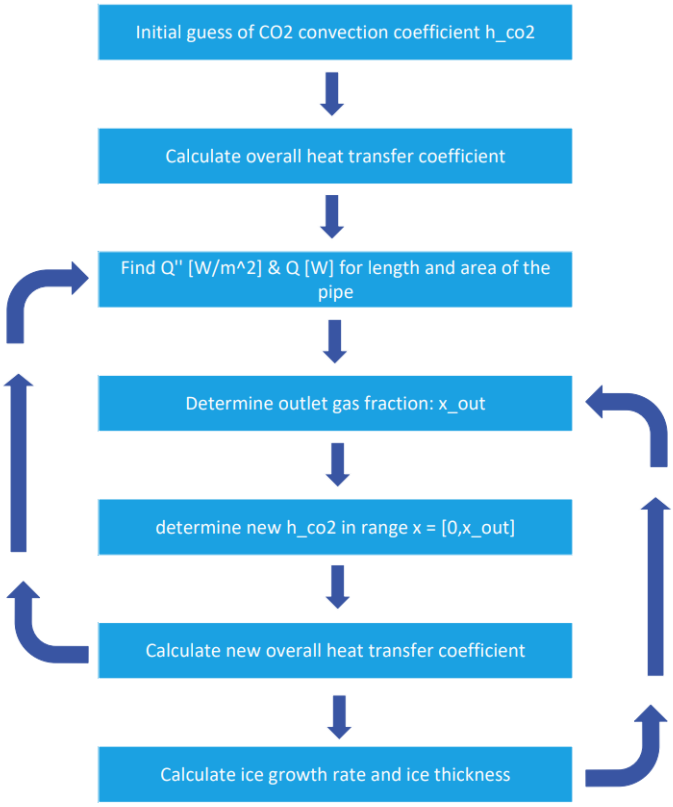

Figure 4.3: Algorithm CO_2 convection coefficient

make it possible to find the heat transfer as a function of the tube length of the refrigerant and an average overall U-value.

An iteration through time will be necessary in order to make the equations above transient. The main value that change as a function of time is the ice growth rate which is coupled with the heat transfer coefficient. Due to the relatively low conduction coefficient of the ice being $k_{ice} = 2.2[W/mK]$, there will be a reduction in the heat transfer as the ice layer grows. Due to the continuous motion of the scrape, the change of the U-value will be cyclic and reset due to the ice layer being removed every time the scrape cycles the cylinder.

There phase change on both sides of the wall will cause the temperature difference to change little over the geometry of the heat transfer. The increasing ice formation will however cause some freezing point depression to happen. The initial freezing point for the hydrolysate mixture of 6.8% concentration is found to be -0.61°C while the freezing point at 30% concentration is approximately -4°C [7] as seen in figure 2.6. The change is small and for simplicity, the water freezing at the wall is assumed to have the properties and temperature of 0°C.

4.4 Contact Freezing Vessel

The contact freezing vessel or just vessel has the geometry of a cylinder. The size of the vessel varies with the radius and the height chosen. The cross-sectional area, volume, and surface area of the vessel is derived from the following equations:

$$A_{cyl} = \pi \times r_{cyl}^2 \tag{23}$$

$$V_{cyl} = A_{cyl} \times h_{cyl} = \pi \times r_{cyl}^2 \times h_{cyl} \tag{24}$$

$$A_{surf} = 2\pi \times r \times h_{cyl} \tag{25}$$

Increasing the diameter of the vessel increases the volume by an exponential amount compared to the surface area. Increasing the height and reducing the diameter increases the surface-to-volume ratio and can be done in cases of low heat transfer. In the cases of high heat transfer, the diameter can be increased to minimize the number of vessels necessary per unit of hydrolysate.

The vessel simulated is constructed of aluminum with the thermal conductivity determined by the average temperature through the construction. Since the majority of force from the water is directed downwards and a minor load will be imposed on the walls horizontally, a thickness of 2.5mm is assumed to be sufficient for the structural integrity of the vessel.

$$Q = UA_{surf}\Delta T \tag{26}$$

Due to the geometry, the heat transfer from the hydrolysate is calculated by using equation 26. The required heat transfer rate Q is determined by the bulk going through the process. The U-value is calculated for a number of given parameters, amongst them vessel diameter and saturation temperature. The required surface area can then be calculated by varying the saturation temperature and using the calculated U-value. For the initial assumption for processing of a batch of 1000 kg RRM and 1000 kg water mixture, the required cooling load $Q = 143kW$ and volume is constant.

$$A_{suface,req} = \frac{Q}{U\Delta T} \tag{27}$$

$$\frac{V_{vessel}}{A_{surface}} = \frac{h \times \pi r^2}{h \times 2\pi r} = \frac{r}{2} \tag{28}$$

By using equation 27 it is possible to calculate the required surface area using the U-value and temperature difference. As seen by equation 28, the ratio between the volume and surface area depends solely on the diameter of the vessel. By using the required surface area and volume of the bulk, the maximum diameter can be calculated for the given processing rate.

4.5 Compressor

The suggested design includes two compressors; one sub-critical, low-pressure compressor compressing the vapor to the intermediate stage. The second high-pressure (HP), trans-critical compressor discharges the gas in the super-critical region.

Compressor efficiency

When regarding the energy consumption of the compressor, an isentropic efficiency $\eta_{is} = 0.70$ will be assumed. The isentropic efficiency is expressed by the following equation.

$$\eta_{is} = \frac{\dot{W}_{ideal}}{\dot{W}_{real}} \tag{29}$$

$$W_{comp} = \frac{\dot{W}_{ideal}}{\eta is} = \frac{\dot{m}_{ref} \times (h_{2s} - h_1)}{\eta_{is}} = \dot{m}_{ref} \times (h_2 - h_1) \tag{30}$$

Where $W_{ideal}[kW]$ is the ideal isentropic compressor work, $W_{real}[kW]$ is the real compressor work and $h_{2s}[kJ/kgK]$ is the specific enthalpy at the outlet of the compressr of an isentropic compression,$h_2[kJ/kgK]$ is the specific enthalpy at the compressor outlet of a real compression, $h_1[kJ/kgK]$ is the specific enthalpy at the compressor inlet, and $\dot{m}_{ref}$ $[kg/s]$ is the mass flow of refrigerant.

Volumetric flow rate $\dot{V}_{suction}$ is the volume of fluid moved per time unit ahead of the compressor and can be expressed from the following equation.

$$\dot{V}_{suction} = \dot{m}_{suction} \times v \times 3600 = \frac{\dot{m}_{ref}}{\rho} \times 3600[m^3/h] \tag{31}$$

Where v $[m^3/kg]$ is the specific volume and ρ is the density. The maximum volumetric suction and discharge flow rate is given by the compressor manufacturer. The density of the refrigerant is determined using the CoolProp and EES libraries based on the temperature and pressure of the gas. The density of the refrigerant gas is highly affected by pressure and temperature. Higher temperatures and pressures decrease the density, increasing the volumetric flow and lowering the capacity of the compressor.

Sub-critical Compressor

The initial saturation temperature set in the evaporator and low-pressure vessel is -40°C and the initial saturation temperature in the intermediate vessel is set to 10°C.

The commercial compressors in the ranges are scarce and are predominantly screw compressors with considerably larger capacities than the required flow for the presumed bulk size.

Using the RTSelect software [24] developed by GEA compressors in order to determine CO_2 compatible compressors available in the suggested refrigeration capacity. The software presented compressors in the GEA Grasso 5HP series. The models range from a swept volume of 101 $[m^3/h]$ and a cooling capacity of 130 $[kW]$ with the 35HP model to 202 $[m^3/h]$ and 260 $[kW]$ with the 65HP. The compressors stated has a field of operations shown in figure 4.4. According to GEA.com the compressors has a high stage design pressure of 50 bar and a maximum pressure difference of 30 bars between the low and high-pressure stage.

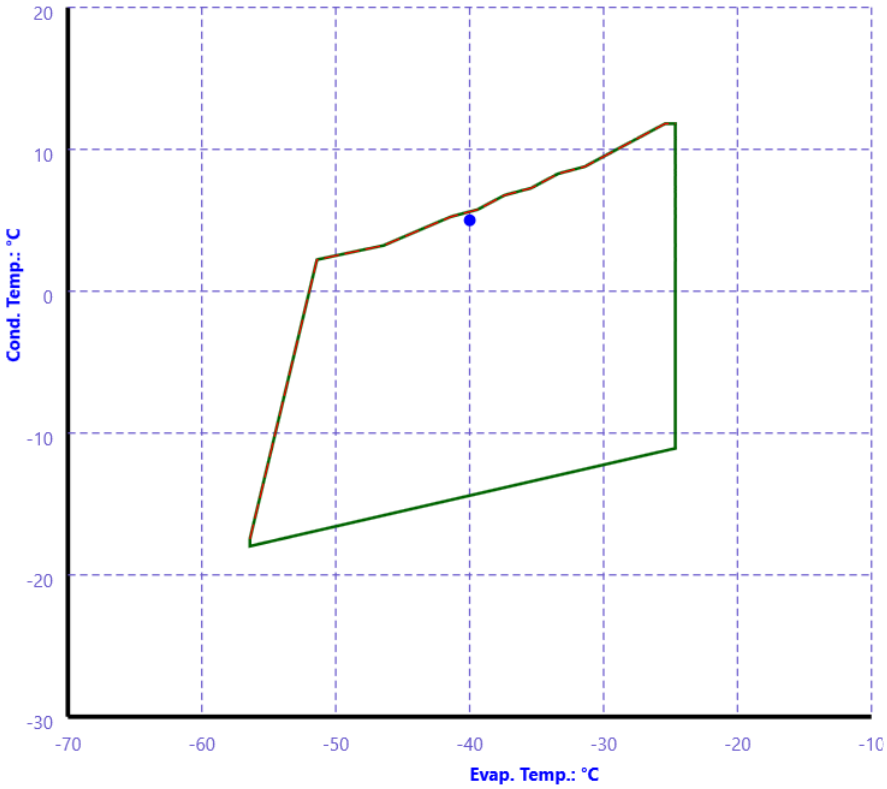

Figure 4.4: Field of operation for GEA Grasse 35HP using R744[24]

The operational range is a challenge for the initial pressure-level set. As figure 4.4 depicts the saturation temperature of 10°C of the intermediate pressure vessel is outside the range of the low-pressure compressor considering the initial evaporation temperature of -40°C. The limited range requires a change in evaporation pressure for CASE 1 due to the condensation happening at the intermediate pressure, while either pressure level can be adjusted for CASE 2 in order to operate.

Trans-critical Compressor

The second, high-pressure compressor is maintaining the pressure in the intermediate pressure receiver and raises the pressure of the vapor to the supercritical region.

Although the pressure difference is large, the pressure ratio of the high-pressure compressor is relatively low. There are numerous compressors available in the pressure range and the volumetric displacement considered in the commercial market.

Examples of this are found at several compressor suppliers, such as the ecoline+ at BITZER [25] which can operate with pressure levels of up to 160 bar on the high-pressure side.[25]

5 Results

This section will encompass the result of the calculations and simulations performed with python and EES. The heat transfer coefficient results are mainly focused on the effect of the geometry and factors impacting the U-value in order to identify restricting circumstances and a roughly estimated heat transfer rate to be expected. The EES calculations aim to map the energy efficiency of the refrigeration system by altering the parameters in the process.

5.1 Evaporator & Heat transfer Coefficient

The overall heat transfer coefficient is calculated using the CO_2 convection coefficient h_{CO_2}, the average 1-dimensional conduction through the pipe, thermal gel, and aluminum wall, and convection coefficient in the vessel h_{hyd}.

The results are conducted setting a saturation temperature of $T_{sat} = -40°C$ and bulk temperature $T_{bulk} = 0.0°C$. The assumption of the bulk having properties similar to water is the reason for the temperature being set at 0°C. The saturation temperature is changed when investigating the saturation temperature is investigated.

The size of the vessel investigated is of height, $h_{cyl} = 2.4m$ & $D_cyl = 0.7m$ and the volume of the vessel equals $V_{cyl} \approx 0.9m^3$. The dimensions are initially chosen to fit half the bulk of $V_{bulk} \approx 1.8m^3$ one batch filtrated hydrolysate. The exception of the dimension is for the investigations of varying diameter and coiled vs vertical pipe configurations, where the diameter is varied. The length of the pipe in the vertical configuration is set to $L_{pipe} = H_{cyl} = 2.4m$, while the length of the pipe in coiled configuration is set to $L_{pipe} = 5.6m$. All results has a scraping cycle rate of 15 RPM.

5.1.1 Coiled pipes vs Vertical pipes

Determining the difference between the coiled and vertical pipe configuration is important to understand how varying other factors will impact the geometry. The vertical pipe configuration has the pipe length tied to the height of the vessel, and the pipe length of the coiled configuration is affected by the diameter of the cylindrical freezing vessel. The diameter of the vessel affects the thickness of the thermal gel layer between the pipes and cylinder for the vertical configuration, but not the coiled pipe configuration. Investigating the conductive resistance for the two configurations has therefore been presented for a range of diameters.

Additionally, the initial requirement for the convection coefficient for the CO_2 evaporation to be valid is $Fr > 0.04$, which is true for all cases tested.

Table 5.1 shows the inverse of the average thermal conductive resistance $\frac{1}{R_{cond}}$ for the coiled and vertical pipes. It is clear that varying the diameter has a negligible impact ($< 1\%$) on the average conduction resistance through the wall. Therefore, it is reasonable to assume that the variation in average conductive resistance between the coiled and vertical configuration can be disregarded. The following results will therefore be indicative of both the coiled and vertical pipe configuration.

Diameter $[m]$	$1/R_{cond}$ $[W/m^2K]$
Coiled	**7150**
0.35	7130
0.70	7140
1.05	7145
1.40	7145
1.75	7145

Table 5.1: Conductive resistance with varying diameters

5.1.2 Varying mass flux

The results of the calculations and simulations of the heat transfer coefficient with varying mass flux, $G[kg/m^2s]$ through the pipes. The outlet gas quality and average h_{CO_2} are determined by running the algorithm explained in chapter 4 and using the average heat flux over the surface area of the pipe each iteration, and finally finding the values as the values converge.

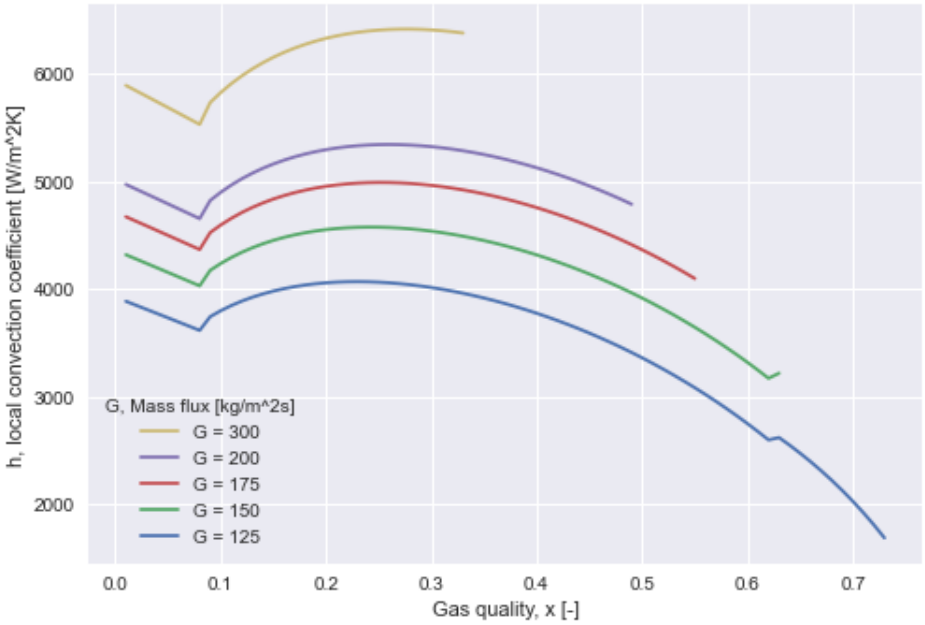

Figure 5.1: Initial CO_2 convection coefficient with increasing gas quality, coiled configuration

Figure 5.1 illustrates the initial convection coefficient as a function of the increasing gas quality [kg/kg] of the CO_2 in the pipes and different mass fluxes.

The heat transfer coefficient increases with increasing mass flux as anticipated. The only variable being changed is the mass flux, which increases proportionally with the volumetric and mass flows through the pipe. The Reynolds number increases at higher flows and causes lower thermal resistance and higher heat transfer for the evaporating CO_2. The convection coefficient h_{CO_2} increases for boiling at higher Reynolds numbers and higher heat flux $Q''[W/m^2]$.

For all the values of G plotted, the convection coefficient starts off decreasing at the initial gas fractions prior to $x = 0.1$, before increasing and reaching the highest value near a gas quality of 0.25, then reducing with increasing quality. The correlation is only valid for heat transfer up to

0.8 The sudden increase of is likely a combination of the correlation being somewhat imprecise at the gas quality in combination of the low saturation temperature of -40°C. At higher saturation temperatures of [-20, 0]°C the "bump" at around 0.1-0.3 is still present, although less pronounced, and does not exceed the initial h_{CO_2} values at ≈ 0.0.

G $[kg/m^2 2s]$	h_{avg} $[W/m^2K]$	x_{out} $[kg/kg]$	$\dot{m}$ $[kg/s]$
125	3450	0.74	0.0075
150	4170	0.65	0.009
175	4709	0.57	0.01
200	5100	0.51	0.012
300	6120	0.35	0.018

Table 5.2: Average values for CO_2 convection

Table 5.2 shows the average convection coefficients as well as the outlet gas quality and mass flow through the pipes. Raising the mass flux from 150 to 300 $[kg/m^2s]$ increases the average convection coefficient by approximately 47% and reduces the outlet gas quality by approximately 0.3 $[kg/kg]$. The gas quality at the exit is however highly dependent on the mass flux through the pipes, and thus the length of the pipes. For the coiled configuration, the pipe length is set to 5.6 meters, the consequences will be further discussed in Chapter 6: Discussion.

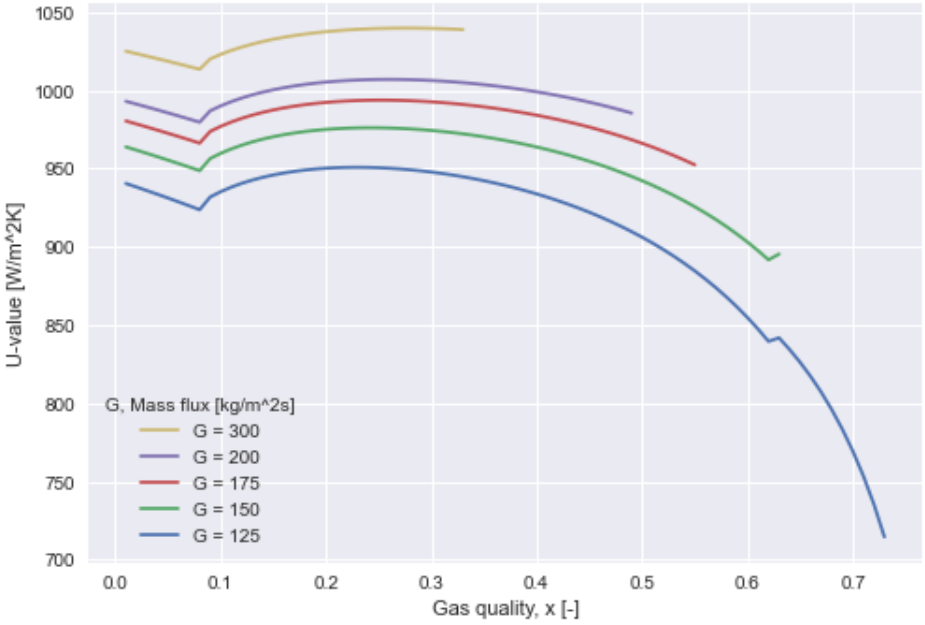

Figure 5.2: Initial overall heat transfer coefficient with increasing gas quality, coiled configuration

Figure 5.2 illustrated the initial overall heat transfer rate, U-value with increasing gas quality of CO_2 and mass flux. Since the convection coefficient of CO_2 is the only thermal resistance varying with the gas quality, the graphs have similar shapes.

From figure 5.2 it is clear that the increase in h_{CO_2} leads to an increase in U-value, but the increase is smaller in magnitude and decreases with higher mass flux. Since the increase in mass flux leads to higher pressure loss in the system, there will eventually be diminishing returns at higher mass fluxes.

G [kg/m2s]	h_avg [W/mˆ2K]	Increase	U-value [W/mˆ2K]	Increase
125	3450		905	
150	4170	21%	955	5.5%
175	4709	13%	980	2.6%
200	5100	8%	1000	2.0%
300	6120	20%	1030	3.0%

Table 5.3: Initial convection coefficient and U-value with increasing G

Table 5.3 shows the average h_{CO_2} and U-values, as well as the increase with each G value. It makes it clear that the increase in convection coefficient has a smaller impact on the U-value. Comparing a mass flux of 125 and 300 shows an increase of 77% for convection coefficient only increases the corresponding U-value of approximately 14%. These findings imply that the convection coefficient is not the limiting factor in heat transfer.

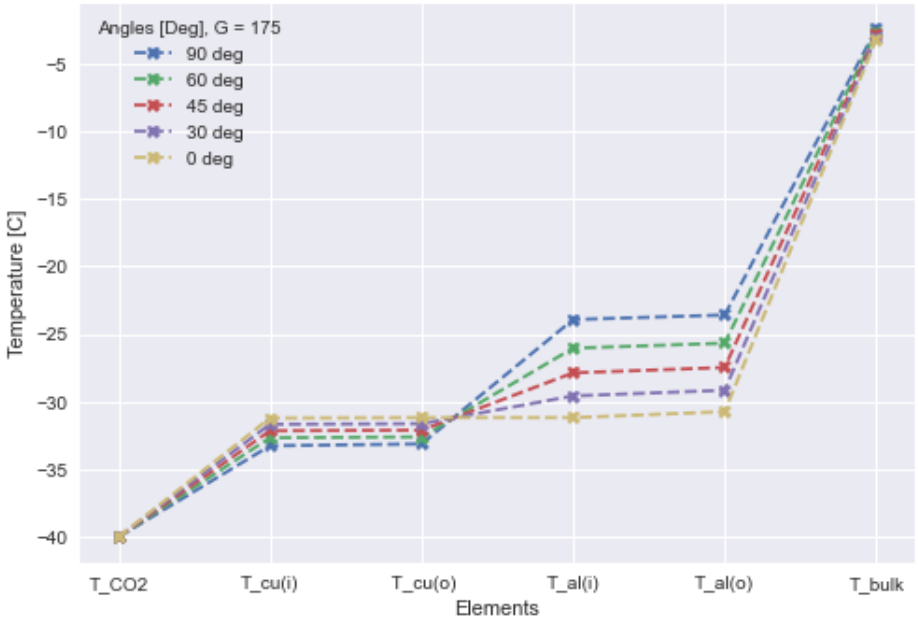

Figure 5.3: The temperature through thermal resistance elements at different heights, coiled configuration

Name	Placement description
T_CO_2	Temperature of CO_2
T_cu(i)	Inside copper pipe, surface temperature
T_cu(o)	Crossection between copper and gel/aluminum
T_al(i)	Crossection between copper/gel and aluminum
T_al(o)	Surface temperature for the
T_bulk	Temperature of the hydrolysate

Table 5.4: Elements corresponding to figure 5.3 and placement decriptions

In figure 5.3 the temperature distribution through the elements through the wall is illustrated. The heat flow is assumed to be 1-dimensional and moving horizontally through the wall. The pipe is discretized, where 90 degrees corresponds to the top of the pipe angled vertically, while 0 degrees is horizontally in the center-line of the pipe as the figure 4.1 is illustrated. The range [0,90] is chosen due to the symmetric geometry below and over the center-line. As illustrated in the schematic of the pipe in figure 4.1 and figure 4.2. The distance between the copper pipe and aluminum increases with higher angles reaching a maximum at 90 degrees. The space is filled with thermal gel.

The temperature distribution is a measure of the magnitude of thermal resistance through the different elements of the wall. From the figure it is clear that the significant resistances are the convection coefficient of the CO_2 at smaller angles, thermal gel and convection coefficient inside the cylinder. Optimizing the convection coefficient in the cylinder will lead to a higher CO_2 convection coefficient due to the increased Q'', providing significant on the overall heat transfer through the wall.

The thermal resistances are smallest at the center-line of the pipe and increase with higher angles due to the increasing distance from the bulk hydrolysate to the refrigerant. The Q'' will therefore decrease with increasing angles as well since the bulk and refrigerant have constant temperatures. The crossing occurring between $T_{cu(o)}$ and $T_{al(i)}$ visualizes the increased thermal resistance of the thermal gel, and the reduction of heat transfer it leads to since $Q'' = U \times (T_{bulk} - T_{CO_2}) = h_{cyl} \times (T_{bulk} - T_{al_o})$.

In practice, there will be vertical heat transfer due to the temperature gradients in the wall. The temperature distribution will also look different as the transient nature of the freezing adds more thermal resistance, and the cyclic scraping induces higher heat transfer due to the increase in Reynolds number earlier in the cycle.

Figure 5.4 plots the growth of the ice layer through a cycle with a scraping speed of 15 rpm for the values of G ranging from [125,300]. The convection coefficient in the cylinder at this scrape rate is equal to $h_{hyd} \approx 1500$, and the average ice production per round is approximately 2,9 mm per 4 seconds.

The figure makes it clear that the impact of mass flux is minuscule as a factor in increasing the ice growth per cycle. The overall maximum difference at the end of the cycle is in the range of $< 10\%$. As time increases the ice growth rate decreases, leading to more ice being generated early in the cycle.

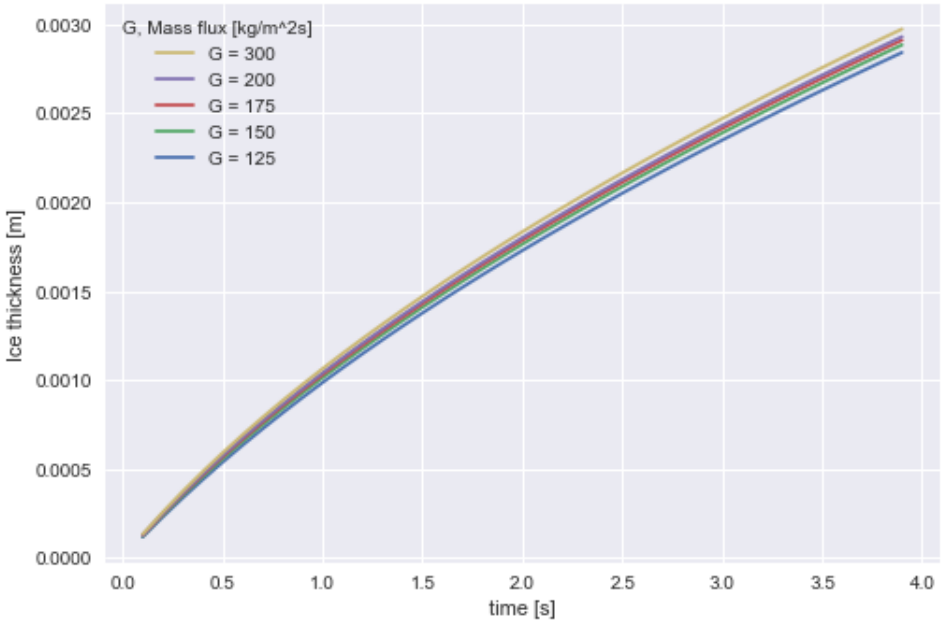

Figure 5.4: Ice thickness as a function of time, coiled configuration

G $[kg/m^2s]$	U_{0s} $[W/m^2K]$	U_{4s} $[W/m^2K]$	U_{avg} $[W/m^2K]$
125	915	407	**530**
150	955	409	**537**
175	980	410	**541**
200	995	412	**545**
300	1030	415	**552**

Table 5.5: U-values ice formation

Figure 5.5 shows the dramatic drop in U-value as the ice layer grows, and by the end of the cycle, the average U-value is more than halved at the scraping speed of 15 rpm at all values of G. As table 5.5 depicts, the impact of the mass flux has a notable impact initially, but the difference decreases with increasing time and ice layer formation. The average values are all in the range of 530 - 552 $[W/m^2K]$ and it is clear that the mass flux of CO_2 has little impact on the overall heat transfer coefficient as the ice layer forms.

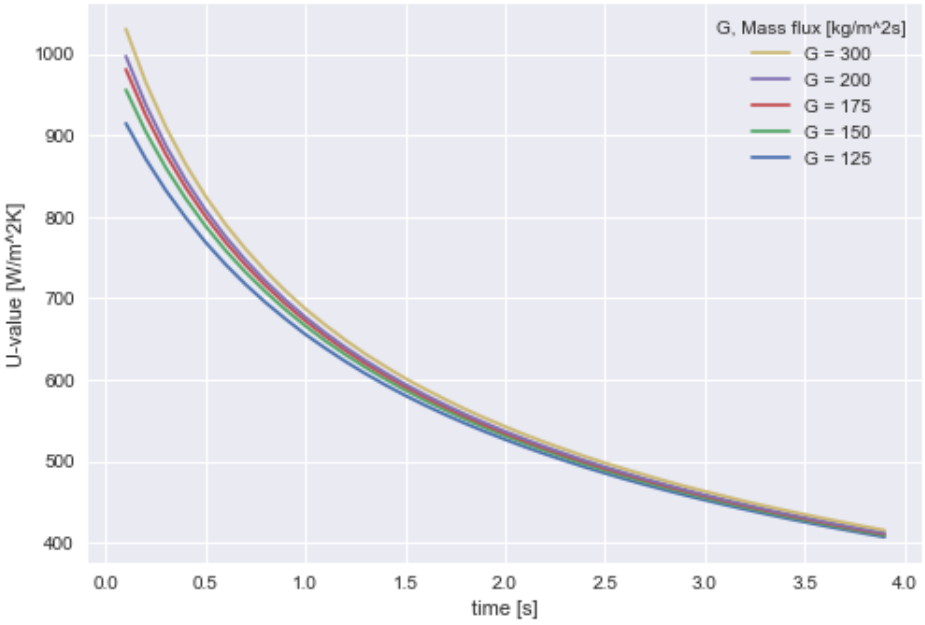

Figure 5.5: Average U-value of ice-formation, coiled configuration

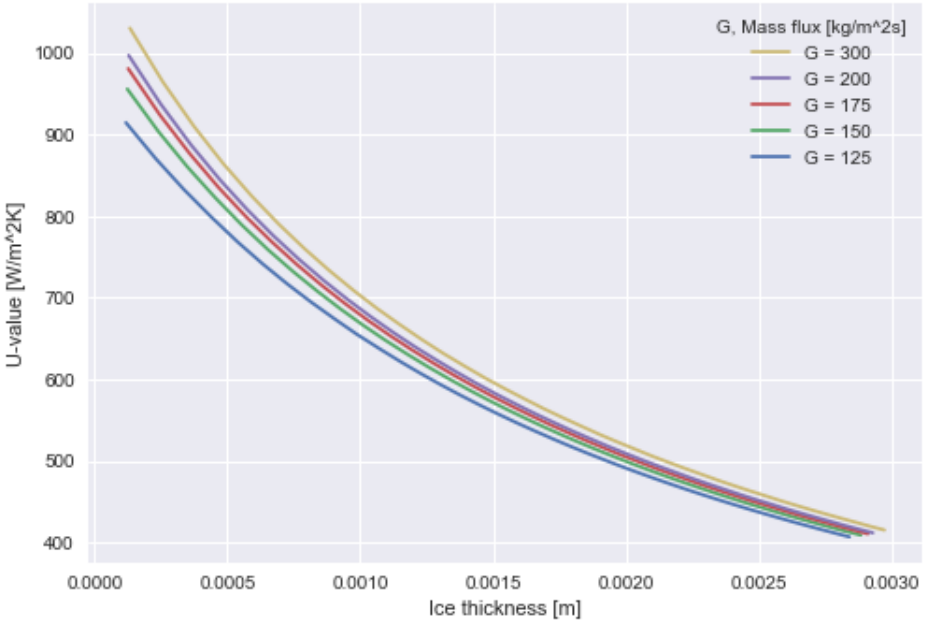

Figure 5.6: U-value vs Ice thickness, coiled configuration

Figure 5.6 is relates figure 5.4 & 5.5 and shows the connection of U-value and the ice thickness for the given parameters. The slight increase in ice formation for the higher mass fluxes is visible, while the trending U-value reduction is clear. At 1.5mm of ice forming, a reduction of 30-40% in overall heat transfer is observed for the values of G. The slope is decreasing as the ice thickness builds and the growth rate slows as the heat transfer reduces.

It is clear that the conductive thermal resistance through the wall becomes the dominating factor as the ice layer continues to grow. A challenge with increasing the time interval of the scraping cycle is the impact on the convection coefficient of the hydrolysate in the vessel. The thermal

resistance increases by slowing the scrape, leading to lower heat transfer to the evaporating CO_2 and slower overall ice formation. Thus leading to the paradox of slower ice forming for longer intervals dramatically increasing the time necessary for thicker ice layers. Although the force required to operate the scrape lowers, the economic ramifications for higher heat transfer area per volume need to be considered. Alternatively, other elements for keeping a high convection coefficient should be considered in the case of requiring wider ice layers.

5.1.3 Uniform Thermal Gel Layer

Imperfect execution of building the vessel can lead to unwanted gaps between the copper pipe and aluminum wall. The absence of contact between the elements leads to increased thermal resistance where applicable. Figure 5.7 shows the impact a uniform layer of growing thermal gel has on the initial heat transfer coefficient.

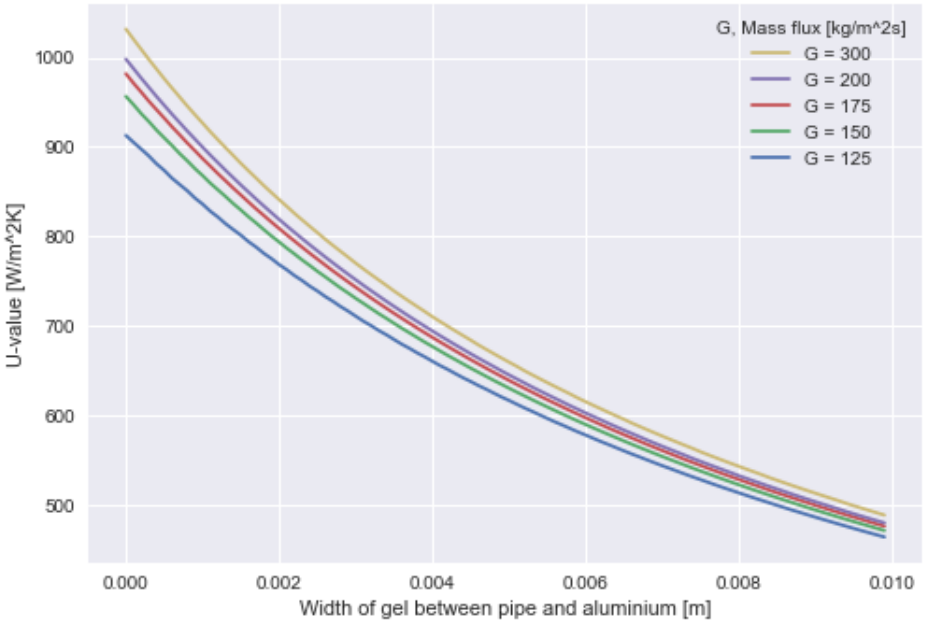

Figure 5.7: Overall heat transfer coefficient with excess gel width, coiled configuration

Due to the relatively low conduction of the gel $k_{gel} = 10[W/m^2K]$, the impact of the initial u-value is considerable. The results are similar when compared to the growing ice layer, but have less impact due to the higher conductive coefficient k_{gel} of the thermal gel. As with the ice, the mass flux through the pipes has a minuscule impact compared to the thickness of the layer, particularly as the layer increases.

The plot is in the range of 0 - 10mm in figure 5.7. The case of 10 mm is unlikely, but an impact of a small layer of approximately 2mm is impactful with a reduction of $10-20\%$ of the initial U-value for all mass fluxes.

5.1.4 Varied Diameter Impact

The thermal resistance of the conduction varies with values of the vessel diameter at constant scraping intervals.

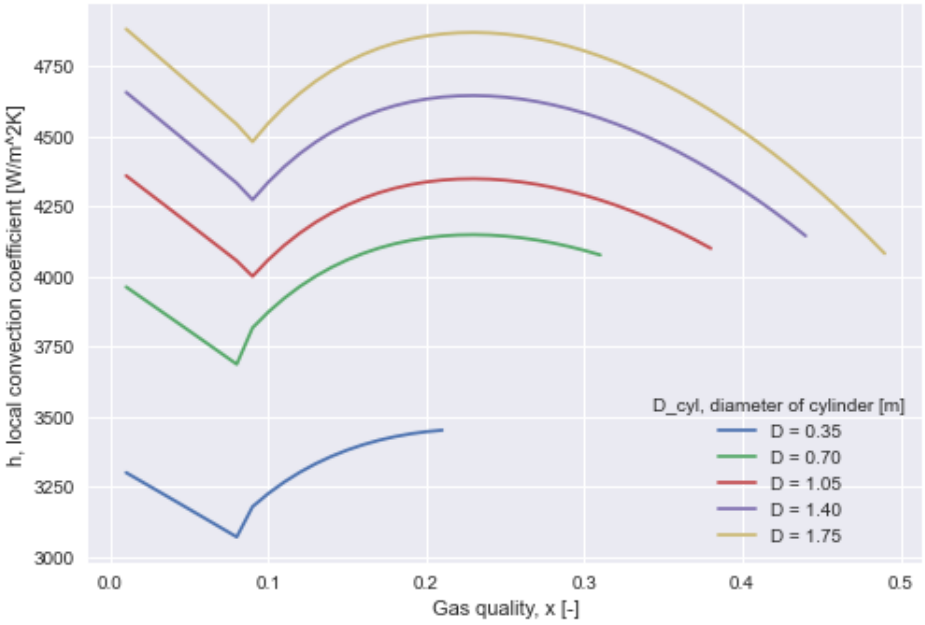

Figure 5.8: Impact of D_{cyl} on CO_2 convection coefficient with constant RPM = 15, $G = 125[kg/m^2s]$, vertical configuration

Figure 5.8 shows the initial convection coefficient as a function of gas quality plotted for diameters in the range [0.35, 1.75]. Increasing the diameter has a notable impact on the initial CO_2 convection coefficient. The height of the cylinder wall is the same as the coiled configuration, and equal to $h_{cyl} = 2.4m$. The mass flux through the pipe has an impact on the convection coefficient as seen in the coiled configuration, although the largest impact is on the outlet gas quality x_{out}.

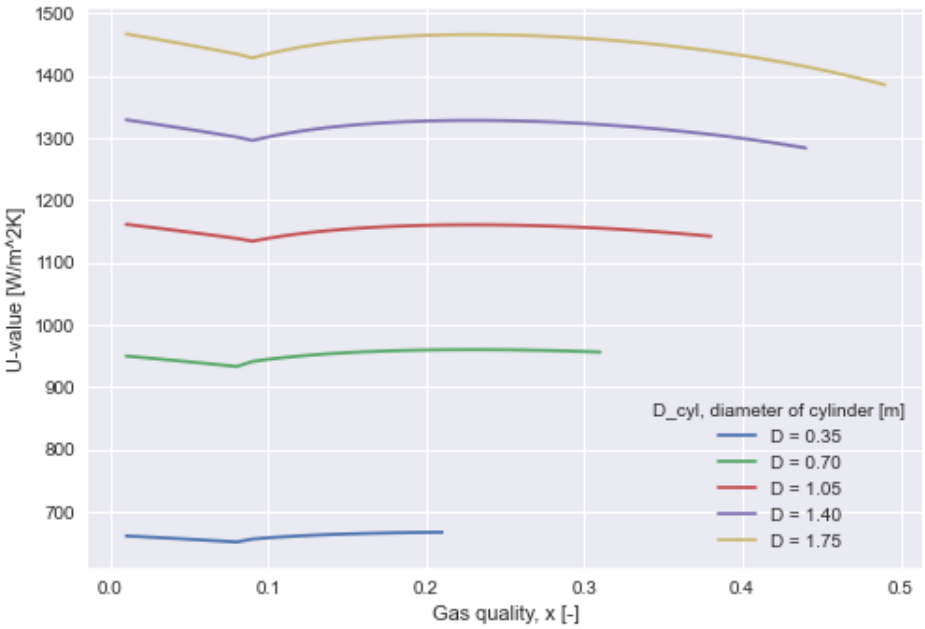

Figure 5.9: Impact of D_{cyl} on U-value, $G = 125[kg/m^2s]$, coiled configuration

The initial impact on the overall heat transfer coefficient significant is seen in figure 5.9, and table 5.6. Compared to h_{CO_2}, the diameter affects the U-value to a greater extent. It is clear from table

Diameter $[m]$	h_{CO_2} $[W/m^2K]$	$1/R_{cond}$ $[W/m^2K]$	h_{hyd} $[W/m^2K]$	x_{out} $[kg/kg]$	U_{avg} $[W/m^2K]$
0.35	3290	7130	930	0.21	**660**
0.70	4010	7140	1500	0.31	**950**
1.05	4240	7145	2010	0.38	**1150**
1.40	4490	7145	2480	0.44	**1315**
1.75	4660	7145	2920	0.49	**1445**

Table 5.6: Initial thermal resistances, outlet gas quality, and average U-value as a function of diameter

5.6 that the convection coefficient inside the cylinder remains the limiting factor as the diameter decreases. h_{hyd} increases with the diameter as the scraping cycle of 15RPM remains constant, leading to a higher scrape speed and inducing a higher Reynolds number. As both the graphs and tables depict, the diameter of the vessel is highly impactful on the initial heat transfer coefficient for the vertical geometry and the coiled configuration. Another observation that can be made is that h_{CO_2} increases considerably without changing the mass flux G. The increase is due to the higher boiling number as the heat flux Q'' grows.

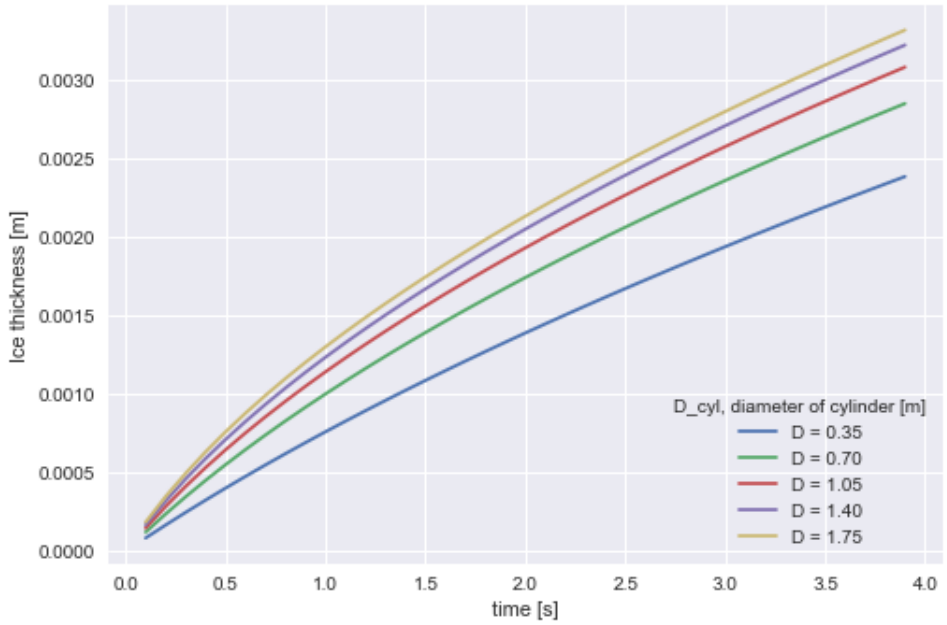

Figure 5.10: Ice growth with varying diameters, $G = 125[kg/m^2s]$, vertical configuration

Figure 5.10 & 5.11 shows respectively the growing thickness of the ice layer and the U-value for a cycle of scraping. As the ice builds, the conductive resistance will increase further. The initial U-value is important since the ice growth rate is largest at the beginning of the cycle.

Table 5.7 contains the average U-value for a scraping cycle. The table makes it clear that the impact of increased scrape speed which comes with higher diameters raises the average U-value of the cycle. The difference is particularly notable for the lower diameters. The U-value increases by approximately 30% from a diameter of 0.35 to 1.05 meters and a 20% increase from 0.35 to 0.70 meters. Since the circumference is proportional to the diameter, an increase in diameter is also proportional to the Reynolds number. The reduction of U_{avg} is due to the conductive resistance increasing further in the cycle as the ice builds on the wall, making the conductive resistance the

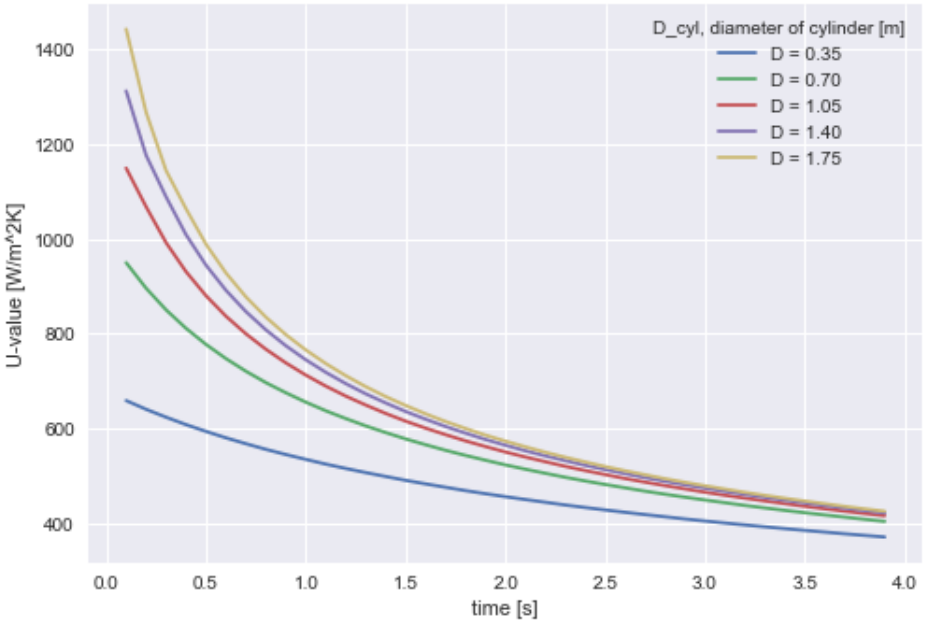

Figure 5.11: U-value as ice grows with different diameters, $G = 125[kg/m^2s]$, vertical configuration

D_{cyl} $[m]$	U_{avg} $[W/m^2K]$	Ice thickness $[mm]$
0.35	**475**	**2.38**
0.70	**570**	**2.85**
1.05	**615**	**3.01**
1.40	**640**	**3.22**
1.75	**660**	**3.32**

Table 5.7: Average U-value for a scraping cycle and ice layer thickness for $G = 125[kg/m^2s]$

"bottleneck" of the heat transfer.

As figure 5.11 shows, higher initial U-values induce faster ice layer growth, which in turn reduces the U-value. From 3.0s to 4.0s the difference in U-value is minor since the ice layer is becoming large. In order to maintain a high U-value, rapid and continuous removal of the ice layer is paramount.

5.1.5 Saturation temperatures

Varying the saturation temperature of the refrigerant will directly affect the temperature gradient driving the heat transfer, which affects the boiling coefficient and ice propagation on the cylinder wall. The properties of the refrigerant also change with temperature, specifically gas density decreases with higher pressures which are intertwined with the saturation temperature.

Figure 5.12 shows the U-values plotted for a scraping cycle at different saturation temperatures. As the figure shows, the initial U-value is only slightly impacted. Through the cycle, it is clear that the lower temperatures have a larger drop in U-value. At the end of the cycle, the heat transfer coefficient is noticeably higher for the higher temperatures.

The ice thickness for the scraping cycle at different saturation temperatures is shown in figure 5.13. The figure shows the lower saturation temperatures has considerably higher ice propagation. Table

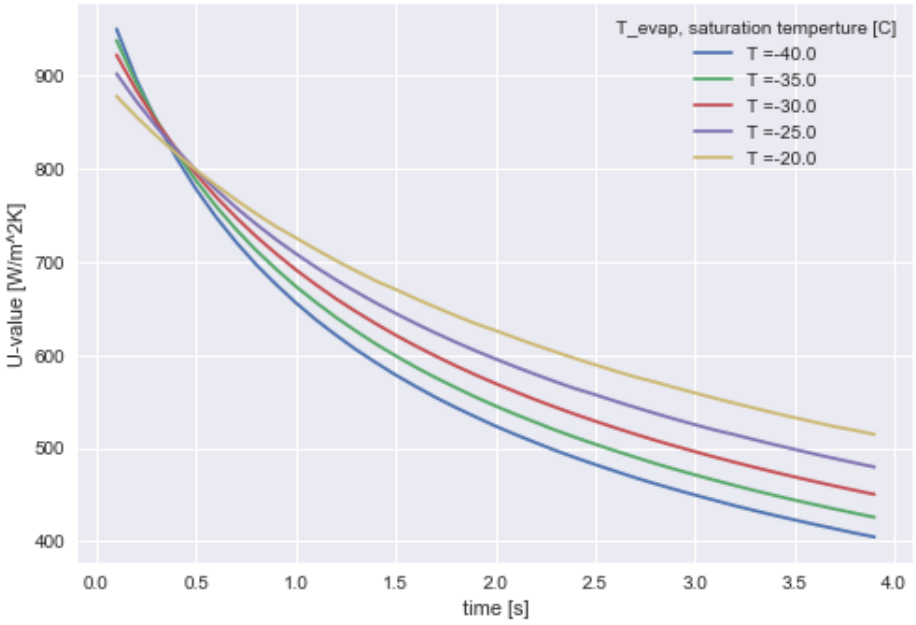

Figure 5.12: U-value through cycle of scraping at different saturation temperatures, $G = 125[kg/m^2s]$, $L_{pipe} = 2.4[m]$, vertical configuration

5.8 further relates figure 5.12 & 5.13. The average U-value is higher for the higher temperatures, which is the case because of the smaller temperature difference and further Q''_{avg}. Since the heat transfer is lower, the ice propagation is smaller and less impactful on the overall U-value. Lowering the evaporation temperature from -20°C to -40°C increases the ice growth per cycle by 78%.

Evaporation temperature $°C$	U_{avg} $[W/m^2K]$	Ice thickness $[mm]$	Q''_{avg} $[kW/m^2]$
-40	**565**	**2.85**	**23.1**
-35	**585**	**2.56**	**20.9**
-30	**605**	**2.26**	**18.5**
-25	**625**	**1.94**	**16.0**
-20	**650**	**1.60**	**13.4**

Table 5.8: Heat transfer coefficient, heat transfer rate and ice thickness for $G = 125[kg/m^2s]$ & $L_{pipe} = 2.4[m]$

The saturation temperature will directly affect the ice removal, and freeze concentration of the bulk. As the bulk temperature decreases at lower temperatures and higher concentrations, the reduction in heat flux has a proportionally larger impact at higher saturation temperatures. The boiling rate is higher at large Q'' which also lower with increasing temperatures. The lower saturation temperatures will however impact the refrigeration system, and the consequences of investment-, operating cost, and production rate have to be assessed.

Contact freezing vessel size

In order to decide the dimensions of the vessel, the volume of the bulk is determined and the average U-values are gathered from table 5.8. As equation 28 displays, the volume to surface area

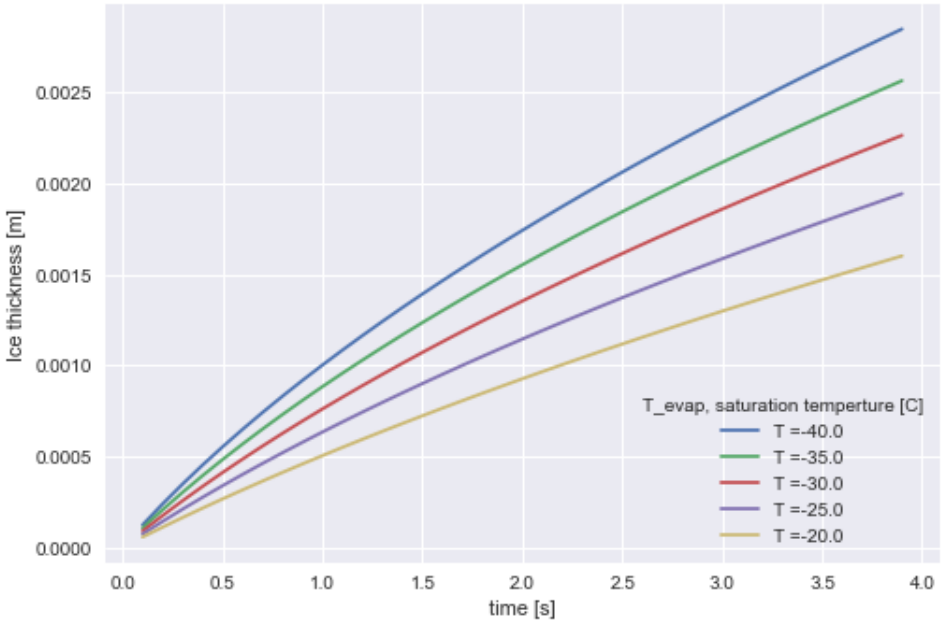

Figure 5.13: Growing ice layer between scraping at different saturation temperatures, $G = 125[kg/m^2s]$, vertical configuration

of the vessel remains constant as the height varies, but increases with higher diameter with a factor of $\frac{r}{2}$ or $\frac{d}{4}$. Low diameters imply several vessels for higher hydrolysate production, while larger diameters imply slower production.

The maximum diameter in order to satisfy the required surface area for the cooling load of $143kW$ is calculated at the given saturation temperatures.

Evaporation temperature C	U_{avg} W/m^2K	D_{max} $[m]$	height $[m]$
-40	**565**	**1.14**	**1.73**
-35	**585**	**1.04**	**2.10**
-30	**605**	**0.92**	**2.66**
-25	**625**	**0.80**	**3.56**
-20	**650**	**0.67**	**5.08**

Table 5.9: Maximum diameters and corresponding heights for U-values and saturation temperatures.

Table 5.9 shows the maximum diameter for the bulk volume of $1.783m^3$ to satisfy the cooling load. The corresponding height of the cylinder is calculated to fit the entirety of the bulk. Decreasing the diameter will increase the height and skew the surface area to volume ratio, and increase the overall cooling load. Increasing the diameter leads to a lower cooling load, or several vessels working in parallel.

The values in table 5.9 are calculated for a mass flux of $G = 125[kg/m^2s]$ and U_{avg} from table 5.8. For the smaller diameters in vertical configuration, it can be reasonable to increase the mass flux in order to avoid fully evaporating the refrigerant, thus reducing the overall heat transfer coefficient.

5.2 CO_2 refrigeration system performance

The steady state system performance for the two cases are investigated here, with focus on the optimal pressure levels for the intermediate and high-pressure stage and different evaporation temperatures considering the findings from the heat transfer calculations.

Being able to fulfill the heat demand of the process as presented in chapter 4 is important in order to evaluate the entire energy demand of the refrigeration system. The heating and cooling loads imposed on the refrigeration system are found in table 5.10. In both CO_2 systems the evaporator duty is set to $Q_E = 143.0kW$ and decides the mass flow compressor of the low side compressor.

Utility	Thermal Load
(4) Sterilization 50 - 90 C	**87.2 kW**
Wash column (Ice-melting)	**39.8 kW**
Thawing of fish*	**68.7 kW***
Freeze Concentration	**-143.0 kW**

*When RRM is frozen at arrival

Table 5.10: Heating and cooling loads of the FPH process

CO_2 system CASE 1

The first case CO_2 system has the requirement of a minimum intermediate saturation temperature of 10°C, which equates to a pressure of 45 bar. The intermediate temperature is set due to the necessary temperature difference to the heat sink, being seawater at 5°C. The limitation of the compressor investigated is a maximum pressure difference of 30 bars. Therefore CASE 1 can only operate while maintaining a minimum evaporator pressure of 15 bars, the corresponding saturation temperature is -28°C.

Evaporation temperature $[°C]$	COP_R	$\dot{W}_{low}$ $[kW]$	$\dot{V}_{low}$ $[m^3/h]$	$T_{out,comp}$ $[°C]$	$\dot{Q}_{desuperheater}$ $[kW]$	$\dot{Q}_{condenser}$ $[kW]$
-28	**1.76**	45.3	61.4	64.9	54.8	28.6
-26	**1.83**	42.2	57.4	60.1	51.7	28.6
-24	**1.91**	39.1	53.7	56.4	48.7	28.6
-22	**1.98**	36.2	50.3	52.9	45.7	28.6
-20	**2.06**	33.3	47.2	49.4	42.8	28.6

Table 5.11: COP_R & Intermediate pressure performance, CASE 1

Table 5.11 shows the main performance for the low and intermediate components that change as the evaporation temperature varies. $Q_{desuperheater}$ & $Q_{condenser}$ is the heating duty of the intermediate desuperheater and partial condensing, and $T_{out,comp}$ is the gas temperature exiting the low pressure compressor. The COP_R increases by 17% by increasing the saturation temperature from -28°C to -20°C. The required volumetric flow is in the range [61.4, 47.2m^3/h], which is considerably less than the 35HP compressor mentioned earlier, making it possible for a larger cooling capacity or smaller compressors.

The COP_R is calculated using the ratio of the cooling load $\dot{Q}_c = 143kW$ and total power consumption $\dot{W}_{tot} = \dot{W}_{low} + \dot{W}_{high}$. The intermediate pressure gas is de-superheated and partially condensed, meaning the liquid part of the mass flow expands to the evaporator, and the gas is compressed to the super-critical pressure stage. The mass flow of the high-pressure side is decided by the required heat load for the heating of sterilizing the hydrolysate $\dot{Q}_{hyd} = 87.2kW$ while the excess heat load at the high-pressure side is $\dot{Q}_{55-30} = 55.8kW$. The high pressure stage is therefore not affected by the varying evaporation temperature, as the steady-state flow rate is constant at constant intermediate pressure.

P_{high} $[bar]$	$\dot{W}_{high}$ $[kW]$	$\dot{m}_{high}$ $[kg/s]$	$\dot{V}_{high}$ $[m^3/h]$	$\dot{Q}_{hyd}$ $[kW]$	$\dot{Q}_{55-30}$ $[kW]$
120	36.0	0.56	18.3	87.2	55.7

Table 5.12: High pressure performance at 120 bar

Varying the pressure of the gas cooler will however affect the mass flow of the high-pressure compressor and further COP_R of the system. At a high side pressure of 120 bar the compressor power and performance is seen in table 5.12.

In case 1, the total heating duty excluding Q_{hyd}, is minimum $Q_{rest} = 139.1kW$, which is 30.6kW higher than the heating duty of the wash column and thawing of fish $Q_{WC} + Q_{thaw} = 108.5kW$. The total thermal load imposed on the refrigeration system is covered for all the evaporation temperatures investigated.

CO_2 system CASE 2

The second CO_2 system has fewer components than CASE 1 and since there is no condensing at the intermediate stage, the evaporation, intermediate, and high side pressure can be varied. In order to fulfill the heat demand of the sterilization of the hydrolysate $Q_{hyd} = 87.2kW$ and the temperature lift of $90 - 50°C$ as well as the minimum temperature difference of 5°C, an optimum high side pressure was determined for a range of intermediate pressures.

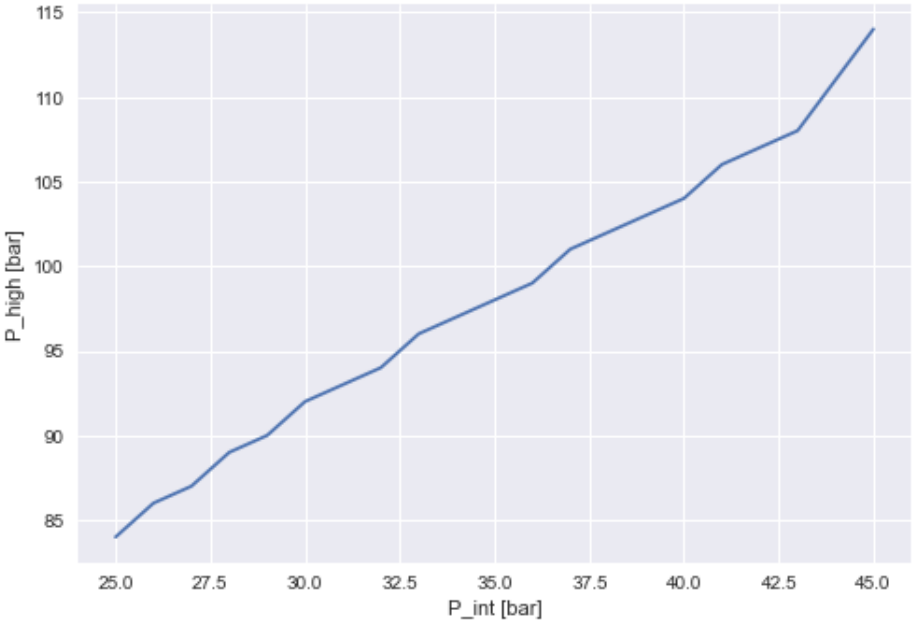

Figure 5.14: Minimum high side pressure vs intermediate pressure

The optimum high pressure is plotted in figure 5.14. The high pressure increases with higher intermediate pressures due to the required high temperature and hot duty exiting the compressor. At the lower intermediate pressures, the hot duty is the limiting factor until $P_{int} = 42bar$, where the temperature becomes the bottleneck. The pressure ratio between the high and intermediate pressures varies from approximately 3.4 to 2.5.

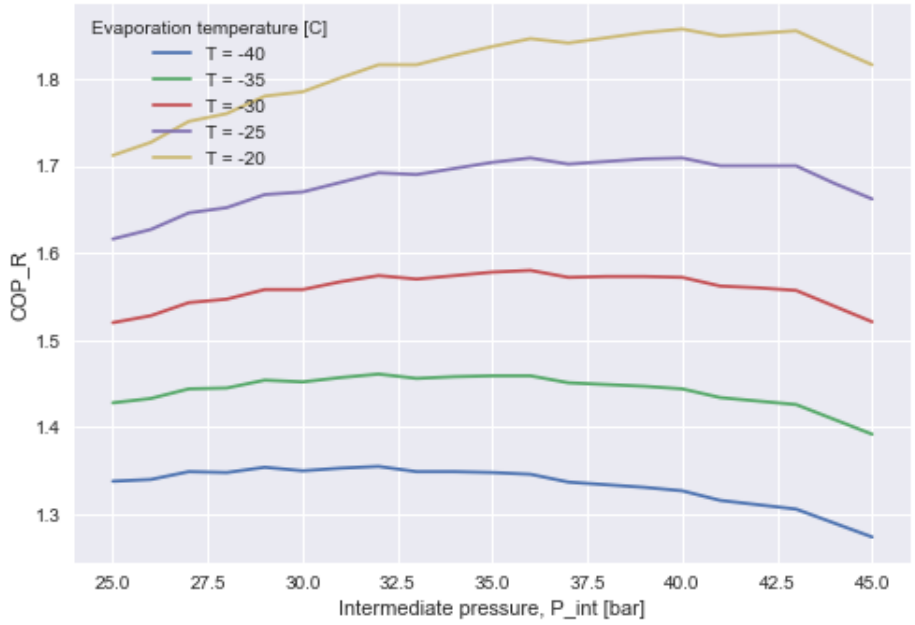

Figure 5.15: COP_R with varying P_{int} for a range of evaporation tempertaures

Figure 5.15 shows the COP_R as a function of P_{int}. It is clear that there exists an optimal intermediate pressure for the system. At all evaporation temperatures the COP decreases at intermediate pressures over 42 bars, which can be explained by the temperature becoming the limiting factor for

Evaporation temperature C	COP_R	P_{int} [Bar]	P_{high} [Bar]	$\dot{V}_{low}$ [m^3/h]	$\dot{V}_{high}$ [m^3/h]	$\dot{Q}_{desuperheater}$ [kW]	$\dot{Q}_{hyd}$ [kW]	$\dot{Q}_{55-30}$ [kW]
-40	**1.35**	32	94	81.1	40.7	32.6	87.8	131.6
-35	**1.46**	35	98	69.9	36.0	33.6	88.1	123.6
-30	**1.58**	36	99	59.3	34.6	29.3	87.3	121.4
-25	**1.71**	36	99	50.1	34.6	22.7	87.2	121.3
-20	**1.86**	38	102	43.5	32.0	21.4	88.8	115.4

Table 5.13: Performance of CASE 2 CO_2 system

the high-pressure side. This leads to compression to higher pressures to increase the temperature difference, increasing $Q_{hyd} > 87.2kW$. The COP is additionally lower at pressures below 30bars. The lower intermediate pressure results in a increased specific enthalpy difference and larger pressure ratio of the high side compressor, which in turn increases the work. Another observation that can be made is the increase of optimal intermediate pressure as the evaporation temperature increases.

The main system performance can be seen in table 5.13. The increase of 5°C increases the overall COP for the configuration between 8% & 9%. Due to the higher saturation pressure of the evaporator, the volumetric flow decreases dramatically at higher temperatures. The hot duty from the de-superheater decreases and is not high enough to solely fulfill the heat demand of the water-loop.

Since the cooling load Q_E is the same for CASE 1 & 2, the excess heat of CASE 2 is higher as the COP_R is lower. The total heating load excluding Q_{hyd} ranges from is $Q_{rest} = [136.8, 163.2kW]$ which is more than sufficient to cover the thermal loads imposed on the CO_2 system of $108.5kW$.

6 Discussion

6.1 Assumptions

The results presented are dependent and shaped by the assumptions made in chapter 4 & 3. The established bulk sum of 1000 kg water and 1000 kg of RRM produces large amounts of low concentration hydrolysate considering the RRM consists of a mass fraction of approximately 75-80% water prior to mixing. The water added is directly tied to the cooling and heating demand imposed on the system and further the energy costs per unit of produced hydrolysate at 30% concentration.

6.2 Heat Transfer Coefficient

In practice, there will be deviations due to the heat transfer coefficient being derived from existing correlations and no experimental data being obtained for the geometry of the evaporator. The correlations used are made for evaporating pipe flow and since the geometry of the evaporator only imposes heat load on half of the pipe, some deviation from the correlation is reasonable to expect.

The conduction is calculated assuming 1-dimensional heat transfer from the bulk hydrolysate inside of the cylinder, through the wall to the evaporating CO_2 flowing in the pipes. Realistically the heat transfer will not be solely 1-dimensional leading to an expected deviation from the results of the calculations.

The coiled and vertical configurations produce similar values since the main difference is the conductive resistance, which produces negligible differences for the investigated diameters. The heat transfer investigated will therefore be practically indistinguishable for the different geometries for the same pipe length and outlet gas quality. The difference in pressure loss and flow rate for the two configurations will likely have a larger impact due to the density-driven propulsion of the flow because of the density difference in the phase change.

The practical challenge of the diameter is the length of the pipes in the coiled configuration depends on the circumference of the vessel. The number of pipes will be dependent on the height of the vessel and the length of the coils. The opposite is true for the vertical configuration, as the number of pipes depend on the diameter of the contact freezing vessel, and length on the height. Shorter pipes prompt lower mass fluxes as the evaporation rate is tied with the surface area. The results show however that the impact of changing the mass flux is minor compared to the scraping speed and frequency.

The overall heat transfer of the vessel, heat transfer area, and bulk volume are tightly correlated. To increase the amount of produced hydrolysate per hour, a high ratio of heat transfer area to bulk volume is desired and a low evaporation temperature, to increase the overall heat transfer Q.

The calculations include analysis of a single copper pipe and do not consider spacing between parallel copper pipes. Realistically there will be an even spacing between the pipes for both configurations, which will be found using an optimum between the cost of production/assembly and the subsequent impact on the desired heat transfer. In order to find the optimum, an experimental rig should be tested to determine the experimental heat transfer rate.

The investigation of the significance of minimizing the distance between the copper pipes and aluminum showcases the importance of precise construction and assembly of the components in

order to maximize heat transfer.

The evaporation temperature and increased scrape speed at higher diameters have the highest impact on the heat transfer of all the factors varied. In order to increase the production rate, these factors should first be considered. The drawback of the SSHE freeze concentrators compared to bulk and layer FC is the smaller ice crystals formed which makes the separation more difficult, making it a very complicated and expensive process[9]. Lower evaporation temperatures increase the growth rate and size of the crystals, which makes them easier to separate.

The calculations are made using constant temprature of 0°C, as the freezing point of the hydrolysate mixture. The initial freezing point of the hydrolysate is -0.61°C. The hydrolysate enters the vessel at 4°C and due to the freezing point depression explained in chapter 2, the temperature of the solution will drop as the concentration increases. The Q'' will therefore differ slightly depending on the temperature of the bulk.

The overall result from the simulations show that an expected $U_{avg} = [475, 660]$ can be expected from the contact freezing vessel. The convection in the vessel is the limiting factor initially, and as the ice builds, the conductive resistance becomes the bottleneck due to the low conduction coefficient of ice $k_{ice} = 2.2W/mK$. In order to increase the Q'', high scrape velocity and frequency and low evaporation temperature are efficient measures.

6.3 Performance of Systems

Both configurations are able to fulfill the required heat loads of the processing. The difference between the two configurations the complexity and number of components required for the system, and the operational range.

The CASE 1 configuration achieves a higher COP for the limited range of saturation temperatures [-28°C, -20°C] with 9.4% better COP_R at -25°C and 10.1% better at -20°C compared to CASE 2. The operational range of CASE 2 investigated is [-40°C, -20°C]. The flexibility of CASE 1 is limited to the maximum pressure difference of 30 bars for the sub-critical compressor to the condensing temperature of 10°C, the configuration will not be able to produce the same amount of product rate as CASE 2 potentially can due to the higher temperature difference at lower saturation temperatures.

At higher evaporation pressure the volumetric flow decreases due to the density change of the gas. Specific volume v at -40°C is 0.03819 m^3/kg while it lowers to 0.01932 at -20°C, nearly 2 times lower, leading to a higher cooling capacity for the same size compressor.

It is however important to see the performance of the two systems under the circumstances of the process. A lower evaporation temperature increases the heat flux and ice production rate while decreasing the COP_R. Lowering the evaporation temperature from -25°C to -40°C increases the heat flux for the investigated contact freezing vessel Q'' $[W/m^2]$ by approximately 45%. The potential increase in the production rate of hydrolysate may outweigh the lower energy efficiency at lower evaporation temperatures as the energy cost per unit of hydrolysate kWh/kg is a crucial factor for economic sustainability and incentive.

Lower ambient temperatures open for the possibility of rejecting heat at a lower pressure and temperature. The ambient temperature is frequently lower than 0°C during the winter in Norway, particularly in the northern parts. Rejecting heat at a lower temperature will lower the overall energy consumption for the refrigeration system, although more components will be required to

ensure the operation in summer conditions.

The dynamic performance of the two system configurations is not investigated and can affect the viability and overall performance.

Higher saturation pressures in the evaporator of $P > 20bar$ also open for the possibility of 1-stage trans-critical compression, removing the need for 2-stage compression. It is reasonable to assume that this refrigeration system will be less complex and have a higher energy consumption. Less complexity usually means cheaper capital costs. Unfortunately, higher evaporation pressure simultaneously implies lower diameter vessels, meaning considerable height, multiple ones, or less production.

7 Conclusion

Heat Transfer Coefficient

An analysis of the heat transfer for a geometry consisting of a contact freezing cylinder with cyclic ice removal, with evaporating CO_2 pipes in contact with the wall has been conducted. Using correlations, the convection coefficient of the evaporating CO_2, the undeveloped flow within the cylinder, and the average 1-dimensional conduction coefficient are determined.

Two different configurations were investigated; coiled pipes around the cylindrical freezing vessel, and vertical pipes parallel to the vessel.

The impact on the overall heat transfer coefficient was analyzed by varying the following factors:

- **Coiled & vertical configuration:** The results indicate that the configuration of the copper pipes has a negligible difference in the average conductive resistance of $< 1\%$. As the average conduction is the least of the resistances prior to ice building, the difference can safely be discarded.
- **CO_2 mass flux** is simulated for the range $G = [125, 300]$ shows a notable impact in the initial heat transfer coefficient, however the difference decreases as time increases and the ice layer builds. The average U-value ranges from $U_{avg} = [530, 552]$.
- **Thermal Gel:** a Uniform layer of thermal gel with thickness $[0, 10mm]$ between the copper pipe and aluminum cylinder wall impacts the initial heat transfer considerably. 2mm reduces the initial U-value by 10-20% and the larger 10mm layer reduces the initial U-value by 40-50%.
- **Diameter & scrape speed:** The overall heat transfer for diameters in range $D_h = [0.35, 1.75m]$ were investigated at 15RPM scraping cycle. The diameter is tied to the speed of scraping, and yields the greatest impact on the U-values of $U_{avg} = [475, 660]$ significantly impacting the thickness of the ice layers produced.
- **CO_2 saturation temperatures** in range $[-40°C, -20°C]$ showed U-values ranging from $U_{avg} = [565, 650]$ proving less thermal resistance for lower temperature since the lower heat transfer Q'' causing slower ice layer propagation. By using the values for different U_{avg} and relating surface area and volume of the bulk, maximum diameters and corresponding heights of the vessel were determined.

CO_2 Refrigeration System

Two CO_2 systems were designed in order to meet the cooling and heating demands of the processing and freeze concentrating of the fish protein hydrolysate processing. Both systems have 2-stage compression and heat rejection. An investigation of the steady-state performance of the systems was conducted using EES. The cooling and heat load is satisfied by both systems. The deciding factors are the cooling load $Q_R = 143kW$, minimum heat rejection temperature of $T = 10°C$ and heating load of $Q_{hyd} = 87.2kW$

- **CASE 1:** includes an intermediate pressure stage with partial condensing at $T_{sat} = 10°C$ and an intermediate pressure vessel. The COP and system is calculated for saturated evaporating temperatures ranging from $[-28°C, -20°C]$ The resulting COP_R ranges from $[1.76, 2.06]$.

- **CASE 2** has de-superheating at the intermediate stage to $T = 10°C$ and two-step expansion, with gas by-passing to the high-stage compressor at the intermediate expansion stage. The optimal high side pressure is determined based on the intermediate pressure, and the COP_R was calculated for evaporation temperatures ranging from $[-40°C, -20°C]$. The resulting COP_R ranged from $[1.35, 1.86]$.

8 Further Work

Due to the limiting time and resources possible to spend on the project, several topics and ideas were not investigated. Here is listed topics can be reviewed for further work.

CFD & experimental investigation of flow in cylinder

There are uncertainties regarding the Reynolds number within the cylinder where the crystallization/freezing occurs. Since this thesis concludes that the convection coefficient of the solution is the limiting factor prior to ice formation, further analysis and experimental heat testing could enlighten the viability of the design and realistic sizes of components. The scraping speed effect on the ice layer can also be investigated to minimize the fouling of the ice, thus finding an optimum interval for ice removal.

Analysis of all thermal systems for a complete hydrolysate production facility

The thesis concludes that there is surplus heat in all system configurations. Gathering the heat & cooling demand of the entire facility and further analysis of the waste heat recovery would give a better view of the utility of the CO_2 system compare to other refrigerants and system configurations.

Introducing hydrolysate production to established fish processing facilities

There are many fish processing facilities along the Norwegian coast. Using case studies to investigate the economic gain of implementing the process of fish protein hydrolysate in existing fish processing facilities with surplus or reserve cooling or heating capacity.

References

[1] Peter John Fellows. *Food processing technology: principles and practice*. CRC Press LLC, 2000.

[2] Sintef, coolfish project. https://www.sintef.no/en/projects/2019/coolfish/. Accessed 08.04.2022.

[3] Inna Petrova, Ignat Tolstorebrov, and Trygve Magne Eikevik. Production of fish protein hydrolysates step by step: technological aspects, equipment used, major energy costs and methods of their minimizing. *International Aquatic Research*, 10(3):223–241, 2018.

[4] Arun Tapal and Purnima Kaul Tiku. Nutritional and nutraceutical improvement by enzymatic modification of food proteins. *Enzymes in Food Biotechnology*, 2019.

[5] Trygve Magne Eikevik. Compendium for heat pumping processes and systems tep 4255, 2015.

[6] ASHRAE Handbook Refrigeration and SI Edition. American society of heating, refrigerating and air-conditioning engineers. *Inc. Atlanta*, 2010.

[7] Muhammad Umar Khan. Design and analysis of freeze concentrator for processing of fish protein hydrolysate. 2021.

[8] Ken Morison and R.W. Hartel. *Evaporation and freeze concentration*, pages 495–552. 01 2006.

[9] Shafirah Samsuri, Nurul Aini Amran, Norshafika Yahya, and Mazura Jusoh. Review on progressive freeze concentration designs. *Chemical engineering communications*, 203(3):345–363, 2016.

[10] J. Sánchez, E. Hernández, J.M. Auleda, and M. Raventós. Review: Freeze concentration technology applied to dairy products. *Food Science and Technology International*, 17(1):5–13, 2011.

[11] Prem Kumar Sherman. Sustainable architecture in producing fish protein hydrolysates. 2021.

[12] T.L. Bergman, A.S. Lavine, and F.P. Incropera. *Fundamentals of Heat and Mass Transfer, 7th Edition*. John Wiley & Sons, Incorporated, 2011.

[13] Yu Xu and Xiande Fang. A new correlation of two-phase frictional pressure drop for evaporating flow in pipes. *International journal of refrigeration*, 35(7):2039–2050, 2012.

[14] Lutz Friedel. Improved friction pressure drop correlation for horizontal and vertical two-phase pipe flow. 1979.

[15] Jomar Mandal Leth-Olsen. Design of co2 heat pump and refrigeration system for hydrolyzation freeze concentration processes. 2021.

[16] Wieland. k65 product data sheet. https://resources.renkulde.no/renkulde/files?file=/resources/58458_20220512085500000.pdf. Accessed 25.05.2022.

[17] Gregory Nellis. *Heat transfer*. Cambridge University Press, Cambridge, 2009.

[18] M. Mohammed Shahs. Evaluation of general correlations for heat transfer during boiling of saturated liquids in tubes and annuli. *HVACR research*, 12(4):1047–1063, 2006.

[19] M. Shah. A new correlation for heat transfer during boiling flow through pipes. *ASHRAE Transactions*, 82:66–86, 01 1976.

[20] M. Shah. Chart correlation for saturated boiling heat transfer: Equations and further study. volume 88, 01 1982.

[21] O Krischer. *Die wissenschaftlichen Grundlagen der Trocknungstechnik*, volume 1. Springer-Verlag, Berlin, 3. edition, 1978.

[22] V Gnielinski. Berechnung mittlerer wärme- und stoffübergangskoeffizienten an laminar und turbulent überströmten einzelkörpern mit hilfe einer einheitlichen gleichung. *Forsch Ing Wes*, 41:145–150, 1975.

[23] *VDI Heat Atlas*. VDI-Buch. Springer Berlin Heidelberg, Berlin, Heidelberg.

[24] Rtselect. product configuration software. https://www.gea.com/en/articles/rtselect/index.jsp. Accessed 16.04.2022.

[25] Bitzer. https://www.bitzer.de/gb/en/reciprocating-compressors/ecoline-transcritical/. Accessed 20.05.2022.

Appendix

A: Python programs

Coiled pipes configuration

```
# -*- coding: utf-8 -*-
"""
Created on Wed May 18 14:28:52 2022

@author: jomar
"""
import numpy as np
import CoolProp.CoolProp as CP
import avg_conduction
import avg_conduction_vertical
import matplotlib.pyplot as plt
import Bulk_calculation


#### PLOT STYLE #####
plt.style.use('seaborn')


R744 = 'CarbonDioxide'
HYD = 'Water'
Freezing = 334  # kj/kg

# CONSTANTS
T_inf = 273.16    # [K] Temperature of the hydrolysate in the cylinder

T_evap = -40 + 273.15  # [K]
P_sat = CP.PropsSI('P', 'T', T_evap, 'Q', 0, R744)
m_tot = 1.0  # kg/s
n_pipe = 100
m_r = m_tot / n_pipe  # kg/s

#### PIPE VALUES ####
d_y = 0.009525  # meter
pipe_thick = 0.00076  # [m]
d_i = d_y - pipe_thick  # [m]

# CYLINDER WALL THICKNESS
wall_thick = 0.0025  # [m]


#### CONDUCTION COEFFICIENTS & initial ice thickness ####
k_cu = 403  # [W/m*K] @-40C
k_gel = 10  # [W/m*K]
k_al = 233.3  # [W/m*K] @-3C
k_ice = 2.2 # [W/m*K] @ -30C
x_ice = 0.0 # [m]

### CONTACT FREEZING VESSEL ####
h_cyl = 2.4  # [m]
d_cyl = 0.7  # [m]
A = np.pi * d_cyl * h_cyl
Volume_cylinder = np.pi * d_cyl**2 / 4 * h_cyl
```

```
### AVERAGE THERMAL RESISTANCE OF CONDUCTION ###
resistance, angles, avg, res_cu, res_gel, res_al = avg_conduction.conduction(
    T_evap, d_i, d_y, k_cu, k_al, k_gel, wall_thick, k_ice, x_ice)

# NUMBER OF COIL AND TOTAL LENGTH #
n_coil = round(h_cyl / d_y) - 1
r_coil_cent = (d_cyl+wall_thick)/2 + d_y/2
l_circumference = 2*np.pi*r_coil_cent
tot_length_coil = l_circumference * n_coil / n_pipe
total_rounds_per_pipe = n_coil/n_pipe

###CALCULATION OF CONVECTION COEFFICIENT CO2 SIDE###

def Re_d(u, rho, d, mu):
    Reynolds = (rho * u * d)/mu
    return Reynolds


def u(m, rho, d):
    velocity = m/(rho*((d**2)*np.pi/4))
    return velocity


def friction_coeff(Re):
    f = (0.790 * np.log(Re) - 1.64)**-2  # V&M PAGE 567
    return f


def pressure_loss(f, rho, L, u, d):
    dp = f * (rho/2) * ((u**2)/d) * L
    return dp


def scrape_speed(rpm, diameter):
    circumference = diameter * np.pi
    u = (rpm*circumference)/60
    return u


### CALCULATION OF CONVECTION COEFFICIEN ###
#Two-phase correlation#
mu_f = CP.PropsSI('V', 'T', T_evap, 'Q', 0, R744)
mu_g = CP.PropsSI('V', 'T', T_evap, 'Q', 1, R744)
cp_f = CP.PropsSI('C', 'T', T_evap, 'Q', 0, R744)
cp_g = CP.PropsSI('C', 'T', T_evap, 'Q', 1, R744)
Pr_f = CP.PropsSI('Prandtl', 'T', T_evap, 'Q', 0, R744)
Pr_g = CP.PropsSI('Prandtl', 'T', T_evap, 'Q', 1, R744)
rho_f = CP.PropsSI('D', 'T', T_evap, 'Q', 0, R744)
rho_g = CP.PropsSI('D', 'T', T_evap, 'Q', 1, R744)
h_f = CP.PropsSI('H', 'T', T_evap, 'Q', 0, R744)
h_g = CP.PropsSI('H', 'T', T_evap, 'Q', 1, R744)
h_fg = h_g - h_f
k_f = CP.PropsSI('L', 'T', T_evap, 'Q', 0, R744)
```

```
k_g = CP.PropsSI('L', 'T', T_evap, 'Q', 1, R744)

### CALCULTAING VALUES FOR LIQUID CO2 ###
u_f = u(m_r, rho_f, d_i)
Re_f = Re_d(u_f, rho_f, d_i, mu_f)
f_f = friction_coeff(Re_f)
dp_f = pressure_loss(f_f, rho_f, tot_length_coil, u_f, d_i)
#print('CO2, [m/s]', u_f)
#print('Re, CO2', Re_f)

Nu_f = 0.023 * Re_f**0.8 * Pr_f**0.4  # V&M Page 567

### Hydrolysate on other side - Assuming to be water ###
mu_w = CP.PropsSI('V', 'T', T_inf, 'P', 101325,  HYD)
cp_w = CP.PropsSI('C', 'T', T_inf, 'P', 101325, HYD)
P_w = CP.PropsSI('P', 'T', T_inf, 'P', 101325, HYD)

Pr_w = CP.PropsSI('Prandtl', 'T', T_inf, 'P', 101325, HYD)
rho_w = CP.PropsSI('D', 'T', T_inf, 'P', 101325, HYD)
h_w = CP.PropsSI('H', 'T', T_inf, 'P', 101325, HYD)
k_w = CP.PropsSI('L', 'T', T_inf, 'P', 101325, HYD)

### SCAPE SPEED - FINDING U, RE FOR THE SURFACE ###
rpm = 15  # ROUNDS PER MINUTE
u_scrape = scrape_speed(rpm, d_cyl)  # m/s
Re_w = Re_d(u_scrape, rho_w, d_cyl*np.pi, mu_w)
Nu_wl = 0.664 * Re_w**(1/2) * Pr_w**(1/3)  # VDI HEAT ATLAS G4 Eq 2
Nu_wt = (0.037*Re_w**0.8 * Pr_w)/(1+2.443*Re_w**(-0.1)*(Pr_w**(2/3) -1 )) # VDI
HEAT ATLAS G4 Eq 8

Nu_w = (Nu_wl**2 + Nu_wt**2)**0.5 # VDI HEAT ATLAS G4 Eq 9

h_w = (Nu_w * k_w) / (d_cyl * np.pi)

#### INITIAL CO2 GUESS ####
h_co2 = 100


R_co2 = 1/h_co2
R_hyd = 1/h_w

### CALCULATING U-VALUE AND Q BASED ON CO2 GUESS ###
U_A = 1/(R_co2 + R_hyd + avg)

Q = U_A * d_cyl*np.pi*h_cyl*(T_inf - T_evap)
Q_A = U_A * 37 ### Q PER AREA FOR CALCULATION OF TEMPERATURE ###


### FLOW BOILING ### PAGE 792-793 HEAT TRANSFER

def N(Fr, Co):
    if Fr > 0.04:
        return Co
    else:
```

```
        return 0.38 * Co * Fr**-0.3

def h_cb():
    return 1.8*(N(Fr,Co)**-0.8)

def h_nb(Bo):
    if Bo < 0.3*10**-4:
        return 1 + 46 * Bo**0.5
    else:
        return 230 * Bo**0.5


def h_bs1(Bo):
    if Bo < 11*10**-4:
        return 15.43 * Bo**0.5 * np.exp(2.74*N(Fr,Co)**-0.1)
    else:
        return 14.70 * Bo**0.5 * np.exp(2.74*N(Fr,Co)**-0.1)

def h_bs2(Bo):
    if Bo < 11*10**-4:
        return 15.43 * Bo**0.5 * np.exp(2.47*N(Fr,Co)**-0.15)
    else:
        return 14.70 * Bo**0.5 * np.exp(2.47*N(Fr,Co)**-0.15)

def h_dim(N):
    if N <= 0.1:
        h_new = h_bs2(Bo)
    elif N > 1.0:
        h_new = h_nb(Bo)
    else:
        h_new = h_bs1(Bo)
    if h_new > h_cb():
        return h_new
    else:
        return h_cb()


### FLOW BOILING ### PAGE 792-793 HEAT TRANSFER
Q_1 = (U_A *d_i * tot_length_coil * (T_inf - T_evap))
Q_A1 = U_A * (T_inf - T_evap)
x_out = Q_1 / (h_fg * m_r)

G = m_r / ((d_i**2/4)*np.pi) # mass flowrate per crossectional area per pipe

Q = G * np.pi * d_i**2/4 * h_fg * (1-x_out)
Bo = Q_A1/(G * (h_fg))
Fr = G**2/(rho_f**2 * 9.81 * d_i)
G = m_r / ((d_i**2/4)*np.pi) # mass flowrate per crossectional area per pipe

#### FINDING EQUILIBRIUM FOR hCO2 #####
#### FINDING U VALUES FOR DIFFERENT G ####
G_lst = [125, 150, 175, 200, 300]
m_lst = []
for glist in G_lst:
```

```
    m_lst.append(glist * ((d_i**2/4)*np.pi))
U_G = [[],[],[],[],[]]
k_G_lst = [[],[],[],[],[]]
h_G_local = [[],[],[],[],[]]
counter = 0
for num in G_lst:
    G = num

    for i in range(0,15):
        h_lst = []
        h_liq = []
        n_lst = []
        k_lst = []
        h_local = []
        for i in range(1,int(x_out*100),1):
            k = i/100
            k_lst.append(k)
            Co = (1/k - 1)**0.8 *(rho_g/rho_f)**0.5
            Re_bo = (G * (1-k) * d_i)/(mu_f)
            f_l = (friction_coeff(Re_bo))
            h_l = (((f_l/8) * (Re_bo - 1000) * Pr_f) / (1 +
12.7*((Pr_f**(2/3))-1)*(f_l/8)**0.5)) * (k_f/d_i)
            h_liq.append(h_l)
            n_lst.append(N(Fr,Co))
            h_lst.append(h_dim(N(Fr,Co)))

        for i in range(len(h_lst)):
            h_local.append(h_lst[i]*h_liq[i])
        h_co2_avg = sum(h_local)/len(h_local)
        U_new = 1/(1/h_co2_avg + avg + R_hyd)

        Q_1 = U_new * d_i *  tot_length_coil * (T_inf - T_evap)
        Q_A1 = U_new * (T_inf - T_evap)
        x_out = Q_1 / (h_fg * G * ((d_i**2/4)*np.pi))
        Bo = Q_A1/(G * (h_fg))

    for i in range(len(h_local)):
        U_G[counter].append(1/(1/h_local[i] + avg + R_hyd))

    k_G_lst[counter] = k_lst
    h_G_local[counter] = h_local

    counter = counter + 1
#### CALCULATING AVERAGE CO2 CONVECTION VALUES #####
h_125_avg = sum(h_G_local[0]) / len(h_G_local[0])
h_150_avg = sum(h_G_local[1]) / len(h_G_local[1])
h_175_avg = sum(h_G_local[2]) / len(h_G_local[2])
h_200_avg = sum(h_G_local[3]) / len(h_G_local[3])
h_300_avg = sum(h_G_local[4]) / len(h_G_local[4])

print('h_125_avg =', h_125_avg)
print('h_150_avg =', h_150_avg)
print('h_175_avg =', h_175_avg)
print('h_200_avg =', h_200_avg)
```

```
print('h_300_avg =', h_300_avg)

U_125_avg = sum(U_G[0]) / len(U_G[0])
U_150_avg = sum(U_G[1]) / len(U_G[1])
U_175_avg = sum(U_G[2]) / len(U_G[2])
U_200_avg = sum(U_G[3]) / len(U_G[3])
U_300_avg = sum(U_G[4]) / len(U_G[4])

print('U_125_avg =', U_125_avg)
print('U_150_avg =', U_150_avg)
print('U_175_avg =', U_175_avg)
print('U_200_avg =', U_200_avg)
print('U_300_avg =', U_300_avg)


#### PLOTTING THE CO2 CONVECTION AND U VS GAS QUALITY ####
G_125, = plt.plot(k_G_lst[0], h_G_local[0], label = 'G = 125')
G_150, = plt.plot(k_G_lst[1], h_G_local[1], label = 'G = 150')
G_175, = plt.plot(k_G_lst[2], h_G_local[2], label = 'G = 175')
G_200, = plt.plot(k_G_lst[3], h_G_local[3], label = 'G = 200')
G_300, = plt.plot(k_G_lst[4], h_G_local[4], label = 'G = 300')
plt.xlabel('Gas quality, x [-]')
plt.ylabel('h, local convection coefficient [W/m^2K]')
plt.legend(handles=[G_300,G_200,G_175,G_150,G_125], loc = 'lower left', title =
'G, Mass flux [kg/m^2s]');
plt.show()


G_125, = plt.plot(k_G_lst[0], U_G[0], label = 'G = 125')
G_150, = plt.plot(k_G_lst[1], U_G[1], label = 'G = 150')
G_175, = plt.plot(k_G_lst[2], U_G[2], label = 'G = 175')
G_200, = plt.plot(k_G_lst[3], U_G[3], label = 'G = 200')
G_300, = plt.plot(k_G_lst[4], U_G[4], label = 'G = 300')
plt.xlabel('Gas quality, x [-]')
plt.ylabel('U-value [W/m^2K]')
plt.legend(handles=[G_300,G_200,G_175,G_150,G_125], loc = 'lower left', title =
'G, Mass flux [kg/m^2s]');
plt.show()


### ICE FORMATION ### starting with the inlet with saturated liquid.
h_ice = 334 * 10**3 #J/kg
rho_ice = 917 #kg/m^3
freezing_point = 273.15 - 0.61

U_ice = [[],[],[],[],[]]
time_lst = [[],[],[],[],[]]
ice_lst = [[],[],[],[],[]]

k_G_lst = [[],[],[],[],[]]
h_G_local = [[],[],[],[],[]]
counter = 0

#### CHANGE T_BULK TO WANTED TEMPERATURE ####
```

```
T_bulk = -0.61

### CALCULATING ICE GROWTH AND U-VALUE CHANGE IN A CYCLE ####
for num in G_lst:
    G = num
    ice_formed = 0
    #SETTING STARTING POINT

    none, noone, cond_ice, none1, none2, none3 = avg_conduction.conduction(
        T_evap, d_i, d_y, k_cu, k_al, k_gel, wall_thick, k_ice, ice_formed) ###
is the initial ice formed
    for n in range(1, (1 + int((60/rpm)))*10, 1):
        l = n/10
        for i in range(0,15):
            h_lst = []
            h_liq = []
            n_lst = []
            k_lst = []
            h_local = []
            for i in range(1,int(x_out*100),1):
                k = i/100
                k_lst.append(k)
                Co = (1/k - 1)**0.8 *(rho_g/rho_f)**0.5
                Re_bo = (G * (1-k) * d_i)/(mu_f)
                f_l = (friction_coeff(Re_bo))
                h_l = (((f_l/8) * (Re_bo - 1000) * Pr_f) / (1 +
12.7*((Pr_f**(2/3))-1)*(f_l/8)**0.5)) * (k_f/d_i)
                h_liq.append(h_l)
                n_lst.append(N(Fr,Co))
                h_lst.append(h_dim(N(Fr,Co)))
            for i in range(len(h_lst)):
                h_local.append(h_lst[i]*h_liq[i])
            h_co2_avg = sum(h_local)/len(h_local)
            U_new = 1/(1/h_co2_avg + cond_ice + R_hyd)
            Q_0 = U_new * d_i * tot_length_coil * (freezing_point - T_evap)
            Q_A0 = U_new * (freezing_point - T_evap)
            x_out = Q_0 / (h_fg * G * ((d_i**2/4)*np.pi))
            Bo = Q_A0/(G * (h_fg))
            #print('X_out',x_out)

        Q_0 = U_new * (freezing_point - T_evap)
        ice_formed = ice_formed + Q_0/(h_ice * rho_ice)
        none, noone, cond_ice, none1, none2, none3 = avg_conduction.conduction(
            T_evap, d_i, d_y, k_cu, k_al, k_gel, wall_thick, k_ice, ice_formed)
        U_ice[counter].append(U_new)
        ice_lst[counter].append(ice_formed)
        time_lst[counter].append(l)
    counter = counter + 1

#### PLOTTING ICE, U, TIME ####
G_125_ICE, = plt.plot(time_lst[0], ice_lst[0], label = 'G = 125')
G_150_ICE, = plt.plot(time_lst[1], ice_lst[1], label = 'G = 150')
G_175_ICE, = plt.plot(time_lst[2], ice_lst[2], label = 'G = 175')
G_200_ICE, = plt.plot(time_lst[3], ice_lst[3], label = 'G = 200')
```

```
G_300_ICE, = plt.plot(time_lst[4], ice_lst[4], label = 'G = 300')
plt.xlabel('time [s]')
plt.ylabel('Ice thickness [m]')
plt.legend(handles=[G_300_ICE,G_200_ICE,G_175_ICE,G_150_ICE,G_125_ICE], loc =
'upper left', title = 'G, Mass flux [kg/m^2s]');
plt.show()

G_125_ICE, = plt.plot(time_lst[0], U_ice[0], label = 'G = 125')
G_150_ICE, = plt.plot(time_lst[1], U_ice[1], label = 'G = 150')
G_175_ICE, = plt.plot(time_lst[2], U_ice[2], label = 'G = 175')
G_200_ICE, = plt.plot(time_lst[3], U_ice[3], label = 'G = 200')
G_300_ICE, = plt.plot(time_lst[4], U_ice[4], label = 'G = 300')
plt.xlabel('time [s]')
plt.ylabel('U-value [W/m^2K]')
plt.legend(handles=[G_300_ICE,G_200_ICE,G_175_ICE,G_150_ICE,G_125_ICE], loc =
'upper right', title = 'G, Mass flux [kg/m^2s]');
plt.show()

print('125, AVG: ',sum(U_ice[0])/len(U_ice[0]))
print('150, AVG: ',sum(U_ice[1])/len(U_ice[1]))
print('175, AVG: ',sum(U_ice[2])/len(U_ice[2]))
print('200, AVG: ',sum(U_ice[3])/len(U_ice[3]))
print('300, AVG: ',sum(U_ice[4])/len(U_ice[4]))

G_125_ICE, = plt.plot(ice_lst[0], U_ice[0], label = 'G = 125')
G_150_ICE, = plt.plot(ice_lst[1], U_ice[1], label = 'G = 150')
G_175_ICE, = plt.plot(ice_lst[2], U_ice[2], label = 'G = 175')
G_200_ICE, = plt.plot(ice_lst[3], U_ice[3], label = 'G = 200')
G_300_ICE, = plt.plot(ice_lst[4], U_ice[4], label = 'G = 300')
plt.xlabel('Ice thickness [m]')
plt.ylabel('U-value [W/m^2K]')
plt.legend(handles=[G_300_ICE,G_200_ICE,G_175_ICE,G_150_ICE,G_125_ICE], loc =
'upper right', title = 'G, Mass flux [kg/m^2s]');
plt.show()


P_int = P_sat + 30*10**5
T_sat_int = CP.PropsSI('T', 'P', P_int, 'Q', 0, R744) -273.15


####### TEMPERATURE DISTRIBUTION THROUGH WALL####
###NUMBER IN LIST IS FOUND FOR 90, 60, 45, 30, 0
Temp_lst_90 = []

def temp_lst(number):
    Temp_lst = []
    U_deg = 1/(1/h_co2_avg + res_cu[number] + res_gel[number] + res_al[number] +
1/h_w)
    Q_deg = U_deg * (T_inf - T_evap)
    T_out = Q_deg * 1/(h_175_avg) + T_evap -273.15 #### h_xxx_avg, xxx is G
[kg/m^2s]
    T_cu = Q_deg * res_cu[number] + T_out
    T_gel = Q_deg * res_gel[number] + T_cu
    T_al = Q_deg * res_al[number] + T_gel
```

```
    T_in = Q_deg * (1/h_w) + T_al
    Temp_lst.append(T_evap - 273.15)
    Temp_lst.append(T_out)
    Temp_lst.append(T_cu)
    Temp_lst.append(T_gel)
    Temp_lst.append(T_al)
    Temp_lst.append(T_in)
    return Temp_lst


Temp45 = temp_lst(50)
Temp30 = temp_lst(33)
Temp60 = temp_lst(67)
Temp90 = temp_lst(99)
Temp0  = temp_lst(0)

x_lst = [0,1,2,3,4,5]
temp_xticks = ['T_CO2', 'T_cu(i)', ' T_cu(o)', 'T_al(i)', 'T_al(o)', 'T_bulk']
plt.xticks(x_lst, temp_xticks)

#### PLOTTING TEMERATURE DISTRIBUTION THROUGH WALL ####
temp_plot1, = plt.plot(Temp90, '--', marker = 'X', label = '90 deg')
temp_plot2, = plt.plot(Temp60, '--', marker = 'X', label = '60 deg')
temp_plot3, = plt.plot(Temp45, '--', marker = 'X', label = '45 deg')
temp_plot4, = plt.plot(Temp30, '--', marker = 'X', label = '30 deg')
temp_plot5, = plt.plot(Temp0 , '--', marker = 'X', label = '0 deg')

plt.xlabel('Elements')
plt.ylabel('Temperature [C]')
plt.legend(handles = [temp_plot1, temp_plot2, temp_plot3, temp_plot4,
temp_plot5], loc = 'upper left', title = 'Angles [Deg], G = 175' )
plt.show()



##### adding 10mm to gel thickness  ####
def larger_gel():
    r_gel_thick = []
    r_gel_counter = []

    for i in range(0,100):
        r_gel_thick.append(avg + (i/10000)/k_gel)
        r_gel_counter.append(i/10000)
    return r_gel_thick, r_gel_counter

r_gel_thick, r_gel_counter = larger_gel()




### CALCULATING NEW U FOR GROWING LAYER OF THERMAL GEL BETWEEN PIPE AND ALU WALL
###
U_gel = [[],[],[],[],[]]
thick_gel = [[],[],[],[],[]]
```

```
counter = 0 ### RESETING COUNTER
for num in G_lst:
    G = num
    #SETTING STARTING POINT
    for gel_cond in (r_gel_thick):
        for i in range(0,15):
            h_lst = []
            h_liq = []
            n_lst = []
            k_lst = []
            h_local = []
            for i in range(1,int(x_out*100),1):
                k = i/100
                k_lst.append(k)
                Co = (1/k - 1)**0.8 *(rho_g/rho_f)**0.5
                Re_bo = (G * (1-k) * d_i)/(mu_f)
                f_l = (friction_coeff(Re_bo))
                h_l = (((f_l/8) * (Re_bo - 1000) * Pr_f) / (1 +
12.7*((Pr_f**(2/3))-1)*(f_l/8)**0.5)) * (k_f/d_i)
                h_liq.append(h_l)
                n_lst.append(N(Fr,Co))
                h_lst.append(h_dim(N(Fr,Co)))
            for i in range(len(h_lst)):
                h_local.append(h_lst[i]*h_liq[i])
            h_co2_avg = sum(h_local)/len(h_local)
            U_new = 1/(1/h_co2_avg + gel_cond + R_hyd)
            Q_0 = U_new * d_i * tot_length_coil * (T_inf - T_evap)
            Q_A0 = U_new * (T_inf - T_evap)
            x_out = Q_0 / (h_fg * G * ((d_i**2/4)*np.pi))
            Bo = Q_A0/(G * (h_fg))


        Q_0 = U_new * (T_inf - T_evap)
        U_gel[counter].append(U_new)
    counter = counter + 1


#### PLOTTING GEL THICKNESS VS U-VALUE ####

G_125_GEL, = plt.plot(r_gel_counter, U_gel[0], label = 'G = 125')
G_150_GEL, = plt.plot(r_gel_counter, U_gel[1], label = 'G = 150')
G_175_GEL, = plt.plot(r_gel_counter, U_gel[2], label = 'G = 175')
G_200_GEL, = plt.plot(r_gel_counter, U_gel[3], label = 'G = 200')
G_300_GEL, = plt.plot(r_gel_counter, U_gel[4], label = 'G = 300')
plt.xlabel('Width of gel between pipe and aluminium [m]')
plt.ylabel('U-value [W/m^2K]')
plt.legend(handles=[G_300_ICE,G_200_ICE,G_175_ICE,G_150_ICE,G_125_ICE], loc =
'upper right', title = 'G, Mass flux [kg/m^2s]');
plt.show()
```

Conduction calculation for coiled pipes

```
import numpy as np
def conduction(T_evap, d_i, d_y, k_cu, k_al, k_gel, wall_thick, k_ice, x_ice):
    #### SETTING UP STEP LENGTH ###
    n = 100
    step_length = (np.pi/2)/n  #angle#
    steps = []
    number = 0
    for i in range(n): #FINDING ANGLES#
        steps.append(number)
        number = number + step_length


    def inner_diameter(angle,diameter):
        r = diameter/2
        y = np.sin(angle)*r
        x = np.cos(angle)*r
        return x,y


    def outer_diameter(y,diameter):
        r = diameter/2
        x =(r**2-y**2)**(1/2)
        return x


    new_x,new_y = (inner_diameter(np.pi/4,1))

    #### CALCULATING THE THERMAL RESISTANCE AT DIFFERENT ANGLES #####
    def thermal_resistance(k_cu,k_gel,k_al,k_ice,x_ice):
        R_cond_lst = []
        R_cu = []
        R_gel = []
        R_al = []
        Angle_lst = []
        for step in steps:
            d_inner,width = inner_diameter(step,d_i)
            d_yout = outer_diameter(width,d_y)
            x_cu = d_yout - d_inner
            x_al = wall_thick
            x_gel = d_y/2 - d_yout
            R_cond = x_cu/k_cu + x_gel/k_gel + x_al/k_al + x_ice/k_ice
            R_cu.append(x_cu/k_cu)
            R_gel.append(x_gel/k_gel)
            R_al.append(x_al/k_al)
            R_cond_lst.append(R_cond)
            Angle_lst.append(step)
        return R_cond_lst, Angle_lst, R_cu, R_gel, R_al


    resistance, angles, res_cu, res_gel, res_al =
thermal_resistance(k_cu,k_gel,k_al,k_ice,x_ice)

    avg_resistance = sum(resistance)/n
    return resistance, angles, avg_resistance, res_cu, res_gel, res_al
```

Vertical pipes configuration

```
# -*- coding: utf-8 -*-
"""
Created on Wed May 18 14:28:52 2022

@author: jomar
"""

import numpy as np
import CoolProp.CoolProp as CP
import avg_conduction_vertical
import matplotlib.pyplot as plt
import Bulk_calculation

#### PLOT STYLE #####
plt.style.use('seaborn')


R744 = 'CarbonDioxide'
HYD = 'Water'
Freezing = 334  # kj/kg

# CONSTANTS
T_inf = 273.16    # [K] Temperature of the hydrolysate in the cylinder

T_evap = -40 + 273.15  # [K]
P_sat = CP.PropsSI('P', 'T', T_evap, 'Q', 0, R744)
m_tot = 1.0  # kg/s
n_pipe = 100
m_r = m_tot / n_pipe  # kg/s

#### PIPE VALUES ####
d_y = 0.009525  # meter
pipe_thick = 0.00076  # [m]
d_i = d_y -  pipe_thick  # [m]

# CYLINDER WALL THICKNESS
wall_thick = 0.0025  # [m]

#### CONDUCTION COEFFICIENTS ####
k_cu = 403  # [W/m*K] @-40C
k_gel = 10  # [W/m*K]
k_al = 233.3  # [W/m*K] @-3C
k_ice = 2.2 # [W/m*K] @ -30C
x_ice = 0.0 # [m]

### CONTACT FREEZING VESSEL ####
h_cyl = 2.4  # [m]
d_cyl = 0.7  # [m]
A = np.pi * d_cyl * h_cyl
Volume_cylinder = np.pi * d_cyl**2 / 4 * h_cyl

### AVERAGE THERMAL RESISTANCE OF CONDUCTION ###
resistance, angles, avg, res_cu, res_gel, res_al =
```

```
avg_conduction_vertical.conduction(
    T_evap, d_i, d_y, d_cyl, k_cu, k_al, k_gel, wall_thick, k_ice, x_ice)

# NUMBER OF COIL AND TOTAL LENGTH #
n_coil = round(h_cyl / d_y) - 1
r_coil_cent = (d_cyl+wall_thick)/2 + d_y/2
l_circumference = 2*np.pi*r_coil_cent
tot_length_coil = h_cyl

###CALCULATION OF CONVECTION COEFFICIENT CO2 SIDE###

def Re_d(u, rho, d, mu):
    Reynolds = (rho * u * d)/mu
    return Reynolds


def u(m, rho, d):
    velocity = m/(rho*((d**2)*np.pi/4))
    return velocity


def friction_coeff(Re):
    f = (0.790 * np.log(Re) - 1.64)**-2  # V&M PAGE 567
    return f


def pressure_loss(f, rho, L, u, d):
    dp = f * (rho/2) * ((u**2)/d) * L
    return dp


def scrape_speed(rpm, diameter):
    circumference = diameter * np.pi
    u = (rpm*circumference)/60
    return u


### CALCULATION OF CONVECTION COEFFICIEN ###
#Two-phase correlation#
mu_f = CP.PropsSI('V', 'T', T_evap, 'Q', 0, R744)
mu_g = CP.PropsSI('V', 'T', T_evap, 'Q', 1, R744)
cp_f = CP.PropsSI('C', 'T', T_evap, 'Q', 0, R744)
cp_g = CP.PropsSI('C', 'T', T_evap, 'Q', 1, R744)
Pr_f = CP.PropsSI('Prandtl', 'T', T_evap, 'Q', 0, R744)
Pr_g = CP.PropsSI('Prandtl', 'T', T_evap, 'Q', 1, R744)
rho_f = CP.PropsSI('D', 'T', T_evap, 'Q', 0, R744)
rho_g = CP.PropsSI('D', 'T', T_evap, 'Q', 1, R744)
h_f = CP.PropsSI('H', 'T', T_evap, 'Q', 0, R744)
h_g = CP.PropsSI('H', 'T', T_evap, 'Q', 1, R744)
h_fg = h_g - h_f
k_f = CP.PropsSI('L', 'T', T_evap, 'Q', 0, R744)
k_g = CP.PropsSI('L', 'T', T_evap, 'Q', 1, R744)

### CALCULTAING VALUES FOR LIQUID CO2 ###
```

```
u_f = u(m_r, rho_f, d_i)
Re_f = Re_d(u_f, rho_f, d_i, mu_f)
f_f = friction_coeff(Re_f)
dp_f = pressure_loss(f_f, rho_f, tot_length_coil, u_f, d_i)
#print('CO2, [m/s]', u_f)
#print('Re, CO2', Re_f)

Nu_f = 0.023 * Re_f**0.8 * Pr_f**0.4  # V&M Page 567


### Hydrolysate on other side - Assuming to be water ###
mu_w = CP.PropsSI('V', 'T', T_inf, 'P', 101325,  HYD)
cp_w = CP.PropsSI('C', 'T', T_inf, 'P', 101325, HYD)
P_w = CP.PropsSI('P', 'T', T_inf, 'P', 101325, HYD)

Pr_w = CP.PropsSI('Prandtl', 'T', T_inf, 'P', 101325, HYD)
rho_w = CP.PropsSI('D', 'T', T_inf, 'P', 101325, HYD)
h_w = CP.PropsSI('H', 'T', T_inf, 'P', 101325, HYD)
k_w = CP.PropsSI('L', 'T', T_inf, 'P', 101325, HYD)

### SCAPE SPEED - FINDING U, RE FOR THE SURFACE ###
rpm = 15  # ROUNDS PER MINUTE
u_scrape = scrape_speed(rpm, d_cyl)  # m/s
Re_w = Re_d(u_scrape, rho_w, d_cyl*np.pi, mu_w)
Nu_wl = 0.664 * Re_w**(1/2) * Pr_w**(1/3)  # VDI HEAT ATLAS G4 Eq 2
Nu_wt = (0.037*Re_w**0.8 * Pr_w)/(1+2.443*Re_w**(-0.1)*(Pr_w**(2/3) -1 )) # VDI
HEAT ATLAS G4 Eq 8

Nu_w = (Nu_wl**2 + Nu_wt**2)**0.5 # VDI HEAT ATLAS G4 Eq 9

h_w = (Nu_w * k_w) / (d_cyl * np.pi)

#### INITIAL CO2 GUESS ####
h_co2 = 100

### CALCULATING U-VALUE AND Q BASED ON CO2 GUESS ###
R_co2 = 1/h_co2
R_hyd = 1/h_w

U_A = 1/(R_co2 + R_hyd + avg)

Q = U_A * d_cyl*np.pi*h_cyl*(T_inf - T_evap)
Q_A = U_A * 37 ### Q PER AREA FOR CALCULATION OF TEMPERATURE ###


### FLOW BOILING ### PAGE 792-793 HEAT TRANSFER

def N(Fr, Co):
    if Fr > 0.04:
        return Co
    else:
        return 0.38 * Co * Fr**-0.3

def h_cb():
```

```
    return 1.8*(N(Fr,Co)**-0.8)

def h_nb(Bo):
    if Bo < 0.3*10**-4:
        return 1 + 46 * Bo**0.5
    else:
        return 230 * Bo**0.5


def h_bs1(Bo):
    if Bo < 11*10**-4:
        return 15.43 * Bo**0.5 * np.exp(2.74*N(Fr,Co)**-0.1)
    else:
        return 14.70 * Bo**0.5 * np.exp(2.74*N(Fr,Co)**-0.1)

def h_bs2(Bo):
    if Bo < 11*10**-4:
        return 15.43 * Bo**0.5 * np.exp(2.47*N(Fr,Co)**-0.15)
    else:
        return 14.70 * Bo**0.5 * np.exp(2.47*N(Fr,Co)**-0.15)

def h_dim(N):
    if N <= 0.1:
        h_new = h_bs2(Bo)
    elif N > 1.0:
        h_new = h_nb(Bo)
    else:
        h_new = h_bs1(Bo)
    if h_new > h_cb():
        return h_new
    else:
        return h_cb()


### FLOW BOILING ### PAGE 792-793 HEAT TRANSFER
Q_1 = (U_A * d_i * tot_length_coil * (T_inf - T_evap))
Q_A1 = U_A * (T_inf - T_evap)
x_out = Q_1 / (h_fg * m_r)

G = m_r / ((d_i**2/4)*np.pi) # mass flowrate per crossectional area per pipe

Q = G * np.pi * d_i**2/4 * h_fg * (1-x_out)
Bo = Q_A1/(G * (h_fg))
Fr = G**2/(rho_f**2 * 9.81 * d_i)
G = m_r / ((d_i**2/4)*np.pi) # mass flowrate per crossectional area per pipe


#### FINDING EQUILIBRIUM FOR hCO2 #####
#### FINDING U VALUES FOR DIFFERENT G ####
G_lst = [125, 150, 175, 200, 300]
U_G = [[],[],[],[],[]]
k_G_lst = [[],[],[],[],[]]
h_G_local = [[],[],[],[],[]]
counter = 0
```

```
for num in G_lst:
    G = num

    for i in range(0,15):
        h_lst = []
        h_liq = []
        n_lst = []
        k_lst = []
        h_local = []
        for i in range(1,int(x_out*100),1):
            k = i/100
            k_lst.append(k)
            Co = (1/k - 1)**0.8 *(rho_g/rho_f)**0.5
            Re_bo = (G * (1-k) * d_i)/(mu_f)
            f_l = (friction_coeff(Re_bo))
            h_l = (((f_l/8) * (Re_bo - 1000) * Pr_f) / (1 +
12.7*((Pr_f**(2/3))-1)*(f_l/8)**0.5)) * (k_f/d_i)
            h_liq.append(h_l)
            n_lst.append(N(Fr,Co))
            h_lst.append(h_dim(N(Fr,Co)))

        for i in range(len(h_lst)):
            h_local.append(h_lst[i]*h_liq[i])
        h_co2_avg = sum(h_local)/len(h_local)
        U_new = 1/(1/h_co2_avg + avg + R_hyd)

        Q_1 = U_new * d_i * tot_length_coil * (T_inf - T_evap)
        Q_A1 = U_new * (T_inf - T_evap)
        x_out = Q_1 / (h_fg * G * ((d_i**2/4)*np.pi))
        Bo = Q_A1/(G * (h_fg))

    for i in range(len(h_local)):
        U_G[counter].append(1/(1/h_local[i] + avg + R_hyd))

    k_G_lst[counter] = k_lst
    h_G_local[counter] = h_local

    counter = counter + 1

#### CALCULATING AVERAGE CO2 CONVECTION VALUES #####
h_125_avg = sum(h_G_local[0]) / len(h_G_local[0])
h_150_avg = sum(h_G_local[1]) / len(h_G_local[1])
h_175_avg = sum(h_G_local[2]) / len(h_G_local[2])
h_200_avg = sum(h_G_local[3]) / len(h_G_local[3])
h_300_avg = sum(h_G_local[4]) / len(h_G_local[4])

#### PLOTTING THE CO2 CONVECTION AND U VS GAS QUALITY ####
G_125, = plt.plot(k_G_lst[0], h_G_local[0], label = 'G = 125')
G_150, = plt.plot(k_G_lst[1], h_G_local[1], label = 'G = 150')
G_175, = plt.plot(k_G_lst[2], h_G_local[2], label = 'G = 175')
G_200, = plt.plot(k_G_lst[3], h_G_local[3], label = 'G = 200')
G_300, = plt.plot(k_G_lst[4], h_G_local[4], label = 'G = 300')
plt.xlabel('Gas quality, x [-]')
plt.ylabel('h, local convection coefficient [W/m^2K]')
```

```
plt.legend(handles=[G_300,G_200,G_175,G_150,G_125], loc = 'lower left', title =
'G, Mass flux [kg/m^2s]');
plt.show()


G_125, = plt.plot(k_G_lst[0], U_G[0], label = 'G = 125')
G_150, = plt.plot(k_G_lst[1], U_G[1], label = 'G = 150')
G_175, = plt.plot(k_G_lst[2], U_G[2], label = 'G = 175')
G_200, = plt.plot(k_G_lst[3], U_G[3], label = 'G = 200')
G_300, = plt.plot(k_G_lst[4], U_G[4], label = 'G = 300')
plt.xlabel('Gas quality, x [-]')
plt.ylabel('U-value [W/m^2K]')
plt.legend(handles=[G_300,G_200,G_175,G_150,G_125], loc = 'lower left', title =
'G, Mass flux [kg/m^2s]');
plt.show()

### ICE FORMATION ### starting with the inlet with saturated liquid.
h_ice = 334 * 10**3 #J/kg
rho_ice = 917 #kg/m^3
freezing_point = 273.15 - 0.61

U_ice = [[],[],[],[],[]]
time_lst = [[],[],[],[],[]]
ice_lst = [[],[],[],[],[]]

k_G_lst = [[],[],[],[],[]]
h_G_local = [[],[],[],[],[]]
counter = 0
#### CHANGE T_BULK TO WANTED TEMPERATURE ####
T_bulk = -0.61

### CALCULATING ICE GROWTH AND U-VALUE CHANGE IN A CYCLE ####

for num in G_lst:
    G = num
    ice_formed = 0
    #SETTING STARTING POINT

    none, noone, cond_ice, none1, none2, none3 =
avg_conduction_vertical.conduction(
        T_evap, d_i, d_y, d_cyl , k_cu, k_al, k_gel, wall_thick, k_ice,
ice_formed) ### is the initial ice formed
    for n in range(1, (int((60/rpm)))*10, 1):
        l = n/10
        for i in range(0,15):
            h_lst = []
            h_liq = []
            n_lst = []
            k_lst = []
            h_local = []
            for i in range(1,int(x_out*100),1):
                k = i/100
                k_lst.append(k)
                Co = (1/k - 1)**0.8 *(rho_g/rho_f)**0.5
```

```
                Re_bo = (G * (1-k) * d_i)/(mu_f)
                f_l = (friction_coeff(Re_bo))
                h_l = (((f_l/8) * (Re_bo - 1000) * Pr_f) / (1 +
12.7*((Pr_f**(2/3))-1)*(f_l/8)**0.5)) * (k_f/d_i)
                h_liq.append(h_l)
                n_lst.append(N(Fr,Co))
                h_lst.append(h_dim(N(Fr,Co)))
            for i in range(len(h_lst)):
                h_local.append(h_lst[i]*h_liq[i])
#           print(h_local)
            h_co2_avg = sum(h_local)/len(h_local)
            U_new = 1/(1/h_co2_avg + cond_ice + R_hyd)
            Q_0 = U_new * d_i * tot_length_coil * (freezing_point - T_evap)
            Q_A0 = U_new * (freezing_point - T_evap)
            x_out = Q_0 / (h_fg * G * ((d_i**2/4)*np.pi))
            Bo = Q_A0/(G * (h_fg))
            #print('X_out',x_out)


        Q_0 = U_new * (freezing_point - T_evap)
        ice_formed = ice_formed + Q_0/(h_ice * rho_ice)
        none, noone, cond_ice, none1, none2, none3 =
avg_conduction_vertical.conduction(
            T_evap, d_i, d_y, d_cyl, k_cu, k_al, k_gel, wall_thick, k_ice,
ice_formed)
        U_ice[counter].append(U_new)
        ice_lst[counter].append(ice_formed)
        time_lst[counter].append(l)

    counter = counter + 1
#### PLOTTING ICE, U, TIME ####

G_125_ICE, = plt.plot(time_lst[0], ice_lst[0], label = 'G = 125')
G_150_ICE, = plt.plot(time_lst[1], ice_lst[1], label = 'G = 150')
G_175_ICE, = plt.plot(time_lst[2], ice_lst[2], label = 'G = 175')
G_200_ICE, = plt.plot(time_lst[3], ice_lst[3], label = 'G = 200')
G_300_ICE, = plt.plot(time_lst[4], ice_lst[4], label = 'G = 300')
plt.xlabel('time [s]')
plt.ylabel('Ice thickness [m]')
plt.legend(handles=[G_300_ICE,G_200_ICE,G_175_ICE,G_150_ICE,G_125_ICE], loc =
'upper left', title = 'G, Mass flux [kg/m^2s]');
plt.show()

G_125_ICE, = plt.plot(time_lst[0], U_ice[0], label = 'G = 125')
G_150_ICE, = plt.plot(time_lst[1], U_ice[1], label = 'G = 150')
G_175_ICE, = plt.plot(time_lst[2], U_ice[2], label = 'G = 175')
G_200_ICE, = plt.plot(time_lst[3], U_ice[3], label = 'G = 200')
G_300_ICE, = plt.plot(time_lst[4], U_ice[4], label = 'G = 300')
plt.xlabel('time [s]')
plt.ylabel('U-value [W/m^2K]')
plt.legend(handles=[G_300_ICE,G_200_ICE,G_175_ICE,G_150_ICE,G_125_ICE], loc =
'upper right', title = 'G, Mass flux [kg/m^2s]');
plt.show()
```

```
G_125_ICE, = plt.plot(ice_lst[0], U_ice[0], label = 'G = 125')
G_150_ICE, = plt.plot(ice_lst[1], U_ice[1], label = 'G = 150')
G_175_ICE, = plt.plot(ice_lst[2], U_ice[2], label = 'G = 175')
G_200_ICE, = plt.plot(ice_lst[3], U_ice[3], label = 'G = 200')
G_300_ICE, = plt.plot(ice_lst[4], U_ice[4], label = 'G = 300')
plt.xlabel('Ice thickness [m]')
plt.ylabel('U-value [W/m^2K]')
plt.legend(handles=[G_300_ICE,G_200_ICE,G_175_ICE,G_150_ICE,G_125_ICE], loc =
'upper right', title = 'G, Mass flux [kg/m^2s]');
plt.show()


P_int = P_sat + 30*10**5
T_sat_int = CP.PropsSI('T', 'P', P_int, 'Q', 0, R744) -273.15


####### TEMPERATURE DISTRIBUTION THROUGH WALL####
###NUMBER IN LIST IS FOUND FOR 90, 60, 45, 30, 0
Temp_lst_90 = []

def temp_lst(number):
    Temp_lst = []
    U_deg = 1/(1/h_co2_avg + res_cu[number] + res_gel[number] + res_al[number] +
1/h_w)
    Q_deg = U_deg * (T_inf - T_evap)
    T_out = Q_deg * 1/(h_175_avg) + T_evap -273.15 #### h_xxx_avg, xxx is G
[kg/m^2s]
    T_cu = Q_deg * res_cu[number] + T_out
    T_gel = Q_deg * res_gel[number] + T_cu
    T_al = Q_deg * res_al[number] + T_gel
    T_in = Q_deg * (1/h_w) + T_al
    Temp_lst.append(T_evap - 273.15)
    Temp_lst.append(T_out)
    Temp_lst.append(T_cu)
    Temp_lst.append(T_gel)
    Temp_lst.append(T_al)
    Temp_lst.append(T_in)
    return Temp_lst



Temp45 = temp_lst(50)
Temp30 = temp_lst(33)
Temp60 = temp_lst(67)
Temp90 = temp_lst(99)
Temp0  = temp_lst(0)

x_lst = [0,1,2,3,4,5]
temp_xticks = ['T_CO2', 'T_cu(i)', ' T_cu(o)', 'T_al(i)', 'T_al(o)', 'T_bulk']
plt.xticks(x_lst, temp_xticks)

### PLOTTING TEMPERATURE DISTRIBUTION THROUGH WALL #####
temp_plot1, = plt.plot(Temp90, '--', marker = 'X', label = '90 deg')
temp_plot2, = plt.plot(Temp60, '--', marker = 'X', label = '60 deg')
```

```
temp_plot3, = plt.plot(Temp45, '--', marker = 'X', label = '45 deg')
temp_plot4, = plt.plot(Temp30, '--', marker = 'X', label = '30 deg')
temp_plot5, = plt.plot(Temp0 , '--', marker = 'X', label = '0 deg')

plt.xlabel('Elements')
plt.ylabel('Temperature [C]')
plt.legend(handles = [temp_plot1, temp_plot2, temp_plot3, temp_plot4,
temp_plot5], loc = 'upper left', title = 'Angles [Deg], G = 175' )
plt.show()



##### adding 10mm to gel thickness  ####
def larger_gel():
    r_gel_thick = []
    r_gel_counter = []

    for i in range(0,100):
        r_gel_thick.append(avg + (i/10000)/k_gel)
        r_gel_counter.append(i/10000)
    return r_gel_thick, r_gel_counter

r_gel_thick, r_gel_counter = larger_gel()




### CALCULATING NEW U FOR GROWING LAYER OF THERMAL GEL BETWEEN PIPE AND ALU WALL
###
U_gel = [[],[],[],[],[]]
thick_gel = [[],[],[],[],[]]

counter = 0 ### RESETING COUNTER
for num in G_lst:
    G = num
    #SETTING STARTING POINT
    for gel_cond in (r_gel_thick):
        for i in range(0,15):
            h_lst = []
            h_liq = []
            n_lst = []
            k_lst = []
            h_local = []
            for i in range(1,int(x_out*100),1):
                k = i/100
                k_lst.append(k)
                Co = (1/k - 1)**0.8 *(rho_g/rho_f)**0.5
                Re_bo = (G * (1-k) * d_i)/(mu_f)
                f_l = (friction_coeff(Re_bo))
                h_l = (((f_l/8) * (Re_bo - 1000) * Pr_f) / (1 +
12.7*((Pr_f**(2/3))-1)*(f_l/8)**0.5)) * (k_f/d_i)
                h_liq.append(h_l)
                n_lst.append(N(Fr,Co))
                h_lst.append(h_dim(N(Fr,Co)))
```

```
            for i in range(len(h_lst)):
                h_local.append(h_lst[i]*h_liq[i])
            h_co2_avg = sum(h_local)/len(h_local)
            U_new = 1/(1/h_co2_avg + gel_cond + R_hyd)
            Q_0 = U_new * d_i * tot_length_coil * (T_inf - T_evap)
            Q_A0 = U_new * (T_inf - T_evap)
            x_out = Q_0 / (h_fg * G * ((d_i**2/4)*np.pi))
            Bo = Q_A0/(G * (h_fg))


        Q_0 = U_new * (T_inf - T_evap)
        U_gel[counter].append(U_new)

    counter = counter + 1

#### PLOTTING GEL THICKNESS VS U-VALUE ####

G_125_GEL, = plt.plot(r_gel_counter, U_gel[0], label = 'G = 125')
G_150_GEL, = plt.plot(r_gel_counter, U_gel[1], label = 'G = 150')
G_175_GEL, = plt.plot(r_gel_counter, U_gel[2], label = 'G = 175')
G_200_GEL, = plt.plot(r_gel_counter, U_gel[3], label = 'G = 200')
G_300_GEL, = plt.plot(r_gel_counter, U_gel[4], label = 'G = 300')
plt.xlabel('Width of gel between pipe and aluminium [m]')
plt.ylabel('U-value [W/m^2K]')
plt.legend(handles=[G_300_ICE,G_200_ICE,G_175_ICE,G_150_ICE,G_125_ICE], loc =
'upper right', title = 'G, Mass flux [kg/m^2s]');
plt.show()
```

Conduction calculation for Vertical pipes

```
# -*- coding: utf-8 -*-
"""
Created on Mon May  2 21:55:25 2022

@author: jomar
"""

import numpy as np
def conduction(T_evap, d_i, d_y, di_cyl, k_cu, k_al, k_gel, wall_thick, k_ice,
x_ice):

    #### SETTING UP STEP LENGTH ###
    n = 100
    step_length = (np.pi/2)/n  #angle#
    steps = []
    number = 0
    h_cyl = d_i/2
    h_length = h_cyl/n
    dy_cyl = di_cyl + 2 * wall_thick


    for i in range(n): #FINDING ANGLES#
        steps.append(number)
        number = number + step_length


    def inner_diameter(angle,diameter):
        r = diameter/2
        y = np.sin(angle)*r
        x = np.cos(angle)*r
        return x,y


    def outer_diameter(y,diameter):
        r = diameter/2
        x =(r**2-y**2)**(1/2)
        return x



    def thermal_resistance_cyl(di, dy,di_cyl, dy_cyl):
        r = (h_cyl**2 + dy_cyl**2)**(1/2)
        max_angle = np.arcsin(h_cyl/r)
        return max_angle

    max_angle = thermal_resistance_cyl(d_i, d_y,di_cyl, dy_cyl)
    cyl_step = max_angle/n
    cyl_steps = []
    number = 0
    for i in range(n):
        cyl_steps.append(number)
        number = number + cyl_step

    #### CALCULATING THE THERMAL RESISTANCE AT DIFFERENT ANGLES #####
```

```
    def thermal_resistance(k_cu,k_gel,k_al,k_ice,x_ice):
        R_cond_lst = []
        R_cu = []
        R_gel = []
        R_al = []
        Angle_lst = []
        i = 0
        for i in range(len(steps)):
            d_inner,width = inner_diameter(steps[i],d_i)
            d_yout = outer_diameter(width,d_y)
            x_cu = d_yout - d_inner
            d_cyl_inner, cyl_width = inner_diameter(cyl_steps[i], di_cyl)
            d_cyl_yout = outer_diameter(cyl_width, dy_cyl)
            x_al = d_cyl_yout - d_cyl_inner
            x_gel_cyl = dy_cyl/2 - d_cyl_yout
            x_gel = d_y/2 - d_yout
            R_cond = x_cu/k_cu + (x_gel+x_gel_cyl)/k_gel + x_al/k_al +
x_ice/k_ice
            R_cu.append(x_cu/k_cu)
            R_gel.append((x_gel+x_gel_cyl)/k_gel)
            R_al.append(x_al/k_al)
            R_cond_lst.append(R_cond)
            Angle_lst.append(steps[i])
        return R_cond_lst, Angle_lst, R_cu, R_gel, R_al


    resistance, angles, res_cu, res_gel, res_al =
thermal_resistance(k_cu,k_gel,k_al,k_ice,x_ice)

    avg_resistance = sum(resistance)/n
    return resistance, angles, avg_resistance, res_cu, res_gel, res_al
```

Calculation of Maximum diameters

```
# -*- coding: utf-8 -*-
"""
Created on Sun May 29 10:25:39 2022

@author: jomar
"""

import numpy as np
import matplotlib.pyplot as plt


#### PLOT STYLE #####
plt.style.use('seaborn')

#### CONSTANTS ####
V = 1.783 #[M]
Q_req = 143*10**3 # [W]

#### U-VALUES FROM DIFFERENT T_SAT ###
U_lst = [565,585,605,625,650]
d_lst = []
for i in range(35, 176):
    d_lst.append(i/100)

dT_lst = []

d_lst_new = []
h_lst_new = []
for U in U_lst:
    dT_d = []
    d_d_lst = []
    h_lst = []
    for d in d_lst:
        h = V / (np.pi * (d**2)/4)
        A_surf = np.pi * d * h
        dT = Q_req / (U * A_surf)
        if (dT-0.61) > 50:
            continue
        else:
            dT_d.append(dT-0.61)
            d_d_lst.append(d)
            h_lst.append(h)
            print(round(d,2), round(h,2), round(dT-0.61,2))


    dT_lst.append(dT_d)
    d_lst_new.append(d_d_lst)
    h_lst_new.append(h_lst)

#### PLOTTING TEMPERATURE VS MAX DIAMETER ####
U_300, = plt.plot(dT_lst[0], d_lst_new[0], label = 'U = ' + str(U_lst[0]))
U_400, = plt.plot(dT_lst[1], d_lst_new[1], label = 'U = ' + str(U_lst[1]))
U_500, = plt.plot(dT_lst[2], d_lst_new[2], label = 'U = ' + str(U_lst[2]))
U_600, = plt.plot(dT_lst[3], d_lst_new[3], label = 'U = ' + str(U_lst[3]))
```

```
U_700, = plt.plot(dT_lst[4], d_lst_new[4], label = 'U = ' + str(U_lst[4]))

plt.xlabel('Saturation temperature [C]')
plt.ylabel('Diameter [m]')
plt.legend(handles=[U_300,U_400,U_500,U_600,U_700], loc = 'upper left', title =
'U, Mass flux [kg/m^2s]');
plt.show()
```

B: EES calculations

CASE 1 EES CALCULATIONS

"Heat & Cooling loads"
Q_e = 143
Q_hyd = 87,17

"Intermediate pressure vessle"
T_int = 10
P_int =**p_sat**(***R744***;***T***=T_int)
x_outlet_low = 0
x_outlet_high = 1
d_h_int =**enthalpy_vaporization**(***R744***;***T***=T_int)
h_f_int = **enthalpy**(***R744***;***T***=T_int;***x***=x_outlet_low)
h_g_int = **enthalpy**(***R744***;***T***=T_int;***x***=x_outlet_high)

"EVAPORATION"
T_e = -20
P_low = **p_sat**(***R744***;***T***=T_e)
x_low=**quality**(***R744***;***T***=T_e;***h***=h_f_int)
x_g_low = 1
h_g_low = **enthalpy**(***R744***;***T***=T_e;***x***=x_g_low)
m_low = Q_e/(h_g_low-h_f_int)
s_g_low =**entropy**(***R744***;***T***=T_e;***x***=x_g_low)

"Low - intermediate Compression with 70% isentropic"
eta_is = 0,70
s_g_int_s = s_g_low
h_Bs = **enthalpy**(***R744***;***P***=P_int;***s***=s_g_low)
h_B = (h_Bs-h_g_low)/eta_is + h_g_low
w_low = h_B - h_g_low
T_outlet_comp_low = **temperature**(***R744***; h = h_B; p = P_int)
dh_superheat_low = h_B - h_g_int

"Intermediate - high Compression with 70% isentropic"
P_high = 120
T_gas_out = 30
T_comp_in = 25
h_comp_in=**enthalpy**(***R744***;***T***=T_comp_in;***P***=P_int)
superheat = h_comp_in - h_g_int
subcool = superheat
h_gas_out =**enthalpy**(***R744***;***T***=T_gas_out;***P***=P_high)
h_ihx_out = h_gas_out - subcool
T_ihx_out =**temperature**(***R744***;***P***=P_high;***h***=h_ihx_out)
s_comp_in = **entropy**(***R744***;***T***=T_comp_in;***P***=P_int)
h_comp_out_s = **enthalpy**(***R744***;***P***=P_high;***s***=s_comp_in)
h_comp_out = (h_comp_out_s - h_comp_in)/eta_is + h_comp_in
w_high = h_comp_out - h_comp_in
T_outlet_comp = **temperature**(***R744***;***P***=P_high;***h***=h_comp_out)
h_high_55 = **enthalpy**(***R744***;***T***=55;***P***=P_high)
dh_hyd_heating = h_comp_out-h_high_55
dh_extra = h_high_55 - h_gas_out
m_min = Q_hyd/dh_hyd_heating

"Expansion"
h_exp = h_ihx_out
x_exp = **quality**(***R744***;***P***=P_int;h = h_exp)
m_exp = m_min

"Continue mass balance intermediate pressure vessle"
m_comp_low = m_low
m_gas_exp = x_exp*m_exp
m_liquid_exp = (1-x_exp)*m_exp

V_comp_low = **volume**(***R744***;***x***=x_g_low;***P***=P_low) * m_comp_low * 3600
V_comp_high = **volume**(***R744***;T = T_comp_in;***P***=P_int) * m_min * 3600

m_gas_high = m_min
m_liq_evaporator = m_low

m_liquid_balance = m_liq_evaporator - m_liquid_exp
m_gas_balance = m_gas_high - m_gas_exp

x_int = m_gas_balance/(m_liquid_balance+m_gas_balance)
h_out_cond = **enthalpy**(***R744***;***x***=x_int;***P***=P_int)

"Heating duties for the condensers and gas coolers"
dq_desuperheater = m_comp_low*dh_superheat_low
dq_condenser = m_comp_low*(h_g_int - h_out_cond)

dq_gc_55 = m_min * dh_hyd_heating
dq_gc_extra = m_min * dh_extra

"COP calculations"
work_low = m_comp_low * w_low
work_high = m_min * w_high

hot_duty_high = (h_comp_out-h_gas_out) * m_min
hot_duty_int = (h_B - h_out_cond) * m_comp_low

COP_high = hot_duty_high/work_high
COP_H_total = (hot_duty_high+hot_duty_int)/(work_high+work_low)
COP_C_total = Q_e/(work_high+work_low)

CASE 2 EES CALCULATIONS

```
$Load Component Library
$Load Mechanical Design
"Heat & Cooling loads"
Q_e = 143
Q_hyd = 87,17



"EVAPORATION"
T_e = - 20
P_low = p_sat(R744;T=T_e)
x_low=quality(R744;T=T_e;h=h_f_int)
x_g_low = 1
h_g_low = enthalpy(R744;T=T_e;x=x_g_low)
m_low = Q_e/(h_g_low-h_f_int)
s_g_low =entropy(R744;T=T_e;x=x_g_low)


"Intermediate pressure vessle"
"P_int = 45"
"29 30 + P_low"
T_int = t_sat(R744;P=P_int)
x_outlet_low = 0
x_outlet_high = 1
d_h_int =enthalpy_vaporization(R744;T=T_int)
h_f_int = enthalpy(R744;T=T_int;x=x_outlet_low)
h_g_int = enthalpy(R744;T=T_int;x=x_outlet_high)

P_ratio_low = P_int/P_low
P_ratio_high = P_high/P_int


"Low - intermediate Compression with 70% isentropic"
eta_is = 0,70
s_g_int_s = s_g_low
h_Bs = enthalpy(R744;P=P_int;s=s_g_low)
h_B = (h_Bs-h_g_low)/eta_is + h_g_low
w_low = h_B - h_g_low
T_outlet_comp_low = temperature(R744; h = h_B; p = P_int)
dh_superheat_low  = h_B - h_g_int

"De-superheater, dT 5 [C] to seawater NEW TO MASTER"
T_sup_out = 10
h_sup_out = enthalpy(R744;P=P_int; T=T_sup_out)

dh_superheat = h_B - h_sup_out
Q_superheat = dh_superheat * m_low

T_sat_int = t_sat(R744;P=P_int)
"Intermediate - high Compression with 70% isentropic"
"P_high = 106"
" Real h value for inlet compressor high"
h_comp_in = (m_low *enthalpy(R744;T=T_sup_out ;P=P_int)) + (m_min*(x_exp) * enthalpy(R744;x = x_outlet_high ;P=
P_int)) / (m_low + (m_min*x_exp))
s_comp_in = entropy(R744;h=h_comp_in;P=P_int)
h_comp_out_s = enthalpy(R744;P=P_high;s=s_comp_in)
h_comp_out = (h_comp_out_s - h_comp_in)/eta_is + h_comp_in
w_high = h_comp_out - h_comp_in
T_outlet_comp = temperature(R744;P=P_high;h=h_comp_out)
h_high_55 = enthalpy(R744;T=55;P=P_high)
h_gas_out = enthalpy(R744; T = 30; P=P_high)
dh_hyd_heating = h_comp_out-h_high_55
dh_extra = h_high_55 - h_gas_out
"m_min  = Q_hyd/dh_hyd_heating"
m_min = m_low/(1-x_exp)
Q_90_55 = m_min * dh_hyd_heating
```

```
Q_55_30 = m_min * (h_high_55 - h_gas_out)

"Volumetric flow through the compressors"
V_high = m_min * volume(R744;h=h_comp_in;P=P_int) *3600
V_low = m_low *   volume(R744;h=h_g_low;P=P_low) *3600


"Expansion and intermediate stage"
h_exp = h_gas_out
x_exp = quality(R744;P=P_int;h = h_exp)
m_exp = m_min
m_gas_exp = m_exp * x_exp

"Continue mass balance intermediate pressure vessle"
m_comp_low = m_low
m_comp_high = m_gas_exp + m_comp_low


"COP calculations"
work_low = m_comp_low * w_low
work_high = m_min * w_high

hot_duty_high = (h_comp_out-h_gas_out) * m_min
hot_duty_int = (h_B - h_sup_out) * m_comp_low

COP_high = hot_duty_high/work_high
COP_H_total = (hot_duty_high+hot_duty_int)/(work_high+work_low)
COP_C_total = Q_e/(work_high+work_low)
```

SOLUTION

Unit Settings: SI C bar kJ mass deg

(Table 3, Run 21)

$COP_{C,total}$ = 1,816	COP_{high} = 4,117	$COP_{H,total}$ = 2,919
dh_{extra} = 106,1	$dh_{hyd,heating}$ = 112,2	$dh_{superheat}$ = 63,1
$dh_{superheat,low}$ = 63,15	$d_{h,int}$ = 197,2	η_{is} = 0,7
$hot_{duty,high}$ = 187,1	$hot_{duty,int}$ = 42,72	h_B = -20,72
h_{Bs} = -35,47	$h_{comp,in}$ = -74,36	$h_{comp,out}$ = -21,33
$h_{comp,out,s}$ = -37,24	h_{exp} = -239,7	$h_{f,int}$ = -281,1
$h_{gas,out}$ = -239,7	$h_{g,int}$ = -83,88	$h_{g,low}$ = -69,89
$h_{high,55}$ = -133,5	$h_{sup,out}$ = -83,83	$m_{comp,high}$ = 0,857
$m_{comp,low}$ = 0,6771	m_{exp} = 0,857	$m_{gas,exp}$ = 0,1799
m_{low} = 0,6771	m_{min} = 0,857	P_{high} = 114
P_{int} = 45	P_{low} = 19,7	$P_{ratio,high}$ = 2,533
$P_{ratio,low}$ = 2,285	$Q_{55,30}$ = 90,96	$Q_{90,55}$ = 96,17
Q_e = 143	Q_{hyd} = 87,17	$Q_{superheat}$ = 42,72
$s_{comp,in}$ = -0,9208	$s_{g,int,s}$ = -0,7905	$s_{g,low}$ = -0,7905
T_e = -20	T_{int} = 9,98	$T_{outlet,comp}$ = 95,85
$T_{outlet,comp,low}$ = 49,35	$T_{sat,int}$ = 9,98	$T_{sup,out}$ = 10 [C]
V_{high} = 24,47	V_{low} = 47,15	$work_{high}$ = 45,45
$work_{low}$ = 33,29	w_{high} = 53,04	w_{low} = 49,16
x_{exp} = 0,2099	$x_{g,low}$ = 1	x_{low} = 0,2522
$x_{outlet,high}$ = 1	$x_{outlet,low}$ = 0	

No unit problems were detected.

Parametric Table: Table 3

	P_{high}	P_{int}	$Q_{90;55}$	$Q_{55;30}$	$Q_{superheat}$	$T_{outlet;comp}$	m_{min}	m_{low}	V_{high}	V_{low}
Run 1	84	25	*88,45*	*147,4*	*-7,334*	*115,7*	*0,9164*	*0,5398*	*55,59*	*37,59*
Run 2	86	26	*89,26*	*144,2*	*-5,372*	*115,3*	*0,9084*	*0,5462*	*52,8*	*38,03*

Parametric Table: Table 3

	P_{high}	P_{int}	$Q_{90;55}$	$Q_{55;30}$	$Q_{superheat}$	$T_{outlet;comp}$	m_{min}	m_{low}	V_{high}	V_{low}
Run 3	87	27	87,88	142,6	-3,382	113,5	0,9053	0,5525	50,41	38,47
Run 4	89	28	89,02	139,3	-1,361	113,1	0,8989	0,5589	48,05	38,92
Run 5	90	29	87,88	137,6	0,6939	111,4	0,8964	0,5653	46	39,36
Run 6	92	30	89,31	134,2	2,787	111,1	0,891	0,5717	43,98	39,81
Run 7	93	31	88,38	132,5	4,922	109,4	0,889	0,5782	42,19	40,26
Run 8	94	32	87,52	130,7	7,102	107,9	0,8871	0,5847	40,51	40,72
Run 9	96	33	89,3	127	9,332	107,6	0,8828	0,5913	38,85	41,18
Run 10	97	34	88,59	125,2	11,62	106,1	0,8812	0,598	37,36	41,64
Run 11	98	35	87,93	123,3	13,96	104,6	0,8797	0,6047	35,94	42,11
Run 12	99	36	87,3	121,4	16,37	103,1	0,8782	0,6115	34,6	42,58
Run 13	101	37	89,39	117,4	18,86	102,8	0,8747	0,6183	33,26	43,06
Run 14	102	38	88,82	115,4	21,42	101,4	0,8734	0,6253	32,04	43,54
Run 15	103	39	88,25	113,3	24,08	99,96	0,8722	0,6324	30,87	44,03
Run 16	104	40	87,65	111,3	26,83	98,54	0,871	0,6395	29,75	44,53
Run 17	106	41	89,73	107,1	29,7	98,15	0,8679	0,6468	28,62	45,04
Run 18	107	42	89,02	105	32,7	96,69	0,8668	0,6541	27,57	45,55
Run 19	108	43	88,2	103	35,85	95,2	0,8656	0,6616	26,55	46,07
Run 20	111	44	92,48	96,78	39,18	95,61	0,8611	0,6693	25,49	46,6
Run 21	114	45	96,17	90,96	42,72	95,85	0,857	0,6771	24,47	47,15

Parametric Table: Table 3

	$work_{high}$	$work_{low}$	$COP_{C;total}$
Run 1	76,34	7,188	1,712
Run 2	74,31	8,504	1,727
Run 3	71,87	9,812	1,751
Run 4	70,13	11,11	1,76
Run 5	67,93	12,41	1,78
Run 6	66,41	13,7	1,785
Run 7	64,41	14,99	1,801
Run 8	62,49	16,27	1,816
Run 9	61,2	17,56	1,816
Run 10	59,42	18,84	1,827
Run 11	57,71	20,13	1,837
Run 12	56,05	21,42	1,846
Run 13	54,97	22,71	1,841
Run 14	53,4	24,01	1,847
Run 15	51,87	25,31	1,853
Run 16	50,38	26,61	1,857
Run 17	49,4	27,93	1,849
Run 18	47,95	29,25	1,852
Run 19	46,52	30,59	1,855
Run 20	46,01	31,93	1,835
Run 21	45,45	33,29	1,816

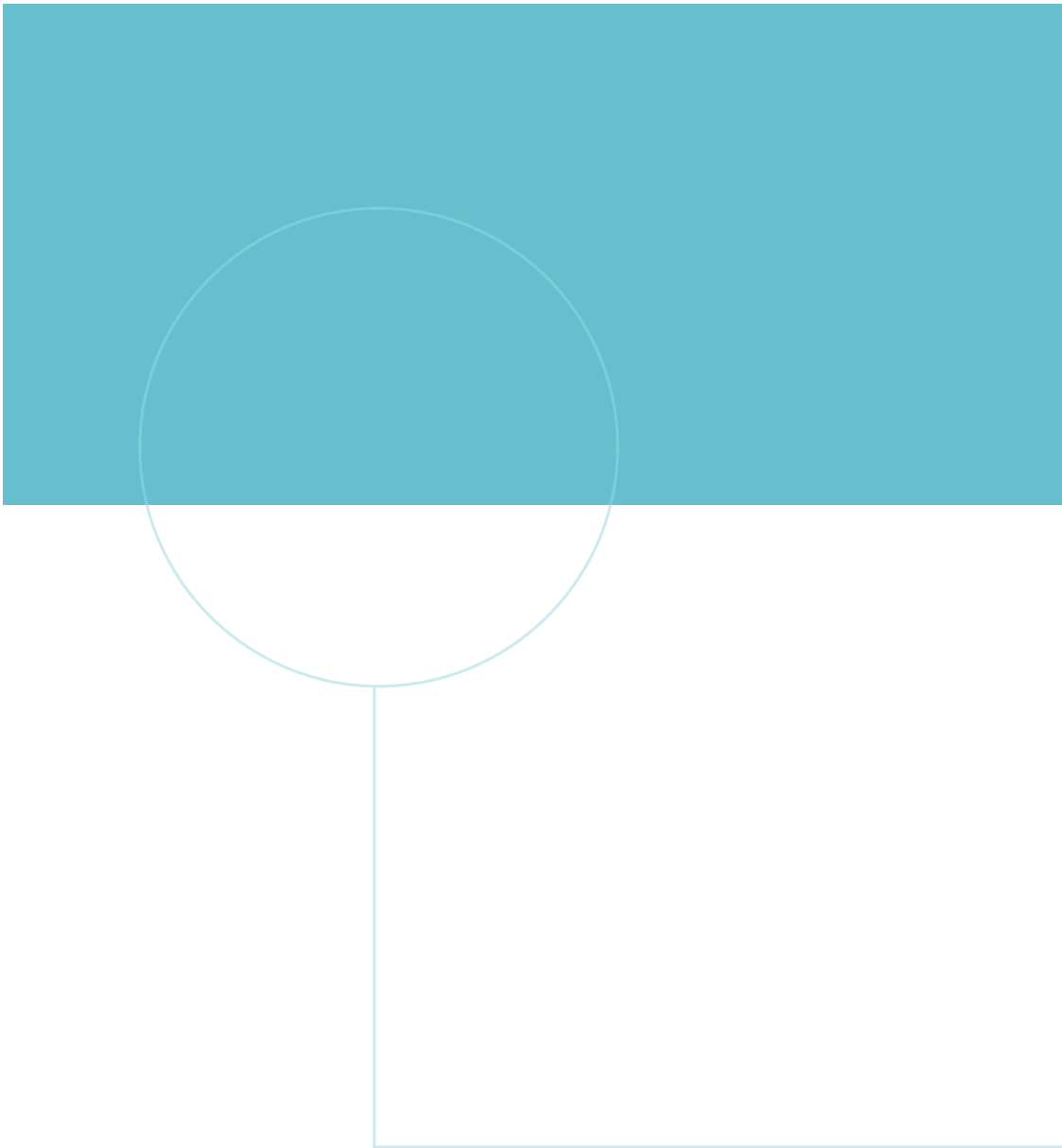

NTNU

Norwegian University of
Science and Technology